5-13-2021

# Evolution of Composite Heat Vulnerability Indices in Atlanta using Multiple Weighting Mechanics

Joseph Karanja

# Evolution of Composite Heat Vulnerability Indices in Atlanta using Multiple Weighting Mechanics

by

Joseph Karanja

Under the Direction of Lawrence Kiage, PhD

A Thesis Submitted in Partial Fulfillment of the Requirements for the Degree of

Master of Science

in the College of Arts and Sciences

Georgia State University

2021

ABSTRACT

Global surface temperatures are projected to escalate in intensity, duration, and frequency, particularly in urban areas, which are dominated by landscapes of imperviousness, accelerating the Urban Heat Island Phenomena (UHI). Geographies of thermal inequality emerge engendered by disproportionality in socioeconomic and demographic characteristics and variances in the magnitude of heat exposure. This study integrated the biophysical exposure index and the socioeconomic index to generate composite heat vulnerability indices at multiple time scales and applying different weighting mechanics. Outputs of the raster-based and vector-based approaches were compared. Remote sensing indices measuring vegetation health, surface water content, urban imperviousness, and bareness were used to characterize the biophysical metric. The objective was to visualize areas most susceptible accurately and precisely to the Urban Heat Island phenomena while ensuring both scientific and policy applications of the spatial representations.

INDEX WORDS: Heatwave, Vulnerability, Hazard, Urban heat island, Exposure, Composite index

# Evolution of Composite Heat Vulnerability Indices in Atlanta using Multiple Weighting Mechanics

by

Joseph Karanja

Committee Chair: Lawrence Kiage

Committee: Ricardo Nogueira

Dajun Dai

Electronic Version Approved:

Office of Graduate Services

College of Arts and Sciences

Georgia State University

May 2021

## DEDICATION

Dedication to Simon Mwaniki and Dan Wanyama, truly altruistic mentors, for the immense sacrifices they have made and taught me virtues of resilience, hard work, and due diligence.

## ACKNOWLEDGEMENTS

I am grateful to my supervisor, Dr. Kiage, for his tireless guidance and commitment to completing this thesis. Dr. Dai was instrumental in shaping my spatial analytical skills. At the same time, Dr. Nogueira consented to be a member of the thesis committee, which was devoted from the preparation to finalization of this document. The graduate director, Professor Kabengi, facilitated the focusing of my study at the nascent stages. My friend, Dan Wanyama, was always available for consultation and provided integral insights into the development of the methodology.

# TABLE OF CONTENTS

# LIST OF TABLES

## LIST OF FIGURES

## LIST OF ABBREVIATIONS

AC – Air Conditioner

EPA – Environmental Protection Agency

GDP – Gross Domestic Product

HPM – Hazard of Place Model

HVI – Heat Vulnerability Index

HWWS – Heatwave Warning Systems

IPCC – Intergovernmental Panel on Climate Change

LCZ – Land Classification Zoning

LDTB – Longitudinal Tract Database

LST – Land Surface Temperature

LULC – Land Use Land Cover Change

MAUP – Modifiable Area Unit Problem

MCA – Multi-Criteria Analysis

MODIS – Moderate Resolution Imaging Spectro-Radiometer

NDBaL – Normalized Difference Bareness Index

NDBI – Normalized Difference Bareness Index

NDISI – Normalized Difference Impervious Surface Index

NDVI – Normalized Difference Vegetation Index

NDWI – Normalized Difference Water Index

NGO – Non-Governmental Organization

NOAA – National Oceanic and Atmospheric Administration

PCA – Principal Component Analysis

RVM – Raster and Vector-Based Model

SoVI – Social Vulnerability Index

UHI – Urban Heat Island

WMO – World Meteorological Organization

# CHAPTER 1: INTRODUCTION

## 1.1 Background Information

The ongoing disruption of the climate system is unprecedented over centuries to millennia (Bera, 2019). The distortions on the climate system have been profound, translating to severe, pervasive, and potentially irreparable ramifications to ecological systems and human systems (Intergovernmental Panel on Climate Change (IPCC), 2014). The explicit evidence for the upset of the climate system is the global warming phenomena manifested in the warming of the oceans, the drastic diminishing of snow and ice, and the rising sea levels (Bera, 2019; The National Oceanic and Atmospheric Association (NOAA), 2020). The five warmest years on record have occurred after 2015, while nine of the ten warmest years in human history have occurred since the year 2005 (NOAA,2020). The average temperature for 2019, which was 0.95º C above the 20$^{th}$ century average of 13.9º C, was ranked as the second warmest year after 2015, since the inception of temperature recordings (NOAA, 2020). 2015 and 2019 witnessed the deadliest heatwaves worldwide (World Meteorological Organization (WMO), 2019). The recent warming of the earth is indisputable and projected to increase to the future (IPCC, 2014), particularly in urban areas that comparatively experience 6º C to 8º C temperature elevations above that of surrounding areas (Habeeb et al., 2015; Weber et al., 2015).

Urbanization has generated disproportional heat hazard exposures and created geographies of thermal inequality globally (Xu et al., 2019; Depiettri et al., 2013; Krstic et al., 2017). The sophistication of urban structures distorts urban landscape cover and alters the urbanscape energy exchange (Wang et al., 2019). The temperature disproportionality between urban and rural areas is the Urban Heat Island (UHI) phenomenon (Figure 1.1) (Wang et al., 2019; Mushore et al., 2018;

Xu et al., 2019). Basu and Ostro (2008) identified the correlation between temperature and mortality, and the growing threat has necessitated studies on the UHI (e.g., Arnds et al., 2017; Basu and Ostro, 2008; Chow et al., 2012; Habeeb et al., 2015; Ho et al., 2018; Wang et al., 2019). For instance, Maier et al. (2013) revealed that extreme heat in Portugal killed 1,990 people in 1981, while the 1990 heat event killed 1,000 people. Further, these studies established that the European heatwave of 2003 increased deaths by 37.7% compared to normal temperature conditions. The recorded temperatures for 14 days ranged between 32˚C and 35˚C. Oppressive hot days increased mortality by about 8 %, although this statistic was inferred from cardiovascular disorders only, hence a conservative estimate (Maier et al., 2014).

Elevated temperatures in urban areas increased urban mortality by four times more than surrounding rural areas in absolute numbers (Borden et al., 2007; Maier et al., 2014). The urban population is at high risk of accelerated morbidity and mortality attributed to heat (Arnds et al., 2017; Habeeb et al., 2015). Some studies ( e.g., Kim et al., 2017; Rizvi et al., 2019) attributed the incessant warming to increased emissions of greenhouse gases and the imperviousness of urban landscapes. They noted that 40% of the emissions remained in the atmosphere that propagated temperature elevation. Carbon dioxide concentrations in the atmosphere have increased by 146% of pre-industrial levels (WMO, 2019). The intensity, magnitude, frequency, and duration of heat events are bound to increase, which calls for resilience plans to cushion potential vulnerabilities (Basu and Ostro, 2008; Reid et al., 2009). Atyia (2015) argued for intelligent and proactive urban planning to limit the severity of natural hazards, including those accentuated by the (UHI) phenomena. Urban areas account for 50% of the world population confined to 3% of the total land area, subjecting massive populations to heat stress vulnerability (Xu et al., 2019).

Heat stress vulnerability shifts across time and space in urban areas, yet the underlying driving factors are only partially understood (Aubrecht and Ozceylan, 2013; Kashem et al., 2016). The heat exposure is irregularly distributed in time and space, while the community's demographics shift continuously, posing a challenge to mapping and tracking vulnerable groups (Eriksen and Kelly, 2007; Wilson and Chakraborty, 2019; Cutter, 2003). The biophysical processes and population dynamics manifest on a range of varying geographic scales and local to regional administration levels, producing the Modifiable Area Unit Problem (MAUP) when mapping (Ho et al., 2015). Fine-scale mapping of coupled biophysical and socioeconomic indices (e.g., composite Heat Vulnerability Index) is often disregarded, resulting in mixed pixel problems attributed to coarse-scale mapping (Aubrecht and Ozceylan, 2013; Mushore et al., 2018). The challenges for spatially explicit information are non-trivial, whereas such visualization is highly on demand (Preston et al., 2011).

### 1.2 Research Problem

Urban environments account for approximately 80% of the population in the United States (Bera, 2019; Atyia, 2015), which is the number of people at risk of heat hazards. The heatwave frequency in the USA is increasing by 20% per decade, and its length is extending by 16% per decade (Habeeb et al., 2015). More worrying statistics indicate that from 2006 to 2010, 620 Americans died annually from heat waves (Weber et al., 2015). The momentum of the heat hazards to increase in frequency, duration, intensity, and magnitude should be a significant concern (Habeeb et al., 2015; Wilson and Chakraborty, 2019). Given the perpetual threats, heat hazards pose, policy formulation and identification require novel vulnerability studies (Eriksen and Kelly, 2007). However, vulnerability is a conceptual clutter and represents the social state preceding a hazard, measured subjectively (Eriksen and Kelly, 2007; Morabito et al., 2014; Eakin and Luers,

2006). Social Vulnerability Indices (SoVIs) are a yardstick for the community's capacity to respond generated through data aggregation techniques. Existing data aggregation methods deplete the authenticity of the information from independent suites of variables (Abson et al., 2012; Kashem et al., 2016). Precise mapping of the susceptible groups is thus impaired, thereby undermining policy direction.

Given the rising challenges posed by increasing exposure to urban heat and the demand for spatially explicit information, the overriding question that this study seeks to answer is, how vulnerable is the population of Atlanta to heat hazards? Answers to the following questions will provide information that would elucidate the vulnerability question:

a) How do biophysical exposure and demographic dynamics interact to create geographies of vulnerability to heat hazards across multiple time scales?
b) What are the primary drivers of evolving patterns of spatio-temporal evolution to heat vulnerability?
c) Are there any hotspots of vulnerability to heat hazards in Atlanta? How have the hotspots to heat hazard (if any) shifted across multiple spatial and temporal scales?
d) How data transformation techniques, including weighting mechanics and choice of spatial models, influence vulnerability?

### 1.3 Research Objectives

The harmonization of scales for both the biophysical exposure index and the SoVI enables data visualization at multiple spatial levels (Ho et al., 2015). However, disciplines utilize different concepts generating diverse methods of measuring vulnerability (Tran et al., 2010). Knowing how vulnerability changes over multiple time scales has a higher value than understanding why a given

trend exists (Eriksen and Kelly, 2007). The objectives cited below allow for the extraction of information at multiple spatial and temporal scales using different spatial weighting mechanics.

a) To produce composite heat vulnerability maps with a higher spatial resolution than socio-demographic datasets at multiple time scales, using different weighting mechanics.
b) To track the variance in indices that drive spatio-temporal evolution to heat vulnerability
c) To suggest possible spatial methodological fixes for representing heat vulnerability

### 1.4 Significance of the Study

Scale choices compromise the accurate representation of heat maps. The debates on precise visualization have been the focus of many studies (e.g., Mushore et al., 2018; Atyia, 2015; Birkmann et al., 2017; Borden et al., 2007). The selection of indicators for analysis should be made at finer scales than the characteristic level of susceptibility patterns (Eriksen and Kelly, 2007). However, Jonsonn and Lundgren (2015) observed that there is no standard and systematic methodology for picking variables. Also, Birkmann et al. (2017) asserted that there is no standard mechanism about how variables load and how their direction of influence should be determined. Therefore, the weighting of layers of biophysical components and socioeconomic indicators is subsequently compromised. This study aims to overcome these challenges to generate a variety of reliable and accurate heat visualizations for a variety of urban practitioners.

# CHAPTER 2[1]

## Perspectives on Spatial Representation of Urban Heat Vulnerability

### 2.0 Synopsis

Extreme heat, the deadliest summer weather-related hazard in the USA, is projected to increase in intensity, duration, frequency, and magnitude, especially in urban areas that account for 80% of the population. Spatial visualization and representation are crucial in establishing the hotspots of vulnerability to the heat hazard. However, despite the progress in the science of vulnerability, there lacks a systematic and consistent conceptual framework. The quantification of variables is unchecked, resulting in subjective decisions regarding the weighting of variables, selection of indicators, and the suitability of the proxies. Moreover, contradicting approaches generate disparate outputs such as inductive versus deductive, area-based versus population-based, and raster versus vector designs. The qualitative approach, meant to provide supplementary data, is often ignored. This review provides a perspective of the lacunae in the existing literature and builds on these gaps to derive a conceptual framework towards harmonizing theoretical and statistical relationships. The framework is anchored on the longitudinal study approach as the socioeconomic, biophysical, and geodemographic dimensions have an inherent temporal variance. The review calls for a precise and accurate depiction of heat vulnerability in urban areas to inform targeted adaptation and mitigation measures and the long-term projection of coupled system behavior.

INDEX WORDS: Social Vulnerability Index (SoVI), Composite Heat Vulnerability Index, Principal Component Analysis (PCA), Biophysical Exposure, Urban Heat Stress

**Highlights:**

[1] This chapter has been published in Science of the Total Environment, February 2021, volume 774. https://doi.org/10.1016/j.scitotenv.2021.145634

- Disparate Perspectives of urban heat vulnerability (figure 2-1)
- Harmonizing theoretical and statistical relationships in spatial representation.
- Accurate detection of heat vulnerability in urban areas for targeted mitigation measures
- The coupled heat vulnerability index with quantitative and qualitative dimensions

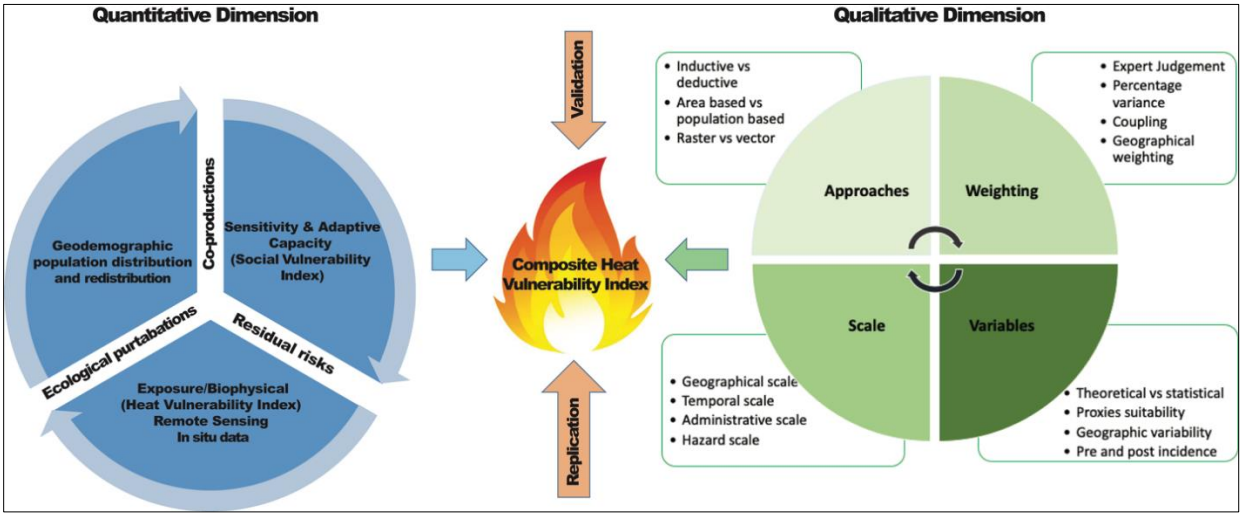


Figure 2-1.Graphical synopsis of the all-inclusive framework, constituting the qualitative and quantitative dimensions of heat vulnerability. Key challenges of heat visualization, such as approaches, weighting mechanics, variable selection, scale, validation, and replication, are highlighted.

## 2.1 Introduction

The progressive detriment of the climate system is unprecedented over centuries to millennia, and the resulting deaths and economic losses continue to rise across the world (Formetta and Feyen, 2019; Intergovernmental Panel on Climate Change (IPCC), 2014). One of the most explicit evidence for the climate system disruption is the ongoing global warming. The average temperature for 2019 was close to 1 degree Celsius above the 20$^{th}$ century average of 13.9$^{o}$C (National Oceanic and Atmospheric Association (NOAA), 2020). 2015 and 2019 witnessed the

deadliest heatwaves (World Meteorological Organization (WMO, 2019). The warming is projected to increase in intensity, magnitude, duration, and frequency, particularly in urbanized environments, which generally experience 6$^{o}$C to 8$^{o}$C higher than surrounding rural locations (Habeeb et al., 2015; Weber et al., 2015). Therefore, urbanization generates disproportionate geographies of thermal inequality, consistent with the Urban Heat Island (UHI) phenomenon (Depiettri et al., 2013; Krstic et al., 2017; Xu et al., 2019). The elevated temperatures in urban areas increase mortality by four times more than in surrounding rural areas (Maier et al., 2014). Despite the heat vulnerability in urban areas, there is minimal attention to heat hazard and its linkages to spatial policy planning in urbanscapes (Hersperger et al., 2018; Masuda et al., 2019).

Intelligent and proactive urban policy strategies are integral to limit the severity of hazards, including those accentuated by the UHI phenomena, hence the demand for spatially explicit information on hotspots (Atyia 2015; Kashem et al., 2016; Preston et l., 2011). However, vulnerability studies represent a pool of conceptual clutter that lacks a systematic and consistent conceptualization to guide spatial representation (Eakin and Luers, 2006; Morabito et al., 2014). Precise and accurate mapping of susceptible groups is impaired, which undermines policy formulation. For instance, heat exposure is irregularly distributed in time and space, while community demographics shift continuously, posing a challenge to mapping and tracking hotspots (Cutter et al., 2003; Eriksen and Kelly, 2007; Wilson Chakraborty, 2019). The biophysical processes and population dynamics manifest on various geographic scales, temporal scales, and administrative levels, producing the modifiable area unit problem (MAUP) when mapping (Ho et al.., 2015). Fine-scale mapping of coupled biophysical and socioeconomic indices (e.g., composite Heat Vulnerability Index (HVI) is often disregarded, resulting in mixed pixel problems attributed to coarse-scale mapping (Aubrecht and Ozceylan, 2013; Mushore et al., 2018). Furthermore, there

are no guidelines for selecting, weighting, and interpreting indicators (Jonsonn and Lundgren, 2015). The existing data aggregation techniques deplete the authenticity of the information from independent suites of variables (Abson et al., 2012; Kashem et al., 2016). Spatially explicit information challenges are non-trivial, whereas such visualization is highly on demand (Preston et al., 2011).

This review provides disparate perspectives on the existing conceptualizations of urban heat vulnerability. It develops a holistic iterative framework that integrates validation and replication to bolster accuracy and precision in spatial representations. The framework is anchored on the longitudinal study approach that effectively captures urban heat events temporal dimension. The quantitative dimension acknowledges the ecological perturbations, the vulnerability co-productions, and residual risks emanating from the interactions of the biophysical exposure Index and the Socioeconomic Vulnerability Index (SoVI). Since heat vulnerability is variable across multiple scale dimensions, and the approaches, weighting mechanics, and determination of variables are inconsistent, our conceptual model provides a novel overview towards a consistent, dynamic, and systematic spatial representation.

## 2.2 Vulnerability in Perspective

### *2.2.1 Climate Change and Heat Vulnerability*

Each of the previous three decades has been consecutively warmer than any preceding decade since 1850 (IPCC, 2014). Surface temperatures are projected to rise in the 21$^{st}$ century across all emission scenarios, thereby amplifying risks and creating new threats that will be disproportionately distributed (Habeeb et al., 2015; IPCC, 2014; Weber et al., 2015; Xu et al., 2019). The current recorded temperatures are at least 1 degree Celsius above those of the pre-industrial period. The associated impacts will be intense and sooner, particularly in urban areas

where 70% of the world population is projected to live by 2050 (Birkmann et al., 2017; Ho et al., 2015; World Meteorological Organization (WMO), 2019). Climatic changes are happening faster than the human capacity to respond, and aggressive mitigation and adaptation responses are indispensable; hence the compelling demand for spatial representation of vulnerability (Bera, 2019; IPCC, 2018). However, the application of vulnerability studies outputs remains limited as they are guided by the interests of the users instead of policy gaps and consistent scientific methodologies (Turner II et al., 2003).

Increased morbidity and mortality have been associated with extreme hot weather in urban environments (Krstic et al., 2017; Reid et al., 2009; Reid et al., 2012). The World Health Organization (WHO) reports that the number of people exposed to heat stress increased by 125 million between 2000 and 2016. Each 4.7 $^{o}$C rise in apparent temperature corresponds to a 2.6% rise in cardiovascular mortality pegged on conservative estimates, while oppressive hot days increased mortality by 7.7% (Basu and Ostro, 2008; Maier et al., 2014). Extreme heat events are already the principal cause of summer weather-related fatalities in the USA, highlighting the imperative for research into heat risk assessment (Environmental Protection Agency (EPA), 2006; Morabito et al., 2014). In the USA, where 80% of the population is already urbanized, 620 residents die annually due to heat stress (Atyia, 2015; EPA, 2006). Data from the WHO indicates that heatwaves were responsible for more than 166,000 mortalities between 2000 and 2017. The 2003 heatwaves killed more than 15,000 people in France, 30,000 for the whole of Europe, while additional 70,000 deaths were recorded in the months following the summer, although the estimates were biased as health data was not specific (EPA, 2006; Laadi et al., 2012; Robine et al., 2008). According to Sheridan and Dolney (2004), these impacts are understated yet underpin the necessity for heat vulnerability studies. It is unclear whether vulnerability is a constituent of the

residual effects once adaptation and mitigation have set in or a pre-existing state or a cumulative hybrid of the two resulting in multiple definitions and conceptualizations that undermine its determination (Eriksen and Kelly, 2007).

### *2.2.2 The Vulnerability Imperative*

Unprecedented demand for spatially explicit visualization of vulnerability hotspots has accelerated the discourse on adaptation and mitigation to the (UHI) (Preston et al., 2011; Rizvi et al., 2019; Zhou et al., 2014). However, a universal conceptualization of vulnerability remains elusive, raveling the conception of formal models (Cutter et al., 2003; Fussel, 2007; Turner II et al., 2003; Zhou et al., 2014). For instance, Lee (2014) defined it as the probability of risk exposure, while Atyia (2015) referred to it as the state of a community preceding a disaster. Other studies (e.g., (Carr et al., 2014; Turner II et al., 2003) define vulnerability as a composite of the biophysical and socioeconomic indices characterized by a temporal dimension. Even with the rare chance of convergence in definitions, disparate assumptions could still mask the accurate and precise representation of hotspots (Fussel, 2007). Despite the growing number of studies on vulnerability (e.g., Abson et al., 2012; Atyia, 2015; Borden et al., 2007; Kelly and Adger, 2000; Stennett et al., 2019), the concept remains overdetermined yet equivocal; hence its application in decision making is limited (Tran et al., 2010). For instance, Fussel (2007) argued that vulnerability encompasses four dimensions, i.e., a system, attributes of concern, the hazard, and its temporal reference, subject to perturbations. Conversely, Brenkert and Malone (2005) equate it to exposure, sensitivity, and adaptive capacity. Therefore, vulnerability is predominantly interdisciplinary, and its precepts evolve over time (Cutter et al., 2003; Otto et al., 2017). Although methodological variations are necessary to expose its full complexity, novel comprehensive and comparative approaches are a pressing concern to mainstream vulnerability in policymaking.

## 2.3 Constructing Heat Vulnerability Indices

### *2.3.1 Exposure/Biophysical Index*

The characterization of biophysical vulnerability remains imprecise, and many studies attempt to justify the approach applied due to the absence of a formal methodology. For instance, Fussel (2007) argued that the exposure index must encompass topographical characteristics, land cover, and environmental parameters. Others (e.g., Maier et al., 2014; Morabito et al., 2014) have advocated for apparent temperature, a measure of the human thermal comfort, but differed on constitutive components. Morabito et al. (2014) incorporated the indoor and outdoor temperature differences, including the insulation provided by clothing. In contrast, Maier et al. (2014) only accounted for humidity and recorded temperatures above the $90^{th}$ and $95^{th}$ percentiles of local average conditions, whereas Weber et al. (2015) used the $85^{th}$ percentile. Heatwave definition varies depending on the length of consecutive days, the temperature metric (maximum, minimum, average), thresholds defined, and accounting for humidity (Shepherd and Zhou, 2009). Despite the acceleration in the number of heat studies, the conceptualization of the exposure index, upon which potential impacts are projected, remains unsettled within the scientific community. The construction of different thermal indicators generates different results across space and time, whose correlations are unknown.

Various studies (e.g., Chen et al., 2006; Chen et al., 2019; Guha et al., 2018; He et al., 2010; Li et al., 2013; Sun et al., 2017; Wang et al., 2019) have derived Land Surface Temperatures (LST) and Spectral Indices such as Normalized Difference Vegetation Index (NDVI), Normalized Difference Built-up Index (NDBI), Normalized Difference Bareness Index (NDBaL), Normalized Difference Water Index (NDWI) and Enhanced Normalized Difference Impervious Surface Index (ENDISI), from satellite images. The spectral indices overcome the mixed pixel problem (Mushore

et al., 2018). However, challenges persist even when using satellite images. LST is produced from different algorithms and using diverse satellite sensors. None has been validated to be optimal as getting sites for *in situ* measurements of LST representative of satellite pixel scale is difficult and limited to a few rare homogenous locations (Chen et al., 2019; Li et al., 2013). Inconsistencies are apparent when coupling LST and heat-related mortality Johnson et al., (2012), while the forcing of air pollutants (Depiettri et al., 2013; Heaton et al., (2014) is often ignored and the associated formation of ground ozone (Habeeb et al., 2015; Lo and Quattrochi, 2003). It is unclear whether the derived spectral indices and LST combine additively and whether they should be assigned equal weighting when coupled. It is underwhelming to validate an instantaneous index based on a snapshot of a scene taken with a satellite lag of 16 days that undermines the capturing of episodic heat waves (Wilson and Chakraborty, 2019). Also, cloudy conditions could impede the accurate capturing of heat events using remote sensing (Johnson et al., 2012).

### *2.3.2 Social Vulnerability Index (SoVI)*

The SoVI measures the adaptive capacity and sensitivity, although methodological shortcomings persist. Limited access to quality data and conceptual limitations derail consistent development of the metric (Cutter and Finch, 2008). The SoVI should capture the social and economic well-being and political, property rights, institutional context, and cultural norms (Clifford and Travis, 2018; Kelly and Adger, 2000). However, processes that define the SoVI are not sufficient, and it may be unwise to conclude that a given prescribed framework should befit the dominant discourse. The rational prediction of the biophysical parameters has limitations; hence answers to how and to what extent social systems are geared to respond are inevitable (Burton et al., 2002; Lee, 2014). Unfortunately, studies on SoVI rarely have one specific hazard, yet it should be the primary yardstick for the potential to prepare, respond and recover (Frigerio

and Amicis, 2016; Johnson et al., 2012). Statistical models that incorporate geodemographic dynamics are needed since population distribution and re-distribution have substantive ramifications on vulnerability whose extent is unknown (Ho et al., 2018; Krstic et al., 2017; Shepherd and Zhou, 2009). The parameterization of the SoVI is thus a fuzzy endeavor, and using different indicators generates different assessment outputs. Also, reliance on census datasets not ideally suited for vulnerability mapping raises queries on the relevance of the indices created (Preston et al., 2011).

Social vulnerability exists in many facets, but only certain specific factors or their proxies can substantially manifest or attenuate the impacts of disasters. For instance, Lee (2014) illustrated that a scientist has to decide on particular and general factors, objective and subjective indicators that pose divergent challenges when constructing the SoVI. These factors compound to generate negative ramifications before, during, and after occurrences of disasters. Existing literature only provides fragmented insights on the relative importance of the factors and fails to capture the co-productions of vulnerability. Arising from these challenges, our current understanding of social vulnerability is in infancy, as Cutter et al. (2003) concluded since their generated SoVI had no correlations with Presidential declarations on disasters. However, the validity test could be inappropriate since Presidential proclamations could have political motives and not purely scientific guidance. Therefore, not only is the construction of SoVI hazy, but parameters for its validation need to be carefully determined. The SoVI lacks an independent variable upon which it can be calibrated (Zhou et al., 2014). The utility value of the SoVI can not be understated; however, the scientific discourse should shift to how well-generated SoVI accurately portrays the intrinsic characteristics of the society.

The credibility of the SoVI is an emerging discourse given that social interactions are indeterminate and multivariate (e.g., Eriksen and Kelly, 2007; Heaton et al., 2014). The pursuit of credibility raises a number of questions. For instance, is it justifiable to correlate the SoVI with heat mortality data when its construction is not hazard specific? Although correlations may exist, how sure are we it is not a statistical chance occurrence attributed to weaknesses of cross-sectional studies? Additionally, data on morbidity and mortality are rarely available and geocoded (Heaton et al., 2014; Weber et al., 2015). While considering new and inclusive models, the pre-incident and post-incident variables differ (Atyia, 2015); therefore, the model must acknowledge these changes. Another perspective by Cutter et al. (2003) raises fundamental concerns on tests of validity. i.e., should validity tests be based on massive singular hazards or small chronic losses? The meanings of variables are consistently contested in respective research disciplines (Cutter and Finch, 2008). For instance, correlating the losses with SoVI presupposes that the most socially vulnerable have most to lose, which may not be the case. The credibility of the SoVI must be interrogated to investigate the relationship of actual damage to the statistically generated indices.

#### *2.3.2.1 Variables for SoVI and their Proxies*

Vulnerability assessment is a multivariable problem that has to capture all dimensions of a society, either directly using variables or through their appropriate proxies (Maier et al., 2014) (Table 2-1). The indicators are both qualitative and quantitative and elicit different interpretations when observed across space and time, with most studies focusing only on the quantifiable indicators (Frigerio and Amicis, 2016). There is also a risk of filtering out variables that can not be spatially represented, which could be crucial determinants of vulnerability (Eakin and Luers, 2006). Consequently, the variety of circumstances that impact vulnerability have not been explored consistently and systematically (Bera, 2019; Borden et al., 2007). There is no consensus on

selecting and interpreting variables likely because SoVI is not hazard-specific, whereas hazard-specific studies tend to apply the broad and general conceptualizations (Reid et al., 2009; Zhou et al., 2014). For instance, is wealth an enabler of quickly absorbing disaster impacts, or does it enhance loss potential?

The adequacy and representativeness of proxies have not been examined in vulnerability studies. Many of the proxies may not be representative and often overlap, failing the test of independence (Brenkert and Malone, 2005). If the actual variables fail the test of credibility, then the results based on proxies cannot be dependable. The lack of a sound methodology designates scientists to arbitrariness in determining proxies. For example, Basu and Ostro (2008) used educational attainment as a proxy for socioeconomic status. In contrast, Kashem et al. (2016) used the poverty rate, income, unemployment, and black race as surrogates for socioeconomic status. Evidently, proxies are at the researcher's discretion, which could undermine the constructed metrics validity. Also, not all factors and proxies are amenable to policy measures; thus, studies differ significantly in the identification of hotspots even after applying similar data reduction techniques such as the Principal Component Analysis (PCA) (Morabito et al., 2014; Eriksen and Kelly, 2007). It is unclear whether theoretical or statistical relationships should determine vulnerability indicators as both approaches have limitations. Besides, the meaning of vulnerability indicators varies with geographical scale (Lee, 2014).

Table 2-1. Examples of variables that have not been used in different studies to generate the Social Vulnerability Index

| **Variables of vulnerability (Percentage or number of)** | **Examples of studies that have utilized the variable** | **Description of the variable** |
|---|---|---|
| Population aged over 25 years without a high school diploma | (Wilson and Chakraborty, 2019; Macnee and Tokai, 2016; Ho et al., 2015; Reid et al., 2009; Zhou et al., 2014; Cutter and Finch, 2008; Sunhui, 2017; Kashem et al., 2016; Borden et al., 2007; Atyia, 2015; Krstic et al., 2017; Ho et al., 2018; Johnson et al., 2012; Lee, 2014; Reid et al., 2012; Maier et al., 2014) | Education |
| Female-headed households with no spouse present | (Wilson and Chakraborty, 2019; Kashem et al., 2016; Borden et al., 2007; Johnson et al., 2012) | Gender |
| Female population | (Reckien, 2018; Kashem et al., 2016; Lee, 2014) | |
| Population aged under 18 years | (Wilson and Chakraborty, 2019; Cutter and Finch, 2008; Sunhui, 2017; Stennet et al., 2019; Zhou et al., 2014) | Age |
| Population aged over 65 years* | (Wilson and Chakraborty, 2019; Reckien, 2018; Macnee and Tokai, 2016; Mushore et al., 2018; Ho et al., 2015; Nayak et al., 2018; Reid et al., 2009; Cutter et al., 2003; Zhou et al., 2014; Cutter and Finch, 2008; Sunhui, 2017; Kashem et al., 2016; Tran et al., 2010; Maier et al., 2014; Borden et al., 2007; Atyia, 2015; Stennett et al., 2019; Mitchell and Chakraborty, 2014; Krstic et al., 2017; Ho et al., 2018; Johnson et al., 2012; Lee, 2014; Reid et al., 2012; Zhou et al., 2014; Aubrecht and Ozceylan, 2013; Maier, et al., 2014) | |
| Population aged under 5 years* | (Mushore et al., 2018; Ho et al., 2015; Cutter et al., 2003; Kashem et al., 2016; Tran et al., 2010; Borden et al., 2007; Mitchell and Chakraborty, 2014; Krstic et al., 2017, Ho et al., 2018; Lee, 2014) | |
| Population of blacks/ African-American* | (Wilson and Chakraborty, 2019; Reckien, 2018; Nayak et al., 2018; Reid et al., 2009; Cutter et al., 2003; Kashem et al., 2016; Maier et al., 2014; Borden et al., 2007; Atyia, 2015; Mitchell and Chakraborty, 2014; Johnson et al., 2012; Reid et al., 2012; Maier, et al., 2014) | Race |

| | | |
|---|---|---|
| Population identifying as some other race | (Wilson and Chakraborty, 2019; Reid et al., 2009; Cutter et al., 2003; Maier et al., 2014; Borden et al., 2007; Atyia, 2015; Reid et al., 2012; Maier, et al., 2014) | |
| Population of Native Americans | (Wilson and Chakraborty, 2019; Reid et al., 2009; Cutter et al., 2003; Kashem et al., 2016; Maier et al., 2014; Borden et al., 2007; Atyia, 2015; Johnson et al., 2012; Reid et al., 2012; Maier, et al., 2014) | |
| Population of Hispanics* | (Wilson and Chakraborty, 2019; Reckien, 2018; Nayak et al., 2018; Reid et al., 2009; Cutter et al., 2003; Kashem et al., 2016; Maier et al., 2014; Borden et al., 2007; Atyia, 2015; Mitchell and Chakraborty, 2014; Johnson et al., 2012; Reid et al., 2012; Maier, et al., 2014) | |
| Population of Asians | (Wilson and Chakraborty, 2019; Reckien, 2018; Reid et al., 2009; Cutter et al., 2003; Kashem et al., 2016; Maier et al., 2014; Borden et al., 2007; Atyia, 2015; Mitchell and Chakraborty, 2014; Johnson et al., 2012; Reid et al., 2012; Maier, et al., 2014) | |
| Population of unemployed | (Macnee and Tokai 2016, Mushore et al., 2018, Ho et al., 2015; Nayak et al., 2018; Zhou et al., 2014; Sunhui, 2017; Kashem et al., 2016; Bera, 2019; Borden et al., 2007; Krstic et al., 2017; Ho et al., 2018; Lee, 2014) | Income |
| Population recipients of social security | (Cutter and Finch, 2008; Kashem et al., 2016; Borden et al., 2007) | |
| Mean household income | (Wilson and Chakraborty, 2019; Mushore et al., 2018; Ho et al., 2015; Cutter et al., 2003; Cutter and Finch, 2008; Sunhui, 2017; Kashem et al., 2016; Krstic et al., 2017; Johnson et al., 2012) | |
| Population below the poverty rate* | (Wilson and Chakraborty, 2019; Reckien, 2018; Nayak et al., 2018; Reid et al., 2009; Cutter and Finch, 2008; Sunhui, 2017; Kashem et al., 2016; Maier et al., 2014; Borden et al., 2007; Mitchell and Chakraborty, 2014; Ho et al., 2018; Lee, 2014; Reid et al., 2012; Aubrecht and Ozceylan, 2013; Abson et al., 2012; Maier, et al., 2014) | |
| Population living alone* | (Reckien, 2018: Macnee and Tokai, 2016; Ho et al., 2015; Nayak et al., 2018; Reid et al., 2009; Maier et al., 2014; Atyia, 2015; Ho et al., 2018; Johnson et al., 2012; Reid et al., 2012; Aubrecht and Ozceylan, 2013; Maier, et al., 2014) | Social Isolation |
| Population change | (Zhou et al., 2014; Cutter and Finch, 2008; Tran et al., 2010; Borden et al., 2007) | Population |
| Urban population | (Zhou et al., 2014; Borden et al., 2007) | |

| | | |
|---|---|---|
| Population using public transport | (Cutter et al., 2003; Kashem et al., 2016; Atyia, 2015) | Transportation |
| Mobile housing units | (Wilson and Chakraborty, 2019; Ho et al., 2015; Cutter et al., 2003; Kashem et al., 2016; Borden et al., 2007; Ho et al., 2018) | Housing |
| The average number of people per household | (Cutter et al., 2003; Kashem et al., 2016) | |
| Population that has disability 18-64 years | (Nayak et al., 2018; Sunhui, 2017; Atyia, 2015; Lee, 2014) | Disability |

*The most commonly used variable

### *2.3.3 Composite Heat Vulnerability Indicator (HVI)*

The composite HVI stems from the necessity for integrative approaches that expand on the computation of contingencies and probabilities associated with a hazard without leaving out its unintended consequences (Cutter, 2003). Areas with the highest exposure vulnerability would not always overlap with areas of most heightened socioeconomic vulnerability (Chow et al., 2012; Cutter and Finch, 2008). Several studies (e.g., Johnson et al., 2012; Zhou et al., 2014) have asserted that hazard is a component of risk and not risk itself given that socioeconomic indicators explained 70% of the variance while biophysical only accounted for 12% of the variance. On the other hand, Macnee and Tokai (2016) emphasized that biophysical exposure must be considered. Despite the progress on vulnerability studies, the relative weights of the biophysical and the socioeconomic paradigms have not been determined when coupling. Integrating the paradigms without a proper definition of relationships could generate arbitral conclusions related to their relative contribution to the combined HVI (Preston et al., 2011). Other studies (e.g., Bera, 2019; Chow et al., 2012; Kim et al., 2017; Wilson and Chakraborty, 2019) explain that a composite HVI should incorporate sensitivity, exposure, and adaptive capacity, although the adaptive capacity dimension is often ignored as it involves qualitative approaches.

## 2.4 The Quantitative Dimension

### *2.4.1 Variable Selection and Weighting*

Studies on heat vulnerability have failed to construct a standard set of variables for uniformity and comparative analysis. Any consensus among studies is driven by the resemblance in chosen measures rather than convergence of insights (Eriksen and Kelly, 2007). The variables selected should encompass sensitivity, adaptive capacity, and exposure (Kim et al., 2017; Wilson and Chakraborty, 2019). Lee (2014) identifies the SoVI as representing the internal state of a system, which is paramount compared to the nature of the threat. Reckien (2018) observed that variables of social vulnerability might differ depending on the stressor, hence giving prominence to physical vulnerability risk. Variable selection could also be altered by the availability of data (Lee, 2014). Therefore, the determination of appropriate indicators is a subjective process that should strike a balance between statistical relationships of variables and the theoretical understanding of relationships (Eriksen and Kelly, 2007).

The general trend in scientific approaches has been to assign equal weights to all indicators for lack of a theoretical underpinning (Abson et al., 2012; Brenkert and Malone, 2005; Kashem et al., 2016). The debate is only limited to the relative influence of variables, yet several studies (e.g., Cutter et al., 2003; Nayak et al., 2018; Reid et al., 2009; Reid et al., 2012; Zhou et al., 2014) have shown that there exists distinct geographical variability in vulnerability that is augmented in downtown areas. Therefore, studies have to explore the weighting of indicators pegged on geographic scale variability and distance from downtown locations. Another dimension of weighting that is least explored occurs when coupling the biophysical and the socioeconomic indices. It is unknown which one should be given prominence. For instance, Mushore et al. (2018) assigned an equal weighting of 25% to four final components that encompassed the NDVI, NDBI,

NDWI, and the SoVI. In this argument, the SoVI was essentially assigned 25%, while the biophysical accounted for 75% of the weighting. It is unknown whether the spectral indices have an additive effect or provide different dimensions of vulnerability. An increase in the number of biophysical indices resulted in a decrease in the proportional weighting of the SoVI without any substantive argument presented. When coupling the spectral indices, it is further assumed that they have equal weighting, which is not supported by any theoretical construct.

Another mechanism fronted by Ho et al. (2015) assigns an equal weighting to the SoVI and the biophysical layers (50% to 50%) regardless of the number of components that define the biophysical. In this approach, the SoVI is a composite of 8 layers, while LST represents the biophysical. Also, there is no theoretical underpinning to assume equal weighting of the biophysical and the SoVI components of vulnerability. Another weighting controversy emanates from the PCA. Several studies (e.g., Borden et al., 2007; Johnson et al., 2012; Nayak et al., 2018: Zhou et al., 2014) have subjected the biophysical and the socioeconomic variables jointly into the PCA. In some instances, the PCA variables are weighted based on the percentage variance they explain (Reckien, 2018). In common practice, equal weighting of final PCA components is favored. No study has evaluated the implications of these weighting mechanics on the final composite HVI developed.

### *2.4.2 Approaches in constructing the Composite HVI*

Challenges abound when constructing the coupled HVI, yet it is inadequately addressed in the literature (Macnee and Tokai, 2016). The socioeconomic and biophysical systems interact across administrative boundaries, while census data are based on administrative units creating a mismatch in spatial representations (Lee, 2014; Li et al., 2019). The use of census data weakens the correlation between population density and LST (Mushore et al., 2018). Census data are

household-based, yet most adults spend most of their daytime elsewhere (Ho et al., 2015). Besides, ecological perturbations may impact the capacity to respond through co-production of vulnerability that creates a challenge on the best way to represent the overlapping stressors. Consequently, relationships between the SoVI and the biophysical hazard need to be explored as vulnerability is a complex multi-dimensionality of causes, outcomes, and pathways (Carr et al., 2014; Cutter et al., 2003). The generated composite index can only have meaning when it measures and represents what was initially intended. For instance, Johnson et al. (2012) used land use and land cover classes to map only residential spaces since the SoVI is a derivative of census data. This is a unique approach that raises weighty concerns as humans are not confined to residential zones. In a different representation, Mitchell and Chakraborty (2014) excluded pixels representing water features and conducted regression analysis with LST as a dependent variable and census data as an independent variable.

The approaches adopted are context-specific and dependent on questions of interest, the audience, and the disciplinary composition of the research team; hence the challenge lies in uniting the disparate perspectives (Depiettri et al., 2013; Eakin and Luers, 2006). Although the diversity of approaches provide rich perspectives on the multi-dimensionality of vulnerability, the lack of a widely applicable theoretical framework could deter progress in the intellectual development of whole encompassing visual representations. For instance, Wilson and Chakraborty (2019) argue that planning interventions favor the built environment and not the socioeconomic conditions; therefore, they opt to solely incorporate sensitivity and adaptive capacity dimensions to align their recommendations with policy interventions. Excluding the exposure dimension could undermine the robustness of the conclusions and subjecting science to vulnerability as elucidated in (Cutter, 2003).

Visual representations are presented as area-based or population-based whose outputs are anchored on the construction methods and input data metrics (Abson et al.., 2012; Reckien, 2018). For additive methods, area-based metrics generated minor deviations and smoother spread than population-based, although vulnerability patterns were relatively the same. Conversely, using PCA in an inductive method, Reckien (2018) established that area based model explained 87% of the total variance while the population-based accounted for 64% of the total variance. According to Abson et al. (2012), variable reduction assumes that highly correlating indicators are interchangeable, hence the idea of using proxies. However, additive approaches should suffice when the influence of individual indicators is known to be high (Reckien, 2018). Generally, Reckien (2018) noted that area-based methods explained more variance and produced lower differences in different models; hence, the technique's infrequent use is unwarranted. However, such an approach of comparing metrics, models, and methods has not been widely replicated in different locations to validate the observation made by Reckien (2018). The techniques adopted in vulnerability studies appear to be guided by convenience and familiarity rather than efficacy (Preston et al., 2011).

The Hazard of Place Model (HPM) (Cutter et al., 2003) and the Vector and Raster Based Model (RVM) (Ho et al., 2015) are the primary conceptual models in vulnerability studies. The HPM holds that risk would always interact with mitigation measures resulting in a hazard potential, modulated by site, situation, proximity, and social fabric of a locality. The model assumes that the hazard is a social construct of demographic characteristics and residual impacts after adaptation and mitigation. However, the HPM fails to provide a weighting mechanism and means for overcoming the MAUP, zonal effects, and the mixed pixel problem. Furthermore, it is not hazard-specific and does not account for unmitigated risks. The decision criteria for spatial representation

perspectives are not specified as the qualitative non-measurable components of vulnerability are not incorporated. On the other hand, the RVM relies on remote sensing datasets and harmonizes the spatial resolutions of the biophysical and socioeconomic through resampling to overcome the MAUP. The RVM allows outputs of raster and vector models enabling for comparative analysis where the selection of variables is expert-based (additive approach); hence PCA is disregarded. It is not clear whether expert judgment studies generate significantly different results compared to systematic studies under PCA. However, both models fail to incorporate the qualitative non-measurable components of vulnerability and do not provide consistent weighting guidelines.

In this review, we modify the HPM (figure 2-2) and narrow it to the heat hazard, which provides a focused approach to the definition of vulnerability. The model acknowledges that a hazard potential is not only defined by interactions between heat risk and mitigation measures, but there exist unexpected perturbations and co-productions of vulnerability which the HPM failed to capture. Therefore, a hazard potential constitutes the residual risks after mitigation, and the unmitigated risks comprising maladaptations and unexpected systemic shocks. The model also provides for broad spatial representation decision considerations, including; area or population-based visualization, theoretical and statistical considerations, inductive and deductive approaches, and weighting mechanics. The conceptualization recognizes the need for hazard specificity, the potential for risk co-productions and unintended perturbations, and enlarging the decision criteria alternatives to allow for comprehensive comparative spatial representations. The decision criteria visualize and define the hazard dimensionality, whereas the hazard potential could influence decision considerations.

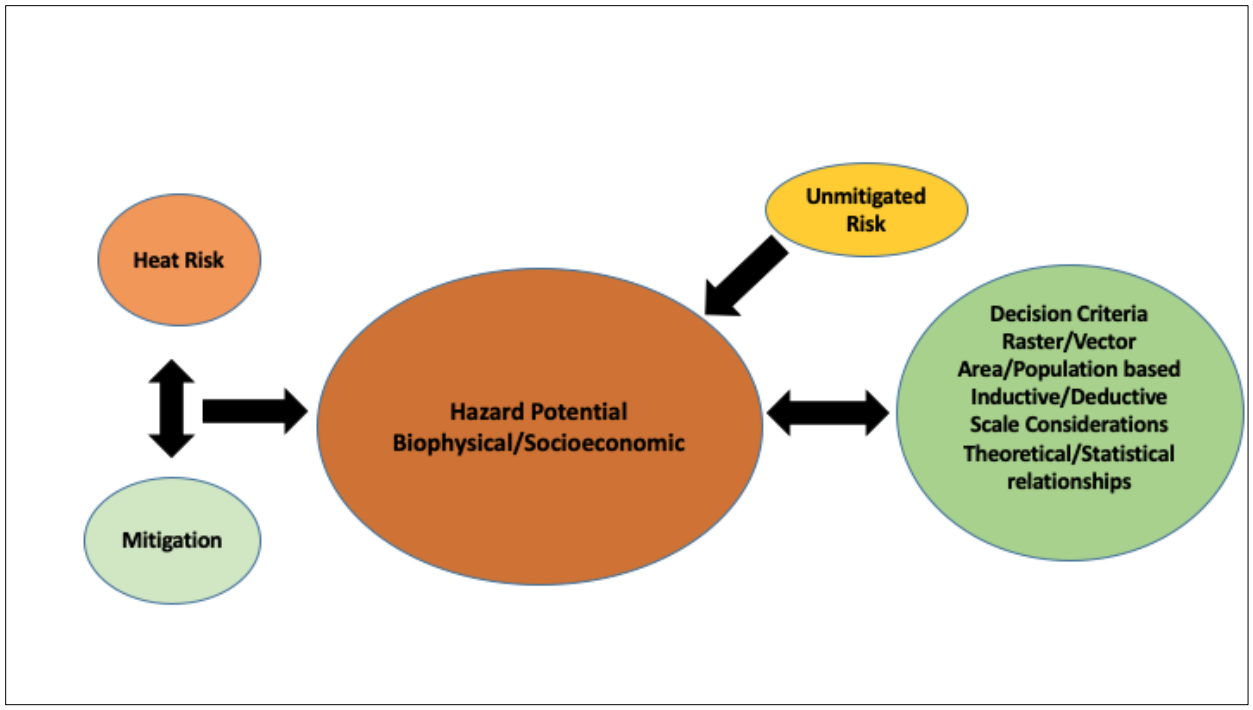


Figure 2-2. The heat hazard potential representation model. Hazard constitutes the biophysical and socioeconomic perspectives, including residual and unmitigated risks. The broad decision criteria offer a range of perspectives that could help generate comparative outcomes. (c.f., Cutter et al., 2003).

### *2.4.3 Principal Component Analysis*

Several studies (e.g., Abson et al., 2012: Tran and Formannn, 2009) have used the PCA as a data reduction technique that allows for a consistent set of indicators to be monitored over time. However, the use of PCA varies in the number of input indicators, variable rotation techniques, criteria for determination of final factor components, and correlational algorithms. Some studies (e.g., Johnson et al., 2012; Maier et al., 2014) have used the varimax rotation method, and the Kaiser criterion then normalized the components and classified them using standard deviations from the mean. Other studies (e.g., Tran and Formannn, 2009) used Parallel Analysis (PA) rather than the Kaiser criterion, which is influenced by sample size and the type of correlation coefficient used. The Kaiser eigenvalue rule has been criticized for not accounting for random fluctuations of correlations and only held true in large samples. Frigerio and Amicis (2016) combined three

selection methods; the Kaiser Criterion, The Broken Stick Model, and the PA. The Kaiser criterion and the PA both retained four components explaining 76% of the total variance, while the broken stick model retained three components explaining 67% of the variance. Therefore, it is not clear which model is sufficient. Also, the criteria for evaluation of the best model is non-existent despite the significant differences. For instance, should a model be assessed as superior based on the number of retained components or percentage variance explained, or should the robustness of the statistical algorithm suffice? Frigerio and Amicis (2016) opted to use the Kaiser criterion, and the PA guided by equivalence in their outputs.

Some studies (e.g., Abson et al., 2012; Johnson et al., 2012) eliminated variables deemed to exhibit a complex structure, which meant their direction of influence could not be ascertained. The excluded variables were total population, males under 5, females under 5, the poor over 65, and populations below the poverty level. However, these factors are significant in other studies. Therefore, we have a justification for doubting the complexity assigned to variables after the PCA. For example, Zhou et al. (2014) had a screening procedure before PCA by using Bartlett's test of sphericity and the Kaiser-Meyer-Olkin test, which determined the suitability of the variables for factor analysis. The effectiveness of the prior screening should be explored to determine its efficacy in eliminating variables with complex structures. Instead of removing variables without a clear direction of influence, some studies (e.g., Cutter et al., 2003; Zhou et al., 2014) assigned them absolute values. Others (e.g., Reckien 2018) opted to adjust for cardinality by multiplying all scores by -1 to transform all components to have unidirectional influence. Also, Nayak et al. (2018) had a series of criteria for determining final components, including; eigenvalue greater than 1, cross-checking elbows of scree plots, each component had to explain a minimum variance of 10%,

and the total variance explained had to be a minimum of 70%. However, neither the relative advantage of the different subjective criteria used nor their utility functionality have been assessed.

The number of input variables differs across studies. For instance, Macnee and Tokai (2016) started with eight variables and ended with three variables that explained 77% of the variance. A study by Reid et al. (2009) began with ten variables and ended with four that explained 75% of the total variance. Cutter et al. (2003) began with 211 variables and ended with 11 variables that accounted for 76% of the total variance. The focus should be on identifying a few substantive variables that explain a significant variation instead of many insignificant indicators and creating clutter in the PCA. A few studies (e.g., Abson et al., 2012; Reckien, 2018) have opined that the PCA merges components based on statistical relationships and not rational content-driven reasoning.

The PCA approach seems useful when the relative strength of vulnerability indicators, correlations, contributions, and roles is unknown (Reckien, 2018). It is challenging to accurately dissolve complex socioeconomic and environmental interactions to a single number (Brenkert and Malone, 2005). The authenticity by suites of individual variables and drivers could be depleted through data aggregation, yet their quantification in isolation may not provide a rich understanding (Abson et al., 2012). The PCA trades off dimensionality and communicability but fails to provide absolute measures of vulnerability for lack of a distinct defensible guidance framework (Hung et al., 2018; Kachigan, 1986). The PCA cannot be performed in datasets with missing values. For instance, Cutter et al. (2003) substituted missing values with the value zero. The implications of such a decision have not been investigated on the eventual vulnerability index. For example, why shouldn't the tracts with missing values be dropped or assigned mean values? Also, what is the criteria for the scientific community to accept a subjective justifiable technique? Although the

PCA has limitations, scientists find it useful since it is difficult for policymakers to strategize based on many discrete variables that could be overlapping and contradictory.

As a consequence of existing limitations, this review modifies the Ho et al. (2015) RVM (figure 2-3), accounting for both low spatial resolution of *in situ* data and coarse temporal resolution for remotely acquired datasets. A weighting mechanics of spectral indices and LST is considered as it is currently unknown whether they act additively while the independence of the indicators has not been explored. Furthermore, the PCA is not only a preserve of the socioeconomic dimension but accommodates arguments about subjecting the biophysical metrics alongside the socioeconomic to data aggregation. The modified model also provides for additive and reductive approaches while incorporating non-quantifiable variables and those incapable of being spatially visualized through the representation considerations. Pre-PCA screening ensures that input variables are suited for the PCA. The retained PCA components are subjected to different comparative statistical procedures, including the Kaiser criterion, the broken stick criteria, scree plot tests, and PA to bolster the robustness of the PCA. The model also acknowledges multiple representation approaches such as raster versus vector, area-based versus population-based, additive and reductive methods. The mixed pixel problem and the MAUP are diminished through resampling and the use of spectral indices. The SoVI is validated through both singular significant hazards and small chronic risks while aligning it with policy formulation and implementation. Ultimately, several composite HVI would be produced and compared for consistency.

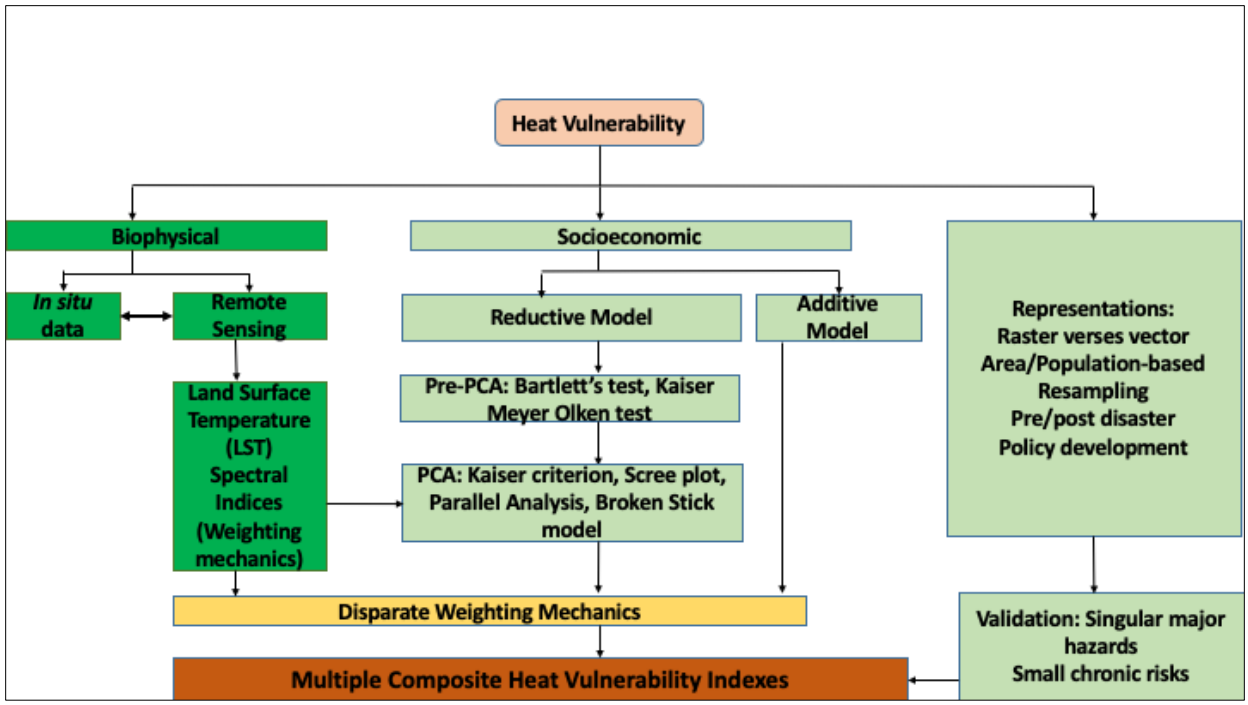


Figure 2-3. The primary components of the multi-dimensional model. In situ data complements remotely acquired datasets, and the PCA process is enhanced by incorporating pre-PCA tests and broadening the criteria for determining final components. Spatial representation considerations are provided for efficacy in outputs (c.f., Ho et al., 2015).

## 2.5 Missing Links

### *2.5.1 The Case for Qualitative Approach*

Vulnerability studies are ostensibly conducted to help decision-making among stakeholders, yet many fail to incorporate direct engagement (Preston et al., 2011). The robustness of spatial representations is evaluated in their capacity to disclose sociopolitical barriers in the decision-making discourse and understanding multiple facets of vulnerability. The SoVI is not exogenous to policy and planning implications; hence the primary causes of the shifts can best be captured by qualitative data (Kashem et al., 2016; Wilson and Chakraborty, 2019). Consequently, the impacts of the various thermal indicators are best illustrated through qualitative and quantitative approaches (Turner II et al., 2003). For instance, Jonsonn and Lundgren (2015)

identified that local contextualized knowledge that elucidated vulnerability drivers and their inter-relations is abundant within communities. However, this knowledge that could complement quantitative studies remains largely untapped by the research community, although it could have a significant influence on the policymaking agenda. Cultural impediments create maladaptations. The stakeholders must be involved in designing methodologies, determining visualization options, aggregation techniques, and mechanisms to communicate the results to align local needs, expectations, and perceptions with the research outcomes (Weber et al.., 2015). Although the calls for qualitative data in vulnerability studies are valid, they are fraught with challenges. It is not clear about the best strategy to capture and integrate data into quantitative vulnerability studies (Depiettri et al., 2013; Eakin and Luers, 2006). For example, our mental representations are limited as time passes, and the scientist has to determine appropriate points in time when recalling events is optimum (Wang et al., 2017).

### *2.5.2 Embracing the Longitudinal Approach*

Vulnerability studies ache for broader, universally acceptable, and comprehensive theoretical and conceptual understanding, yet few attempts have been made to fill the lacunae (Caruana et al., 2015). Majority of the frameworks available have failed to harmonize the divergent scientific perspectives and are anchored on static cross-sectional study designs. Ideally, theories are explicitly and implicitly longitudinal (Ployhart and Vandenberg, 2010). Uncertainty on how to proceed with longitudinal studies could impede stable theoretical and conceptual underpinnings of vulnerability. Scientists shy away with the mindset that there is no guarantee that dynamics in focal variables are inherent when the time dimension is incorporated. Consequently, Ployhart and Vandenberg (2010) opine that differences between individuals at a given time do not constitute a change. Instead, the focus should be guided by substantive dynamic constructs. The existing

theories may not be thoroughly tested unless having been an output of the longitudinal approach. Identifying processes that shape social susceptibility rather than merely aggregating the state of the social system is pertinent in determining representative indicators (Eriksen and Kelly, 2007).

Most vulnerability studies rely on census data, which are subject to consolidation, revisions, and splits. Boundary shifts present a likelihood of drawing invalid conclusions since interpolations are conducted on population and area weighting, which could have substantial variations (Logan et al.., 2014). Adopting the longitudinal approach further presents new challenges, as explained by Wang et al. (2017); for instance, should time be a substantive variable or a notion of temporal dynamics? Also, there is no clarity on how optimal time interval is determined and the number of repeated measures to improve the validity of the inferences that cross-sectional studies fail to achieve. The chosen time interval must sufficiently allow the effect to register and be congruent with the system's inherent change process. The variables in use may not match over time, and their definitions may change when using census data (Cutter and Finch, 2008), hence pushing scientists to opt for closely related variables rather than truly definitive variables. Although shortcomings persist, longitudinal studies provide details on the magnitude and direction of change and ostracize recall bias where data collection is prospective without prior knowledge of successive eventualities (Caruana et al., 2015).

### *2.5.3 Determination of Scale*

The associated effects of heat hazards are not spatially uniform, yet it is central in ascertaining the application and production of scientific knowledge integral for crucial decision making (Lee, 2014; Krstic et al., 2017). Urban heatwaves occur across large functional spatial and temporal extents, complicating response strategies (Kim et al., 2017; Preston et al., 2011). It is challenging to select geographic scales congruent with system dynamics and matching the

biophysical and socioeconomic scales to avoid the MAUP (Ho et al., 2015). Therefore, Johnson et al. (2012) proposed the development of models targeting specific locations that account for local variations. The appropriate scales must capture optimal points where socioeconomic and environmental interactions are most intense while ensuring compatibility with decision-making units (Borden et al., 2007; Eakin and Luers, 2006). It is imperative to doubt the utility of assessing vulnerability dictated by bound economic, population, and regional units to avoid the zoning effect in spatial visualization of hotspots. For instance, Ho et al. (2015) found that a spatial resolution of 500 meters or coarser fails to capture temperature differences between neighborhoods, yet census data are mostly over 1 kilometer.

The interactions between indicators, structures, and stresses of vulnerability manifest on different spatial scales that translate to various dominant vulnerability factors at different geographic levels (Cutter and Finch, 2008; Eriksen and Kelly, 2007). Although this weakness exists, there lacks a formal and consistent methodology for the discernment of ideal spatial units (Bera, 2019). The theoretical conceptualization of processes that ultimately shape vulnerability is not deftly developed as it materializes intermittently (Eriksen and Kelly, 2007). The hazards act within and beyond the unit of analysis, yet the differences are only partially understood (Aubrecht and Ozceylan, 2013; Turner II et al., 2003). Most research work is confined to urban administrative units. Maier et al. (2014) determined that half of the vulnerable counties in Georgia were in rural areas, while some studies even fail to differentiate whether they are urban or rural-focused (Lee, 2014). Although the calls for specific local spatial scales are justified, it is at the national level where adaptation policies and international dialogues occur, hence an emerging debate on whether a top-down or bottom-up scale approaches for vulnerability studies (Preston et al., 2011). To date, debates persist whether vulnerability studies should correspond to the scale of governance and

administration, or correspond to operating processes of the biophysical hazard, or optimal points where socioeconomic and environmental interactions are intense.

### *2.5.4 The Space-Time Dimension*

Heat vulnerability has an exceptionally high degree of spatial and temporal heterogeneity (Abson et al., 2012; Arnds et al., 2017). The dynamism could generate new unintended hazards; hence time should be considered as a substantive variable in longitudinal studies. To unravel the complexity and multi-dimensionality of vulnerability, the spatio-temporal patterns are essential, especially in the coupled HVI (Aubrecht and Ozceylan, 2013; Carr et al., 2014). The space-time analysis helps project future trends, understand shifts in population and their drivers, and how human and environmental conditions attenuate or amplify the changes (Turner II et al., 2003; Wilson and Chakraborty, 2019). However, the use of remote sensing could be limited since it is difficult to select images having similar atmospheric conditions for enhanced comparative analysis over a time lag. A snapshot analysis at a particular instance fails to accommodate the richness of the shifts. Besides, revealing how levels of vulnerability occur over time has more utility functionality than simply illustrating why a particular pattern exists (Eriksen and Kelly, 2007). Therefore, vulnerability assessment needs to be a continuous event that is dynamic and adaptive (Jonsonn and Lundgren, 2015). The population distribution and re-distributions could create new vulnerabilities hence the need to develop standardized datasets that harmonize consolidated or adjusted census tracts across time (Logan et al., 2014: Wilson and Chakraborty, 2019).

### *2.5.5 Shortcomings of the Existing Framework*

The existing framework for characterizing sensitivity, exposure, and adaptive capacity has numerous weaknesses and is highly fragmented. The approaches adopted are not systematic and consistent, primarily guided by convenience and familiarity rather than efficacy. The framework

fails to accommodate qualitative aspects that ensure linkages to policy formulation and incorporation of crucial aspatial variables to minimize overreliance on census datasets. Guidelines for selecting, interpreting, and weighting indicators are absent. The geodemographic dynamics are often ignored, while the theoretical and statistical relationships are not harmonized. Most studies fail to utilize the longitudinal approach, yet the theories are explicitly and implicitly longitudinal, thus failing to explain processes driving vulnerability. The frameworks are not hazard-specific, and correlations of the different metrics are unknown. The validity tests are often not incorporated in the methodology. When validity tests are conducted, they do not distinguish the small chronic events and large singular hazards.

Additionally, shifts in census boundaries remain a challenge when representing vulnerability and tracking its evolution over time. Geographic Information Science challenges related to MAUP, zonal adjustments, and mixed pixel problems are thus inevitable. Scales mismatches at geographic scales, temporal resolution, and administrative levels compromise integration of the biophysical exposure and SoVI metrics. Biophysical characterization is imprecise with the application of different metrics ranging from apparent temperature, surface and near-surface metrics, accounting for humidity, Land Surface temperatures and spectral indices. The existing models also fail to account for pre and post-incident variables. The meanings of indicators vary geographically and across time, and the over-reliance on census datasets, which are not explicitly meant for vulnerability studies, raises doubts about generated indices. More so, no study has evaluated the implications of weighting mechanics on the final derived indices. There is also over-reliance on the PCA as a data reduction technique, which has limitations in determining final components, variable rotational methods, pre-PCA screening, and fails to establish theoretical relationships within variables. The current focus seems to be on aggregating

summative indices instead of identifying processes that shape vulnerability. It is vital to reveal how levels of vulnerability occur over time than merely illustrating how a particular pattern exists. The assortment of weaknesses is non-trivial and calls for new conceptual frameworks to remedy the existing challenges in spatial representation, allowing for comparative analysis of multiple composite indices towards a consistent and systematic spatial model of heat vulnerability. The inclusive framework is thus proposed.

## 2.6 Synthesis: The Inclusive Framework

We are proposing a framework (Figure 2-1) that is anchored on the longitudinal approach, which embraces the dynamism inherent in the systems, cognizant that theoretical and statistical relationships are comprehensively captured using an iterative framework. The quantitative dimension comprises of three components; the biophysical, the SoVI, and geodemographic dynamics, all interacting continuously as a system. The interactions generate unintended and random second-order risks in the form of co-productions, residual risks that occur after adaptation and mitigation have taken effect, and stochastic ecological perturbations. The biophysical index is an output of both *in situ* data and remote sensing techniques, providing a self-validation system on the accuracy of derived metrics.

The geodemographic dynamics represent population distribution and re-distribution, revealing inherent population change patterns, regardless of the socioeconomic characteristics of the populace. The geodemographic dynamics in isolation could result in shifts in vulnerability, thus constituting a substantive suite of variables. Several studies (e.g., Ho et al., 2018; Krstic et al.,2017; Shepherd and Zhou, 2009) acknowledged that the effects of geodemographic dynamics are unknown, yet could have a significant influence on the vulnerability index, thus the necessity for inclusive conceptualizations. The consolidation, revisions, and splits of tracts have a bearing

on the geodemographic dynamics (Wilson and Chakraborty, 2019). Cognizant of the geodemographics, Johnson et al. (2012) used dasymetric mapping only to visualize residential spaces. Therefore, geodemographic factors explain population changes, migration patterns, and census tract changes, occurring continuously, that supplement information derived from socioeconomic variables describing sensitivity and adaptive capacity. However, not all variables can be spatially represented and quantified, thus the imperative for the qualitative approach.

The qualitative dimension comprises four essential components; different approaches, weighting mechanics, scale considerations, selection of variables, and their proxies pre-incident and post-incident. The qualitative dimension mainstreams aggregated indices to policymaking and ensures that the theoretical and statistical perspectives are harmonized. The non-quantifiable attributes such as social capital, political economy, behavioral responses, perceptions of risk, and meaning of indicators are all considered. Qualitative variables bridge the gap between heat hazard and spatial policy planning, pinpointing processes that shape vulnerability, instead of merely aggregating the state of a complex system of interactions (Ericksen and Kelly, 2007). Derived quantitative metrics may not capture institutional context, cultural norms, and property rights, factors that impact communities' vulnerability (Clifford and Travis, 2018; Kelly and Adger, 2000). Integrating the quantitative paradigms of the biophysical and socioeconomic without a comprehensive definition of relationships may lead to arbitral conclusions. For instance, correlating the losses of the SoVI assumes that the most socially vulnerable have most to lose, which may not be the case (Cutter and Finch, 2008).

Communities' susceptibility is an intricate multi-dimensionality of causes, outcomes, and pathways which may not be effectively captured by a single quantitative index. The use of census datasets also limits quantitative studies to the data collected during the census process, which may

not be exhaustive in explaining vulnerability. High biophysical vulnerability locations may not always overlap with areas of high socioeconomic vulnerability; hence, caution is needed when taking the coupled systems approach. Therefore, the qualitative dimension provides context, qualifies the quantitative metrics, ensures stakeholder engagement, enables targeted mitigation measures, clarifies assumptions, and provides supplementary data not captured in census datasets, bridging the gap between statistical and theoretical interpretations. The qualitative dimension is a substantive methodological framework broadly characterizing the adaptative capacity often not deftly captured in socioeconomic variables, thus providing a crucial data collection tool. The selection of ideal indicators should be guided by specific criteria including; hazard specificity, pre-PCA screening, eigenvalue should be more than the value 1, amenable to policy measures, validated by scientific precedence, encompassing sensitivity, adaptive capacity, and exposure. The selection process must go beyond census datasets incorporating spatial and aspatial variables emanating from the qualitative approach.

The conceptual model proposes the use of expert judgment, percentage variance explained, equal weighting when coupling, and geographical weighting with distance from downtown areas as probable weighting mechanics. Several studies (e.g., Brenkert and Malone, 2005; Eriksen and Kelly, 2007; Johnson et al., 2012; Zhou et al., 2014) used different weighting mechanics that significantly affect the derived coupled indices. All the proposed weighting mechanics have logical theoretical justifications, although they vary in spatial characterization. Transitioning to effective, consistent, and accurate spatial representation will require deriving multiple composite indices using different mechanics and subjecting to spatial regressional analysis using geocoded heat-health outcomes. Continuous comparative analysis of the derived indices will provide the best variable weighting mechanics, accurately capturing spatial vulnerability patterns when validated

by heat-health outcomes. The validation approach will provide an empirical and objective conceptualization that should inform subsequent heat vulnerability studies.

The various approaches could be pursued, and outcomes compared and validated towards establishing reliable methodologies. The appropriate geographical scale must capture geographic variability in the dominant variables with changing distance, allowing weighting to pegged on distance. The temporal study scale has to accommodate scales of optimum interactions within coupled systems. The administrative units, reflecting decision-making levels, have to be streamlined with hazard occurrence levels, enabling the selection of indicators amenable to policy strategies.

The ultimate output, a composite HVI, represents a dynamic relative metric that may provide insights into transitioning to absolute measures when subjected to continuous objective validation and replication procedures. Therefore, replications that return similar output over time may form substantive discourse in providing a consistent, holistic, comprehensive, accurate, and precise conceptual framework. The model enriches spatial representations encompassing stochastic incidences and non-linear components, acknowledging that theories are explicitly and implicitly longitudinal, ensuring the use of truly definitive variables to quantify indices. Validation of the derived metrics should be subjected to small chronic hazards and singular significant hazards to guard against weak validation criteria. The composite indices would be the predictor variables in the validation, while geocoded mortality data would be the response variable. Multiple linear regression analysis between composite indices and heat-related mortality could be conducted to test the derived composite indices' effectiveness in predicting heat-health outcomes associated with small chronic hazards. For large singular events, the composite indices could be correlated with the frequency of county or state heat disaster declarations.

Replication is meant to check consistency in the approaches proposed. For instance, proposed techniques include inductive and deductive methods, vector and raster-based, area-based, and population-based, while applying equivalent weighting mechanics. It is expected that replicating similar approaches should generate similar distributions and classifications of vulnerability. Deriving multiple composite indices, and subjecting each to validity tests using heat mortality data, should provide comparative hints on the best approach that best fits with heat mortality outcomes. Therefore, a set of given visualization choices should have similarities in the determination of spatial patterns of vulnerability regardless of locality, providing a robust and consistent pathway for subsequent heat studies. When replicated and subjected to validation tests, comparative spatial visualization choices should determine the optimum methodological framework, identifying the optimal representation of heat vulnerability.

Climatic changes are happening faster than our capacity to respond hence the urgency to harmonize divergent scientific perspectives on heat vulnerability. The policy response strategies are not exogenous to derived composite indices; thus, local needs, perceptions, and cultural attributes have to be integrated into statistically derived indices. The model acknowledges the necessity for accuracy and precision in representing intrinsic characteristics of the society and environmental systems for a robust scientific reference point. The scale mismatches often generate the MAUP and zonal effects in spatial representation; the model provides for raster representation that allows for resampling of datasets to standard spatial scales. The mixed pixel problem is overcome by the generation of spectral indices that quantify each pixel providing a reliable numeric output. The different weighting mechanics guided by expert judgment, percentage variance explained by a variable, and geographical variability of influencing indicators have to be explored while reflecting community stakeholders' input. Therefore, the model summarizes

disparate spatial representation perspectives and applies a systematic synthesis to visualize optimum points of convergence, and enriches aspects of divergence in ideas, creating a harmonious blueprint for comparative scientific outcomes for heat specific hazard.

The conceptual framework provides a significant shift in vulnerability assessment. Although it proposes novel perspectives on heat vulnerability representation, the framework has not been subjected to actual tests using datasets. Our subsequent work would explore the various approaches suggested. Also, satellite and weather station datasets have temporal and spatial scale challenges, respectively, meaning biophysical vulnerability is impaired. The conceptual framework has not explored the possibility of data fusion techniques that could provide multi-temporal, spectral, and spatial resolution sources. The conceptual framework relies on the census data temporal scale, which may not be optimum data for detecting vulnerability changes.

## 2.7 Conclusion

Urban heat stress will increase in magnitude, frequency, intensity, and duration hence the need to accurately and precisely visualize the most susceptible for a targeted policy response. We have provided an iterative holistic conceptual framework that integrates quantitative and qualitative approaches. The UHI phenomenon being multi-dimensional should not be a deterrent to effective spatial representation. Our model acknowledges that the interactions between the biophysical, geodemographics and socioeconomic dimensions generate stochastic ecological perturbations, residual risks, and hazard co-productions, often not accounted for in the existing frameworks. These interactions are iterative and need a longitudinal approach that recognizes that scientific theories are explicitly and implicitly longitudinal.

Targeted policy responses are enhanced when specific, accurate, and precise spatial representations are availed. The imperfections observed in the available frameworks are multiple.

There is a need to harmonize the different approaches, scale choices, weighting mechanics, and manipulation of variables through longitudinal methods that acknowledge spatiotemporal reference. Alternatives pursued by scientists must meet certain thresholds and be subjected to replication and validation while incorporating the qualitative dimension. This review has provided a starting point for scientific discourse towards a consistent iterative spatial representation framework. The theoretical and statistical relationships are enhanced, and the definition of vulnerability is made hazard-specific. We have provided flexible decision criteria that transition from simple data aggregation to understanding processes that shape vulnerability. The model allows for pre and post-hazard variables determination and avails rational content-driven reasoning in developing the composite HVI. It accommodates closely related variables, identifies definitive indicators for vulnerability, and provides a platform for replicating and validating robust, consistent, and systematic conceptualization for spatial representations.

## 2.8 Statement of Authorship

The student, Joseph Karanja, is the lead author for this publication, under the guidance of Dr. Lawrence Kiage.

**References**

Abson, D. J., Dougill, A. J., & Stringer, L. C. (2012). Using Principal Component Analysis for Information-Rich Socio-Ecological Vulnerability Mapping in Southern Africa. *Applied Geography*, 35, 515-524. http://dx.doi.org/10.1016/j.apgeog.2012.08.004

Arnds, D., Bohner, J., & Bechtel, B. (2017). Spatio-Temporal Variance and Meteorological Drivers of the Urban Heat Island in a European City. *Theoretical and Applied Climatology,* 128, 43-61. doi:10.1007s/00704-015-1687-4

Atyia, M. S. (2015). A Framework to Understand the Relationship between Social Factors that Reduce Resilience in Cities: Application to the City of Boston. *International Journal of Disaster Risk Reduction*, 12, 53-80. doi:10.1016/j.ijdrr.2014.12.001

Aubrecht, C., & Ozceylan, D. (2013). Identification of Heat Risk Patterns in the US National Capital Region by Integrating Heat Stress and Related Vulnerability. *Environment Internationa*l, 56, 65-77. http://dx.doi.org/10.1016/j.envint.2013.03.005

Basu, R., & Ostro, B. D. (2008, July 28). A Multi-County Analysis Identifying the Populations Vulnerable to Mortality Associated with High Ambient Temperatures in California. *American Journal of Epidemiology*, 168(6), 632-637. doi:10.1093/aje/kwn170

Bera, K. K. (2019, July). Vulnerability of Rural Areas to Climate Change- Analysis of Similar Units in Terms of Spatial Conditions for Warminsko-Mazurmskie Voivodeship. *Journal of Ecological Engineering*, 20(6), 198-206. https://doi.org/10.12911/22998993/109454

Birkmann, J., Wenzel, F., Grieving, S., Garschagen, M., Vallee, D., Nowak, W., . . . Mitchell, K. J. (2017, March 16). Extreme Events, Critical Infrastructures, Human Vulnerability, and Strategic Planning: Emerging Research Issues. *Journal of Extreme Events*, 3(4). doi:10.1142/s2345737616500172

Borden, K. A., Schmidtlein, M. C., Emrich, C. T., Piergosch, W. W., & Cutter, S. L. (2007). Vulnerability of US Cities to Environmental Hazards. *Journal of Homeland Security and Emergency Management*, 4(2). doi:10.2202/1547-7355.1279

Brenkert, A. L., & Malone, E. L. (2005). Modeling Vulnerability and Resilience to Climate Change: A Case Study of India and Indian States. *Climatic Change*, 72, 57-102. doi:10.1007/s10584-005-5930-3

Burton, I., Huq, S., Lim, B., Pilifosova, O., & Schipper, E. L. (2002). From Impacts Assessment to Adaptation Priorities. *Climate Policy*, 2, 145-159.

Carr, D. L., Pricope, N. G., Aukema, J. E., Jankowska, M. M., Funk, C., Husak, G., & Michaelsen, J. (2014, March 6th). A Spatial Analysis of Population Dynamics and Climate Change in Africa: Potential Vulnerability Hotspots Emerge where Precipitation declines and Demographic Pressures Coincide. *Population and Environment*, 35, 323-339. doi:10.1007/s11111-014-0209-0

Caruana, E. J., Marius, R., Sanchez, J. H., & Solli, P. (2015, October 9). Longitudinal Studies. *Thoracic Disease*, 7(11), 537-545. doi: 10.3978/j.issn.2072-1439.2015.10.63

Chen, J., Yang, K., Chen, S., Yang, C., Zhang, S., & He, L. (2019, January 11). Enhanced Normalized Difference Index for Impervious Surface Area Estimation at the Plateau Basin Scale. *Applied Remote Sensing*, 13(1). doi:10.1117/1.JRS.13.016502

Chen, X. L., Zhao, H. M., Li, P. X., & Yin, Z. Y. (2006). Remote Sensing Image-Based Analysis of the Relationship between Urban Heat Island and Land Use/Cover Changes. *Remote Sensing of Environment*, 104, 133-146.

Chow, W. T., Chuang, W. C., & Gober, P. (2012). Vulnerability to Extreme Heat in Metropolitan Phoenix: Spatio, Temporal, and Demographic Dimensions. *The Professional Geographer*, 64(2), 286-302.

Clifford, K. R., & Travis, W. R. (2018). Knowing Climate as a Social-Ecological-Atmospheric construct. *Global Environmental Change*, 49, 1-9. Retrieved from https://doi.org/10.1016/j.gloenvcha.2017.12.007

Cutter, S. L. (2003). The Vulnerability of Science and Science of Vulnerability. *Annals of the Association of American Geographers*, 93(1), 1-12. doi:10.1111/1467-8306.93101

Cutter, S. L., & Finch, C. (2008, February 19). Temporal and Spatial Changes in Social Vulnerability to Natural Hazards. (B. L. Turner II, Ed.) *Proceedings of the National Academy of Science of the United States of America (PNAS)*, 105(7), 2301-2306.

Cutter, S. L., Boruff, B. J., & Shirley, W. L. (2003, June). Social Vulnerability to Environmental Hazards. *Social Science Quarterly*, 84(2).

Depiettri, Y., Welle, T., & Renaud, F. G. (2013, October 9). Social Vulnerability Assessment of the Cologne Urban Area (Germany) to Heat Waves: Links to Ecosystem Services. *International Journal of Disaster Risk Reduction*, 6, 98-117. doi:10.1016/j.ijdrr.2013.10.001

Eakin, H., & Luers, A. L. (2006, July 18). *Annual Review of Environment and Resources*, 31, 365-394. doi:10.1146/annurev.energy.30.050504.144352

EPA (Environmental Protection Agency) (2006). *Excessive Heat Events Guidebook* (1-60 ed.). Washington, D.C., Pennsylvania Avenue NW: United States Environmental Protection Agency.

Eriksen, S. H., & Kelly, P. M. (2007). Developing Credible Vulnerability Indicators for Climate Adaptation Policy Assessment. *Mitigation and Adaptation Strategies for Global Climate Change*, 12, 495-524. doi:10.1007/s11027-006-3460-6

Formetta, G., & Feyen, L. (2019). Empirical Evidence of Declining Global Vulnerability to Climate-Related Hazards. *Global Environmental Change*, 57. https://doi.org/10.1016/j.gloenvcha.2019.05.004

Frigerio, I., & Amicis, M. D. (2016, June 14). Mapping Social Vulnerability to Natural Hazards in Italy: A Suitable Tool for Risk Mitigation Strategies. *Environmental Science and Policy*, 63, 187-196. Retrieved from http://dx.doi.org/10.1016/j.envsci.2016.06.001

Fussel, H. M. (2007). Vulnerability: A Generally Applicable Conceptual Framework for Climate Change Research. *Global Environmental Change*, 17, 155-167. doi:doi:10.1016/j.gloenvcha.2006.05.002

Guha, S., Govil, H., Dey, A., & Gill, N. (2018). Analytical Study of Land Surface Temperature with NDVI and NDBI using Landsat 8 OLI and TIRS Data in Florence and Naples City, Italy. *European Journal of Remote Sensing*, 51(1), 667-678. doi:10.1080/22797254.2018.1474494

Habeeb, D., Vargo, J., & Stone, B. J. (2015, January 1st). Rising Heat Wave Trends in Large US Cities. *Natural Hazards*, 76, 1651-1665. doi:10.1007/s11069-014-1563-z

He, C., Shi, P., Xie, D., & Zhao, Y. (2010). Improving the Normalized Difference Built-up Index to Map Urban Built-up Areas using a Semiautomatic Segmentation Approach. *Remote Sensing Letters*, 1(4), 213-221.

Heaton, M. J., Sain, S. R., Greasby, T. A., Uejio, C. K., Hayden, M. H., Monaghan, A. J., . . . Wilhelmi, O. V. (2014, January 24). Characterizing Urban Vulnerability to Heat Stress

using a Spatially Varying Co-efficient Model. *Spatio and Spatio-Temporal Epidemiology*, 8, 23-33.

Hersperger, A. M., Oliveira, E., Pagliarin, S., Palka, G., Verburg, P., Bolliger, J., & Gradinaru, S. (2018). Urban Land-Use Change: The Role of Strategic Spatial Planning. *Global Environmental Change*, 51, 32-42. https://doi.org/10.1016/j.gloenvcha.2018.05.001

Ho, H. C., Knudby, A., & Huang, W. (2015, December 18). A Spatial Framework to Map Heat Health Risks at Multiple Scales. *International Journal of Environmental Research and Public Health*, 12, 16110-16123. doi:10.3390/ijerph121215046

Ho, H. C., Knudby, A., Chi, G., Aminipouri, M., & Lai, D. Y.-F. (2018). Spatial-Temporal Analysis of Regional Socio-Economic Vulnerability Change Associated with Heat Risks in Canada. *Applied Geography*, 95, 61-70.

Hung, C. H., Knudby, A., Guanqing, C., Aminipouri, M., & Lai, D. Y. (2018). Spatio-Temporal Analysis of Regional Socio-Economic Vulnerability Change Associated with Heat Risks in Canada. *Applied Geography*, 95, 61-70.

IPCC. (2014). *Climate Change 2014: Synthesis Report: Contributions of Working Group I, II, III to the Fifth Assessment Report of the IPCC*. Intergovernmental Panel on Climate Change. Geneva, Switzerland: IPCC.

IPCC. (2018). *An IPCC Special Report on the Impacts of Global Warming of 1.5ºC above Pre-Industrial Levels and Related Global Greenhouse Gas Emission Pathways, in the Context of Strengthening the Global Response to the Threat of Climate Change, Sustainable Development.* IPCC.

Johnson, P. D., Stanforth, A., Lulla, V., & Luber, G. (2012). Developing an Applied Extreme Heat Vulnerability Index Utilizing Socio-Economic and Environmental Data. *Applied Geography*, 35, 23-31. doi:10.1016/j.apgeog.2012.04.006

Jonsonn, A. C., & Lundgren, L. (2015). Vulnerability and Adaptation to Heat in Cities: Perspectives and Perceptions of Local Adaptation Decision Makers in Sweden. *Local Environment*, 20(4), 442-458. http://dx.doi.org/10.1080/13549839.2014.896326

Kachigan, S. K. (1986). *Multivariate Statistical Analysis: A Conceptual Introduction* (Vol. Second Edition). New York: Radius Press.

Kashem, S. B., Wilson, B., & Zandt, S. V. (2016, January). Planning for Climate Adaptation: Evaluating the Changing Patterns of Social Vulnerability and Adaptation Challenges in Three Coastal Cities. *Journal of Planning Education and Research*, 36(3), 304-318. doi:10.1177/0739456X16645167

Kelly, P. M., & Adger, W. (2000). Theory and Practice in Assessing Vulnerability to Climate Change and Facilitating Adaptation. *Climatic Change*, 47, 325-352.

Kim, D. W., Deo, R. C., Lee, J. S., & Yeom, J. M. (2017, June 5th). Mapping Heat Wave Vulnerability in Korea. *Journal on Natural Hazards*, 89, 35-55. doi:10.1007/s11069-017-2951-y

Krstic, N., Yuchi, W., Ho, H. C., Walker, B. B., Knudby, A. J., & Henderson, S. B. (2017, September 18). The Heat Exposure Integrated Deprivation Index (HEIDI): A Data Driven Approach to Quantifying Neighborhood Heat during Extreme Hot Weather. *Environment International*, 109, 42-52. https://dx.doi.org/10/1016/j.envint.2017.09.011

Laaidi, K., Zeghnoun, A., Dousset, B., Bretin, P., Vandentorren, S., Giraudet, E., & Beaudeau, P. (2012, February). The Impacts of Heat Islands on Mortality in Paris during the August

2003 Heatwave. *Environmental Health Perspectives*, 120(2), 254-259. http://dx.doi.org/10.1289/ehp.1103532

Lee, Y. J. (2014). Social Vulnerability Indicators as a Sustainable Planning Tool. *Environmental Impact Assessment Review*, 44, 31-42. http://dx.doi.org/10.1016/j.eiar.2013.08.002

Li, Y., Wang, L., Liu, M., Zhao, G., He, T., & Mao, Q. (2019, July 21st). Associated Determinants of Surface Urban Heat Islands across 1449 Cities in China. (S. Bonafoni, Ed.) *Advances in Meteorology*, 1-14. https://doi.org/10.1155/2019/4892714

Li, Z. L., Tang, H. B., Wu, H., Ren, H., Yan, G., Wan, Z., . . . Sobrino, J. A. (2013). Satellite-derived Land Surface Temperature: Current Status and Perspectives. *Remote Sensing of Environment*, 131, 14-37. http://dx.doi.org/10.1016/j.rse.2012.12.008

Lo, C. P., & Quattrochi, A. (2003, September). Land Use and Land Cover Change, Urban Heat Island Phenomenon, and Health Implications: A Remote Sensing Approach. *Photogrammetric Engineering and Remote Sensing*, 69(9), 1053-1063.

Logan, J. R., Zengwang, X., & Stults, B. J. (2014, May 13). Interpolating US Decennial Census Tract Data from as Early as 1970 to 2010: A Longitudinal Tract Database. *The Professional Geographer*, 66(3), 412-420.

Macnee, R. G., & Tokai, A. (2016, August). Heat Wave Vulnerability and Exposure Mapping for Osaka Japan. *Journal on Environmental Systems and Decisions*, 36, 368-376. doi:10.1007/s10669-016-9607-4

Maier, G., Grundstein, A., Jang, W., Li, C., Naeher, L. P., & Shepherd, M. (2014, April). Assessing the Performance of a Vulnerability Index During Oppressive Heat Across Georgia, United States. 6, 253-263. doi:10.1175/WCAS-D-13-00037.1

Masuda, Y. J., Castro, B., Aggraeni, I., Wolff, N. H., Ebi, K., Garg, T., . . . Spector, J. (2019). *Global Environmental Change*, 56, 29-40. Retrieved from https://doi.org/10.1016/j.gloenvcha.2019.03.005

Mitchell, B. C., & Chakraborty, J. (2014, October). Urban Heat and Climate Justice: A Landscape of Thermal Inequity in Pinellas County, Florida. *Geographical Review*, 104, 459-480.

Morabito, M., Crisci, A., Messeri, A., Capecchi, V., Modesti, P. A., Gensini, G. F., & Orlandini, S. (2014, January 8th). Environmental Temperature and Thermal Indices: What is the most Effective Predictor of Heat-Related Mortality in different Geographical Contexts. (J. Pinto, & M. Saez, Eds.) *The Scientific World Journal*. doi:http://dx.doi.org/10.1155/2014/961750

Mushore, T. D., Mutanga, O., Odindi, J., & Dube, T. (2018). Determining Extreme Heat Vulnerability of Harare Metropolitan City using Multi-Spectral Remote Sensing and Socio-Economic Data. *Journal of Spatial Science*, 63(1), 173-191. https//:doi.org/10.1080/14498596.2017.1290558

Nayak, S. G., Shrestha, S., Kinney, P. L., Ross, Z., Sheridan, S. C., Pantea, C. I., . . . Hwang, S. A. (2018). Development of a Heat Vulnerability Index for New York State. *Public Health*, 161, 127-137. https//:doi.org/10.1016/j.puhe.2017.09.006

NOAA. (2020, January 15). *Assessing the Global Climate in 2019. NOAA Reports Near-Record Warm Year for the Globe*. (N. O. Administration, Producer) Retrieved from National Oceanic and Atmospheric Administration: https://www.ncei.noaa.gov/news/global-climate-201912

Otto, I. M., Reckien, D., Reyer, C. P., Marcus, R., Masson, V. L., Lindsey, J., . . . Serdeczny, O. (2017, February 27). Social Vulnerability to Climate Change: A Review of Concepts and

Evidence. *Regional Environmental Change*, 17(6) 1651-1662. doi:10.1007/s10113-017-1105-9

Ployhart, R. E., & Vandenberg, R. J. (2010, January). Longitudinal Research: The Theory, Design, and Analysis of Change. *Journal of Management*, 36(1), 94-120. doi:10.1177/0149206309352110

Preston, B. L., Yuen, E. J., & Westaway, R. M. (2011, 24 March). Putting Vulnerability to Climate Change on the Map: A Review of Approaches, Benefits and Risks. (H. M. Fusel, Ed.) *Sustainability Science* 6, 177–202. doi:10.1007/s11625-011-0129-1

Reckien, D. (2018, January 18th). What is in an Index? Construction Method, Data Metric, and Weighting Scheme Determine the Outcome of Composite Social Vulnerability Indices in New York. (C. Reyer, Ed.) *Regional Environmental Change*, 18, 1439-1451. https://doi.org/10.1007/s10113-017-1273-7

Reid, C. E., Gronlund, C. J., O'Neill, M., Brines, S. J., Brown, D. G., Diez-Roux, A. V., & Shwartz, J. (2009, November). Mapping Community Determinants of Heat Vulnerability. *Environmental Health Perspectives*, 117(11), 1730-1735. doi:10.1289/ehp.0900683

Reid, E. C., Mann, J. K., Alfasso, R., English, P. B., King, G. C., Lincoln, R. A., . . . Balmes, J. R. (2012, May). Evaluation of a Heat Vulnerability Index on Abnormally Hot Days: An Environmental Public Health Tracking Study. *Environmental Health Perspective*, 120(5), 715-720. Retrieved from http://dx.doi.org/10.1289/ehp.1103766

Rizvi, S. H., Alam, K., & Iqbal, M. J. (2019). Spatio-Temporal Variations in Urban Heat Island and its Interaction with Heat Wave. *Atmospheric and Solar-Terrestrial Physics*, 185, 50-57. https//:doi.org/10.1016/j.jastp.2019.02.001

Robine, J. M., Cheung, S. K., Roy, S. L., Oyen, H. V., Griffiths, C., Michel, J. P., & Herrmann, F. R. (2008). Death Toll Exceeded 70,000 in Europe During the Summer of 2003. *C.R. Biologies*, 331, 171-178.

Shepherd, M., & Zhou, Y. (2009, May 27). Atlanta's urban heat island under extreme heat conditions and potential mitigation strategies. *Nat Hazards* 52, 639–668. https://doi.org/10.1007/s11069-009-9406-z

Sheridan, S. C., & Dolney, T. J. (2004, September 19). Heat, Mortality, and Level of Urbanization: Measuring Vulnerability Across Ohio, USA. *Climate Research*, 24, 255-265. doi:10.3354/cr024255

Stennett, R. K., Tannecia, S. C., & Taylor, M. A. (2019). Caribbean Climate Change Vulnerability: Lessons from an Aggregate Index Approach. *PLoS One*, 14(7). https://doi.org/10.1371/journal.pone.0219250

Sun, Z., Wang, C., Guo, H., & Shang, R. (2017, September 12). A Modified Normalized Difference Impervious Surface Index (MNDISI) for Automatic Urban Mapping from Landsat Imagery. *Remote Sensing*, 9(942). doi:10.3390/rs9090942

Sunhui, S. (2017, October 4). Social Vulnerability to Heat in Greater Atlanta, USA: Spatial Pattern of Heat, NDVI, Socioeconomics and Household Composition. *Remote Sensing Technologies and Applications in Urban Environments II*, 1043105. Warsaw, Poland. doi:10.1117/12.2278678

Tran, T. L., O'Neill, R. V., & Smith, E. R. (2010). Spatial Pattern of Environmental Vulnerability in the mid-Atlantic Region, USA. *Applied Geography,* 30, 191-202. doi:10.1016/j.apgeog.2009.05.003

Tran, U. S., & Formannn, A. K. (2009, February). Performance of Parallel Analysis in Retrieving Unidimensionality in the Presence of Binary Data. *Educational and Psychological Measurement*, 69(1), 50-61. doi:10.1177/0013164408318761

Turner II, B. L., Kasperson, R. E., Matson, P. A., McCarthy, J. J., Corell, R. W., Christensen, L., . . . Schiller, A. (2003, July 8). A Framework for Vulnerability Analysis in Sustainability Science. *Proceedings of the National Academy of Science of the United States of America (PNAS)*, 100(4), 8074-8079. www.pnas.org/cgi/doi/10.1073/pnas.1231335100

Wang, M., Beal, D. J., Chan, D., Newman, D. A., Vancouver, J. B., & Vandenberg, R. J. (2017). Longitudinal Research: A Panel Discussion on Conceptual Issues, Research Design, and Statistical Techniques. *Work, Aging and Retirement*, 3(1), 1-24. doi:10.1093/workar/waw033

Wang, W., Liu, K., Tang, R., & Wang, S. (2019, January 3). Remote Sensing Image Based Analysis of the Urban Heat Island Effect in Shenzhen, China. *Physics and Chemistry of the Earth*, 110, 168-175. https://doi.org/10.1016/j.pce.2019.01.002

Weber, S., Sadoff, N., Zell, E., & Sherbinin, A. d. (2015, July 17). Policy Relevant Indicators for Mapping the Vulnerability of Urban Populations to Extreme Heat Events: A Case Study of Philadelphia. *Applied Geography*, 63, 231-243. http://dx.doi.org/10.1016/j.apgeog.2015.07.006

Wilson, B., & Chakraborty, A. (2019). Mapping Vulnerability to Extreme Heat Events: Lessons from Metropolitan Chicago. *Journal of Environmental Planning and Management*, 62(6), 1065-1088. doi:10.108009640568.2018.1462475

WMO. (2019). United in Science Report. UN. public.wmo.int/en/resources/united_in_science

Xu, G., Zhu, X., Tapper, N., & Bechtel, B. (2019). Urban Climate Zone Classification using Convolutional Neural Network and Ground Level Images. *Progress in Physical Geography*, 43(3), 410-424. doi:10.1177/0309133319837711

Zhou, Y., Li, N., Wu, W., Wu, J., & Shi, P. (2014). Local Spatial and Temporal Factors Influencing Population and Societal Vulnerability to Natural Disasters. *Risk Analysis*, 34(4), 614-639. doi:10.1111/risa.12193

# CHAPTER 3

## Evolution of Social Vulnerability Index in Atlanta using Raster and Vector Models

### 3.0 Synopsis

The implications of hazards are accentuated or ameliorated by the robustness of social systems, which vary spatially. Little has been explored about the disparate data transformation techniques, weighting mechanics, and visualization models for Social Vulnerability Index (SoVI), crucial for targeted response strategies. This study established that race, language, poverty, gender, living alone, and age are the critical drivers of vulnerability. We also found variance-based weighting to have more clustering and higher magnitude of the SoVI than equal weighting. Downtown Atlanta was disproportionately vulnerable. Varying spatial models, weighting mechanics, and data transformation techniques influence the magnitude and intensity of the SoVI.

INDEX WORDS: Visualization models, Principal Component Analysis, Moran's I, Hazard, Social Vulnerability, Weighting mechanics

**Highlights:**

- Equal weighting and variance-based weighting for both raster and vector models
- Race, language, gender, and age are the critical drivers of social vulnerability
- Variance-based weighting has more clustering than equal weighting in Moran's indices
- Spatial models and weighting mechanics modify the magnitude and intensity of the SoVI

## 3.1 Introduction

Vulnerability constitutes the biophysical hazard and the social system's inherent susceptibility (Binita et al., 2015; Borden et al., 2007; Carr et al., 2014; Karanja and Kiage, 2021). Although the two paradigms are contemporaneous, the biophysical can hardly be mitigated, whereas the social vulnerability can be modified (Cardona 2003). The ramifications attributable to a disaster are not random but predicated on demographic characteristics and the dynamic social-economic conditions quantifiable to generate the Social Vulnerability Index (SoVI) (Atyia 2015; Cutter et al., 2003; Evans et al., 2014; Karanja and Kiage 2021). Spatial disparities in coping, responding, and recovering from disasters are a function of the SoVI (Flanagan et al., 2018; Harlan et al., 2013; Maier et al., 2014). It is imperative to locate the most vulnerable (Alonso and Renard, 2020; Nayak et al., 2018), failure to which may portend a colossal public policy failure when faced with hazards (Goodling et al., 2015; Mitchell and Chakraborty, 2014). The SoVI is essential in effecting climate change policies, exploring climate justice, and advancing the discourse on the "human-centered vulnerability concept" (Chen et al., 2013; Cooley et al., 2012). Despite progress in framing the SoVI, little has been studied about visualization alternatives and the differences in the respective outputs. Geographic Information Science (GIS) provides multiple pathways capable of varying the generated indices' efficacy (Ho et al., 2015). This study explores the raster and vector models with a temporal dimension and compares the outputs, determining how the models impact SoVI visualization.

Principal Component Analysis (PCA) is widely accepted as a reductionist approach before the visualization of the SoVI (Abdi and Williams, 2010; Conlon et al., 2020; Cutter et al., 2003; Nayak et al., 2018; Zhou et al., 2014). However, studies differ on the relevance of pre-PCA tests, including Bartlett's test of sphericity and the Kaiser Meyer-Olkin (KMO) test of sampling

adequacy, which detect multicollinearity in the dataset (Yong and Pearce, 2013). A few studies have applied the two tests (e.g., Alonso and Renard, 2020), while others directly conducted correlational analysis (e.g., Chen et al., 2013). Another divergence point is on variable rotation, which optimizes variable interpretation (Yong and Pearce 2013). There is a profound preference for varimax rotation (Binita et al., 2015; Borden et al., 2007; Dintwa et al., 2019; Eisenman et al., 2016; Reid et al., 2009). Only one study attempted to compare the orthogonal rotational techniques (varimax and equamax) and oblique rotational approaches (promax and oblimin) (Holand et al., 2011). According to Yong and Pearce (2013), orthogonal techniques are relevant when the factors are uncorrelated, while oblique methods are ideal when the components are correlated. The thresholds for determining the number of variables to be retained are not consistent in the literature. Most studies (e.g., Borden et al., 2007; Chen et al., 2013; Dintwa et al., 2019) only use the Kaiser criterion. Other studies (e.g., Hondula et al., 2012) combine the scree plot and Kaiser criterion, while Holand et al. (2011) used parallel analysis, scree plots, Kaiser criterion, and stepwise elimination. A variation in the number of retained components would invariably result in disparate visualization patterns.

Weighting mechanics could have a bearing on the developed SoVI (Karanja and Kiage, 2021; Zhang et al., 2021). Two common mechanics from the literature are equal weighting and weighting based on the percentage variance explained. Several studies (e.g., Alonso and Renard, 2020; Chen et al., 2013; Conlon et al., 2020; Ho et al., 2018; Maier et al., 2014) have adopted equal weighting, while others (e.g., Binita et al., 2015; Kim et al., 2017; Macnee and Tokai 2016) have used percentage variance. Equal weighting is preferred by authors who argue that there is no theoretical underpinning to apportion significance to one component over the other. At the same time, those applying percentage variances proceed from the output of the PCA. Despite the

justifications of preferring one weighting method over the other, the disparities from the two schemes have not been systematically examined and compared and their effect on the intensity and spatial distribution of vulnerability hotspots. In this study, we explore the weighting choices and how they affect the determination of vulnerability hotspots in the Atlanta metropolitan area between 2000 and 2019.

Raster and vector models are the primary visualization pathways on a GIS platform, as explained in Ho et al. (2015), who converted SoVI vector datasets to raster to match up the spatial resolution of either dataset, minimizing the modifiable areal unit problem (MAUP) when overlaying the biophysical and the socioeconomic layers. Most biophysical datasets are in raster format; hence it is essential to consider both raster and vector representations of the SoVI to determine the best fit model for integrating the layers. That is why this study explores both models and compares the outputs across time, which differs from Ho et al. (2015) that was cross-sectional and did not vary weighting mechanics. Several studies (e.g., Eakin and Luers, 2006; Juntunen, 2006; Lee, 2014; Wilson and Chakraborty, 2019) acknowledge that social vulnerability is immensely dynamic. Its evolution can only be captured when knowledge production and application match the dynamic social conditions. The longitudinal approach is preferred to monitor the variations over time, as explained in Caruana et al. (2015) and Ployhart and Vandenberg (2010).

This study adopts a "starting point approach" (Binita et al., 2015). We structure vulnerability as a pre-existing socioeconomic condition whose quantification cannot be understated given its core intervening role when preparing, recovering, and responding to hazard manifestations (Cooley et al., 2012; Hayden et al., 2011; Holand et al., 2011). A hazard transforms into a disaster only when human systems have been impacted. (*ibid*). However, Cardona (2003)

argued that failure to effectively capture the social system's multi-dimensional nature through the existing quantitative models could be the actual vulnerability. Methods of visualization and measuring vulnerability have lagged despite the progress in theoretical constructs (Cutter et al., 2009). The SoVI is applicable across all the phases of a biophysical hazard, yet the literature on disaster overly focuses on the infrastructural setups' susceptibility (Flanagan et al., 2011; Juntunen 2006). The SoVI is also integral pre-and post-disaster (Fothergill and Peek, 2004), and the limited empirical scientific research of this metric is indefensible. It is necessary to reimagine and streamline representations of vulnerability (Mendes, 2009), which this study seeks to achieve by applying disparate weighting mechanics using raster and vector models in a longitudinal study approach.

## 3.2 Methods

### *3.2.1 Study Area*

This study was conducted in Atlanta, Georgia (centered by 33.7490º N and 84.3880º W), covering 17,686 $km^2$. The study included 22 metropolitan Counties, expanding the spatial focus of Lo and Quattrochi (2003) to include Pickens, Dawson, Cherokee, Bartow, Cobb, Paulding, Douglas, Carroll, Coweta, Fayette, Fulton, Clayton, Spalding, Henry, Rochdale, Newton, DeKalb, Gwinnett, Walton, Barrow, Hall, and Forsyth. The 2015-2019 American Community Survey (ACS) estimated Atlanta’s population to be 10,403,847, up from 8,186,453 in the 2010 decennial census, representing a growth rate of 27.1%.

Atlanta is an ideal setting for studying the evolution of the SoVI, given its diversity in race and class (Markley et al., 2020). The "Atlanta paradox" explained by Connor (2015) demonstrates the existence of abject poverty in a city with massive wealth. "White flight" (Connor, 2015; Kruse, 2005) resulted in poverty concentrations within the city core while the suburbs remained affluent,

as the movement entailed capital shifts, new investments, and disinvestments in certain Counties. Atlanta has also been referred to as Black Mecca (Markley et al., 2020), constituting rich Blacks in suburban counties. The racial and class dynamics compel a comprehensive study on the SoVI, its drivers, and the identification of the most vulnerable. The frequency of extreme hydroclimatic events such as heatwaves, floods, and drought is escalating (Binita et al., 2015). It is crucial to determine the most sensitive populations when faced with disasters for targeted mitigation measures. The expansive spatial extent allows for comparison between core city Counties, the suburbs, and those in the periphery.

### *3.2.2 Data Acquisition and Preparation*

The decennial census dataset and the 5-year ACS estimates, alongside GIS-compatible spatial boundary files, were downloaded from the National Historical Geographic Information Systems (NHGIS) website https://www.nhgis.org/ (Manson et al., 2020). For 2000, the decennial datasets provided actual population counts, while the long-form questionnaire provided socioeconomic variables. The other dataset (2005-2009, 2010-2014, and 2015-2019) comprised of ACS 5-year estimates which replaced the long-form questionnaire, thus allowing a longitudinal analysis between 2000 and 2019. The NHGIS datasets facilitate attribute integration by providing a set of comparable statistics across time. A total of 20 variables identified as frequently used variables by Karanja and Kiage (2021) were inductively selected for analysis. The selected variables include percentage Black/African American, percentage Indian/Alaska natives/native Hawaiian/Pacific islander, percentage Asian, percentage some other race, percentage two or more races, and percentage Hispanics. The other variables are percentage population below five years, percentage population below 18 years, percentage population above 65 years, percentage female-headed households, percentage female population, percentage population over 65 living alone, and

percentage population where the English language is not spoken at home. We also used the percentage of the population using public transport, percentage of the population over 25 years without a high school diploma, percentage of the population over 16 unemployed. Additionally, we incorporated the percentage population receiving social security income, percentage of the population below poverty, percentage population living alone, and percentage of the population employed in primary productivity. We normalized the raw data as a percentage of the total population for the four-time periods following (Kashem et al., 2016). The variables specific tables were joined in GIS to the corresponding spatial boundary layer to allow for spatial visualization and data reduction analysis.

### *3.2.3 PCA Analysis*

The datasets' suitability for analysis was evaluated, as explained in Yong and Pearce (2013) and Alonso and Renard (2020). The KMO measure and Bartlett's test of sphericity are crucial in determining whether the correlation matrix is an identity matrix, hence the suitability of the dataset for reduction techniques. The KMO measure should be above 0.6, while the test of significance for Bartlett's test should be less than 0.05. The pre-PCA analysis confirmed that the variables chosen across all periods were suited for data reduction.

The PCA was performed twice using the Statistical Package for the Social Sciences (SPSS) software. The first analysis did not specify the number of components to extract. This process allowed the retention of components that at least represented one variable using the Kaiser criterion. In the second run, the number of components to extract was specified, which varied across time. The varimax rotation method, which minimizes the number of variables that have high loadings on each other and makes small loadings even smaller, was chosen (c.f., Borden et al., 2007; Dintwa et al., 2019; Eisenman et al., 2016; Binita et al., 2015; Reid et al., 2009; Yong

and Pearce, 2013). Variable rotation provides a simple structure that enables each variable to load on as few components as possible. The scores were saved using the regression method, and 999 iterations were chosen. We used both the scree plots and Kaiser criterion to determine the number of components to retain. The Kaiser criterion alone has been found to overestimate the number of components (Kashem et al., 2016). The option, exclude cases listwise, was selected where cases were dropped if they had a missing value, preventing overestimating factors (Yong and Pearce, 2013).

The principal components had both positive and negative values. We scaled the component values between 0 and 1 using the minimum-maximum normalization, with 0 being the least vulnerable and 1 the most vulnerable (e.g., Dintwa et al., 2019). Normalization ensured internal consistency across time and assigned uniform direction of influence for the components while reducing data redundancy. We derived two kinds of SOVIs using percentage variance explained after components rotation (Binita et al., 2015; Kim et al., 2017; Macnee and Tokai 2016) and using equal weighting (Alonso and Renard, 2020; Chen et al., 2013; Conlon et al., 2020; Ho et al., 2018; Maier et al., 2014). We then classified the SOVIs into five classes with consistent class breaks across time. We applied a 0.2 class break, with 0 as the lowest value and 1 as the highest value. Both the Global Moran's I (spatial autocorrelation) and Anselin's local Moran's I (cluster and outlier analysis) were performed on the SOVIs (Ho et al., 2015; Kashem et al., 2006; Zhou et al., 2014). The Global Moran's I established systematized spatial variations while the Anselin's Moran’s I determined statistically significant clustering at 95% confidence level. We then converted the vector models to raster models using the feature to raster conversion tool and resampling to 30-meter resolution. We reclassified the output into five classes similar to the vector model. Resampling to 30-meter resolution was preferred since most raster datasets for the

biophysical parameters are derived from satellite sensors with a spatial resolution of 30 meters. The outcomes of the vector and raster models were then compared across time.

## 3.3 Results and Discussions

### *3.3.1 PCA Analysis*

The KMO measure was 0.709 for 2000, 0.744 for 2005-2009, 0.671 for 2010-2014, and 0.757 for 2015-2019. Bartlett's test was 0 across the periods confirming the suitability of the variables for PCA. The PCA data reduction retained five components for 2000, 2005-2009, and 2010-2014 but retained six components for 2015-2019 (table 3-1). The total percentage variance explained decreased over time despite the increased number of components in 2015-2019. 2010-2014 had the highest percentage variance explained while 2015-2019 had the lowest. For 2000, Hispanic households where the English language was not spoken at home had the highest loadings on component 1. Blacks/African Americans below poverty had the maximum loading for component 2, while recipients of social security income for populations above 65 years old loaded heavily on component 3. Individuals below 18 years essentially explained component 4, whereas those employed in primary productivity (agriculture, forestry, fishing, and hunting) had maximum loadings for component 5.

Table 3-1. Summary statistics for the PCA

| **Periods** | **2000** | **2005-2009** | **2010-2014** | **2015-2019** |
|---|---|---|---|---|
| KMO test | 0.709 | 0.744 | 0.671 | 0.757 |
| Bartlett's test | 0.000 | 0.000 | 0.000 | 0.000 |
| Retained CPNTs | 5 | 5 | 5 | 6 |
| Total variance (%) | 72.650 | 75.322 | 69.274 | 68.548 |
| CPNT 1 | | | | |
| Before rotation | 21.243 | 24.715 | 22.669 | 22.084 |
| After rotation | 17.997 | 21.893 | 20.656 | 18.053 |
| CPNT 2 | | | | |
| Before rotation | 17.750 | 21.932 | 17.659 | 18.130 |
| After rotation | 17.830 | 21.605 | 15.085 | 16.162 |
| CPNT 3 | | | | |
| Before rotation | 17.344 | 11.752 | 13.032 | 9.710 |
| After rotation | 15.559 | 12.301 | 11.580 | 10.717 |
| CPNT 4 | | | | |
| Before rotation | 9.354 | 10.107 | 9.753 | 7.575 |
| After rotation | 13.061 | 11.574 | 11.138 | 9.285 |
| CPNT 5 | | | | |
| Before rotation | 6.959 | 6.817 | 6.560 | 5.812 |
| After rotation | 8.203 | 7.949 | 10.815 | 7.319 |
| CPNT 6 | | | | |
| Before rotation | - | - | - | 5.236 |
| After rotation | - | - | - | 7.011 |

Key:

CPNT=Component

The years 2005-2009 was the only time when the percentage variance explained increased. The highest loading variables for components 1, 3, 4, and 5 mimicked the year 2000. Black/African American female households had the highest loading for component 2. The remarkable similarity observed in 2000 and 2005-2009, with an increase in total percentage variance of 2.7%, could be attributed to the great economic recession between 2007-2009. According to the US Government (2011), the great recession was characterized by layoffs, tighter credit accessibility and availability, foreclosures, and unprecedented unemployment rates. Unemployment rates rose from

8.8% to 13.7% in December 2008. The impacts of the financial crisis in individual US households and businesses could have contributed to a higher percentage variance during this period.

The period 2010-2014 had a significant drop in total percentage variance explained by 6% from the preceding time and by 3.4% compared to 2000 despite retention of 5 components, which could be attributed to economic recovery efforts following the great recession. For the third consecutive period, the Hispanics where the English language is not spoken at home had the highest loading for component 1. New patterns emerged compared to the previous two periods. Blacks above 16 years and unemployed, individuals living alone, and recipients of social security above 65 years had the highest loading for components 2, 3, and 4, respectively. Percentage female population had the maximum loading for component 5. The period 2015-2019 had the least percentage variance despite the retention of 6 components. Five components accounted for 61.5% of the total variance. Components 1, 2, and 5 had an aspect of racial groups. Specifically, Blacks below poverty explained component 1, Hispanics and some other race explained component 2, while two or more races explained component 3. This period was the first time almost all racial groupings explained most of the components. This observation indicates disproportional vulnerability accentuated by racial disparities explored by Connor (2015) and Kruse (2005). Component 3 was explained by the elderly over 65 years receiving social security income, component 4 by the young below 18 years, and component 6 by those living alone.

Our findings identify the drivers of vulnerability as Hispanics where English is not spoken at home, Blacks/African American below poverty level, recipients of social security income, individuals below 18 years, individuals living alone, the elderly above 65, Blacks over 16, and unemployed, and female gender. The PCA analysis established minor variations for the prominent variables across time in Atlanta. The minor variations were in 2015-2019, where race played a

crucial role in establishing vulnerability hotspots. The retained components highlighted the racial disparity and the disproportionate susceptibility of the Hispanics and the Blacks/African Americans racial groups. Hansen et al. (2013) concluded that ethnicity and race could modify the influences of a hazard. Racial differences often translate to language and cultural bias, limiting access to disaster funding and constraining protective behavior acquisition (Aubrecht and Ozceylan., 2013; Cutter et al., 2003). Marginalized races are characterized by environmental justice issues, high comorbidities, and lower-income (Aubrecht and Ozceylan, 2013: Eakin and Luers, 2006). Race, therefore, acts in multiple forms to disadvantage the minority.

### *3.3.2 Global and Local Moran's I*

The values for the global Moran's (spatial autocorrelation) varied between 0.18 and 0.24 for equal weighting of principal components and between 0.21 and 0.35 for weighting based on the variance explained. Weightings based on the variance explained had more clustering compared to equal weighting as its values for the Global Moran's I were consistently higher across time. 2010-2014 had the lowest Global Moran's I index for the weighting mechanics, while 2015-2019 had the highest spatial autocorrelation (table 3-2). 2015-2019 had the lowest total variance explained yet had the highest global Moran's I index, meaning no correlation between the total variance explained and spatial autocorrelation. However, this period had the highest number of retained components. The index generally decreased over time, albeit with a sharp increase for 2015-2019. The global Moran's I index demonstrates instances of concentrated vulnerability, although the percentage variance is decreasing. The statistics suggest that marginalized groups live closer to each other, resulting in a larger global Moran’s I index. The observed pattern of concentrated vulnerability was explored by Shelton (2018), where concentrated affluence and poverty co-occurred and are a vital feature of many USA cities. Pockets of affluence and poverty

become distinct yet co-produced and enmeshed, reflecting the suburban and urban vulnerability dynamics in Atlanta. Despite the variations in the Global Moran's I index's magnitude, both weighting mechanics' values increased and decreased simultaneously, hence consistent patterns. A high global Moran's I index did not always translate to higher proportionality of tracts in the High-High clusters.

Table 3-2. The results of the Global Moran's Index.

| Period | Moran's index equal weighting | Moran's index variance explained |
|---|---|---|
| 2000 | 0.225223 | 0.261082 |
| 2005-2009 | 0.234961 | 0.246750 |
| 2010-2014 | 0.180078 | 0.214248 |
| 2015-2019 | 0.240781 | 0.347430 |

For the local Moran's index (Anselin's local Moran's I), the proportion of tracts in the High-High clustering generally increased from 14.3% in 2005-2009 to 23.7% in 2015-2019 for equal weighting, and from 20.5% to 27.6% for weighting pegged on eigenvalues (table 3-3.). The weighting based on percentage variance consistently returned more High-High clustering than equal weighting, consistent with spatial autocorrelation output. Anselin's Moran's I had different spatial distributions of vulnerability based on the classifications generated for equal weighting and weighting based on the variance explained. The increase in the High-High clustering of the local Moran's I could be attributed to the migration of the Hispanic populations and Blacks to core metro Atlanta counties to pursue jobs, as observed in Binita et al. (2015). The two racial groups were the dominant drivers of vulnerability from the PCA analysis.

Table 3-3. Clusters of H-H have increased over time, and eigenvalues weighting has more dense clusters of H-H compared to equal weighting

| Period | Equal weighting | | | | | Variance explained weighting | | | | |
|---|---|---|---|---|---|---|---|---|---|---|
| | H-H | H-L | L-H | L-L | NS | H-H | H-L | L-H | L-L | NS |
| 2000 | 17.12 | 1.61 | 5.26 | 24.12 | 51.89 | 22.51 | 1.32 | 7.02 | 19.30 | 49.85 |
| 2005-2009 | 14.33 | 5.12 | 2.05 | 26.90 | 51.60 | 20.47 | 2.49 | 3.95 | 23.25 | 49.84 |
| 2010-2014 | 19.75 | 3.76 | 5.43 | 20.48 | 50.58 | 22.15 | 3.34 | 6.00 | 20.48 | 48.03 |
| 2015-2019 | 23.72 | 4.08 | 6.37 | 17.97 | 47.86 | 27.59 | 3.66 | 4.28 | 26.65 | 37.82 |

Key: HH (High-high), H-L (High-low), L-H (Low-high), L-L (Low-low), N-S (Not significant)

The highest clusters in 2000 were in South Fulton, Southeast Cobb, Southwest Gwinnet, Northern DeKalb, Northwest Clayton, and Hall counties, both for equal weighting and variance explained weighting mechanics. However, weighting based on variance explained had more clustering in DeKalb (figure 3-1). In 2005-2009, equal weighting had a more extensive spread indicating pockets of High-High clustering for counties in the periphery such as Pickens, Hall, Bartow, Walton, Carrol, Spalding, and Newton. Southern Fulton still had High-High clustering but shrunk compared to 2000 for equal weighting. Eigen weighting had more High-High clustering in Northwest Clayton, Southern Fulton, Southeast Cobb, Hall, North DeKalb, Southwest Gwinnet, and Spalding counties. For the two periods, counties in the city core had more High-High clustering and succeeded by Low-Low clusters in the suburban. The outliers (Low-High, and High-Low) were fewer. 2010-2014 saw more Low-High clusters emerge in the suburban areas (Cobb, Cherokee, Forsyth, Barrow, and Paulding counties) for both weighting mechanics, which could be explained by the emergence of more affluent Blacks in the suburbs. Similarly, High-Low clusters emerged in Fulton, DeKalb, and Clayton counties that we attribute to gentrification. Gentrification is often associated with capital investment. Shelton (2018) observed that wealth creation and

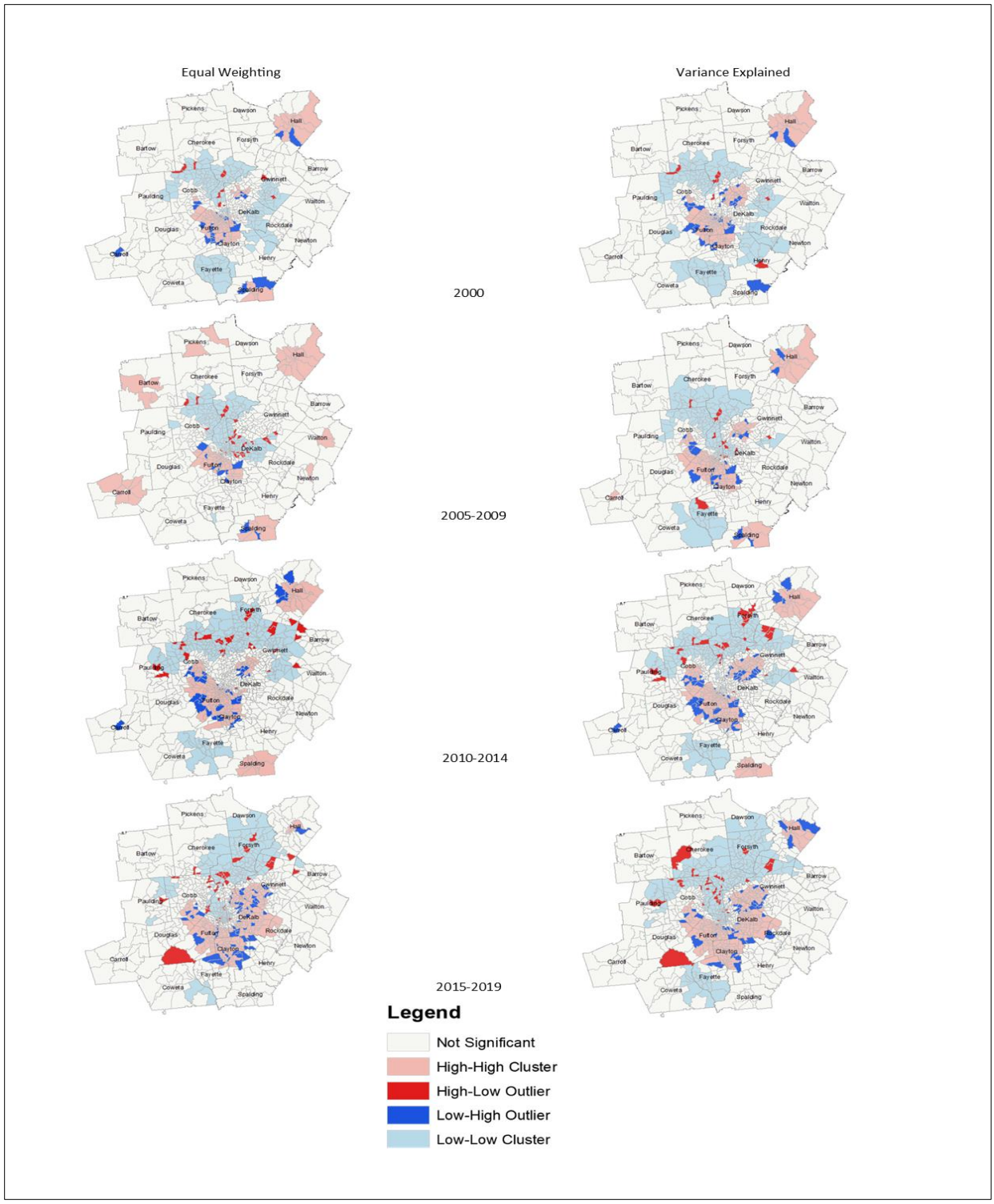


Figure 3-1. Equal weighting and percentage variance weighting produced disparate distributions of clusters using Anselin's Moran's. Core city counties had dense H-H clusters succeeded by L-L clusters in the suburbs. Most peripheral counties had no significant clusters. The H-L and L-H clusters increased over time.

poverty generation are dialectical, escalating unequal development. A similar pattern of distribution was observed for 2015-2019. However, the High-High clusters were denser in the core counties, and the Low-High clusters also increased. The general observation for the entire period was that High-High clusters were dense in core city counties. The High-High clusters were succeeded by Low-Low clusters in the suburban, while most of the peripheral counties did not have significant clusters. Although Low-High clusters' pockets and High-Low clusters increased over time, the clusters' spatial distribution varied with weighting mechanics. We also noted a pattern of concentrated vulnerability in the core metro counties and Hall county.

### *3.3.3 Vector Model*

The vector model established a low number of census tracts for very low, high, and very high classes for equal weighting and percentage variance weighting. Although the distribution indicated relatively low vulnerability levels, a large proportion of the population is potentially at risk of increased vulnerability when the SoVI is integrated with a hazard or when deterioration of social conditions occurs. It is necessary to create integrated metrics that make the SoVI hazard-specific. Equal weighting distributed almost a 50-50 ratio in the low and moderate classes, whereas variance explained weighting had approximately a 60-35 ratio for the low and moderate classes (table 3-4). For both weighting mechanics, 2005-2009 had the highest proportion of tracts in the high category, which tallied with the global economic recession. The two weighting mechanics had observable differences in the distribution of vulnerability for the SoVI. The variance weighting had a higher percentage in the high and very high classes than equal weighting, which corroborates Anselin's Moran I results. Both weighting mechanics had a reduced trend of the proportion of tracts in the high and very high classes for the entire period, which differed with the local Moran's index. The differences could be an indicator of how data transformation and visualization options such

as the choice of classification method may have a bearing on the nature of the SoVI, as observed by Zhang et al. (2021).

Table 3-4. Results of equal weighting and variance explained weighting for the vector model.

| Period | Equal weighting | | | | | Variance explained weighting | | | | |
|---|---|---|---|---|---|---|---|---|---|---|
| | Very low | Low | Moderate | high | Very high | Very low | Low | Moderate | High | Very high |
| 2000 | 0.44 | 53.80 | 44.59 | 1.17 | 0.00 | 0.44 | 64.18 | 33.48 | 1.75 | 0.15 |
| 2005-2009 | 1.02 | 49.56 | 47.95 | 1.47 | 0.00 | 1.46 | 60.82 | 35.53 | 2.19 | 0.00 |
| 2010-2014 | 0.73 | 49.32 | 49.01 | 0.84 | 0.10 | 0.73 | 61.02 | 36.90 | 1.25 | 0.10 |
| 2015-2019 | 0.63 | 49.11 | 49.32 | 0.84 | 0.10 | 0.31 | 60.19 | 38.56 | 0.84 | 0.10 |

Analysis of the spatial visualization indicated that for the year 2000, weighting based on variance explained had more vulnerable tracts in the city core compared to equal weighting. A similar pattern was observed in Anselin's Moran's analyses. The most susceptible counties were Fulton, DeKalb, Gwinnett, Cobb, Clayton, Cherokee, and Hall (figure 3-2). High vulnerability pockets were more pronounced in the city core counties throughout the period, followed by the least vulnerable counties in the suburban counties. In contrast, the peripheral counties were mostly moderately vulnerable, except Hall, Pickens, Carroll, and Spalding counties. The Anselin's Moran's and the vector SoVI indicated that downtown areas were disproportionately susceptible, while the suburban areas were least vulnerable both for equal weighting and variance explained weighting mechanics. The Local Moran's visualizations seem best suited for identifying hotspots compared to the vector model where the researcher has to conduct extra data transformation techniques. However, we are unsure of the consistency of the global and local Moran’s for longitudinal studies. The downtown areas essentially represent Southern Fulton, whose vulnerability was augmented by “White flight” and rich Blacks' movement to the suburbs (Connor, 2015; Kruse, 2005). The movement of capital characterized the demographic shifts.

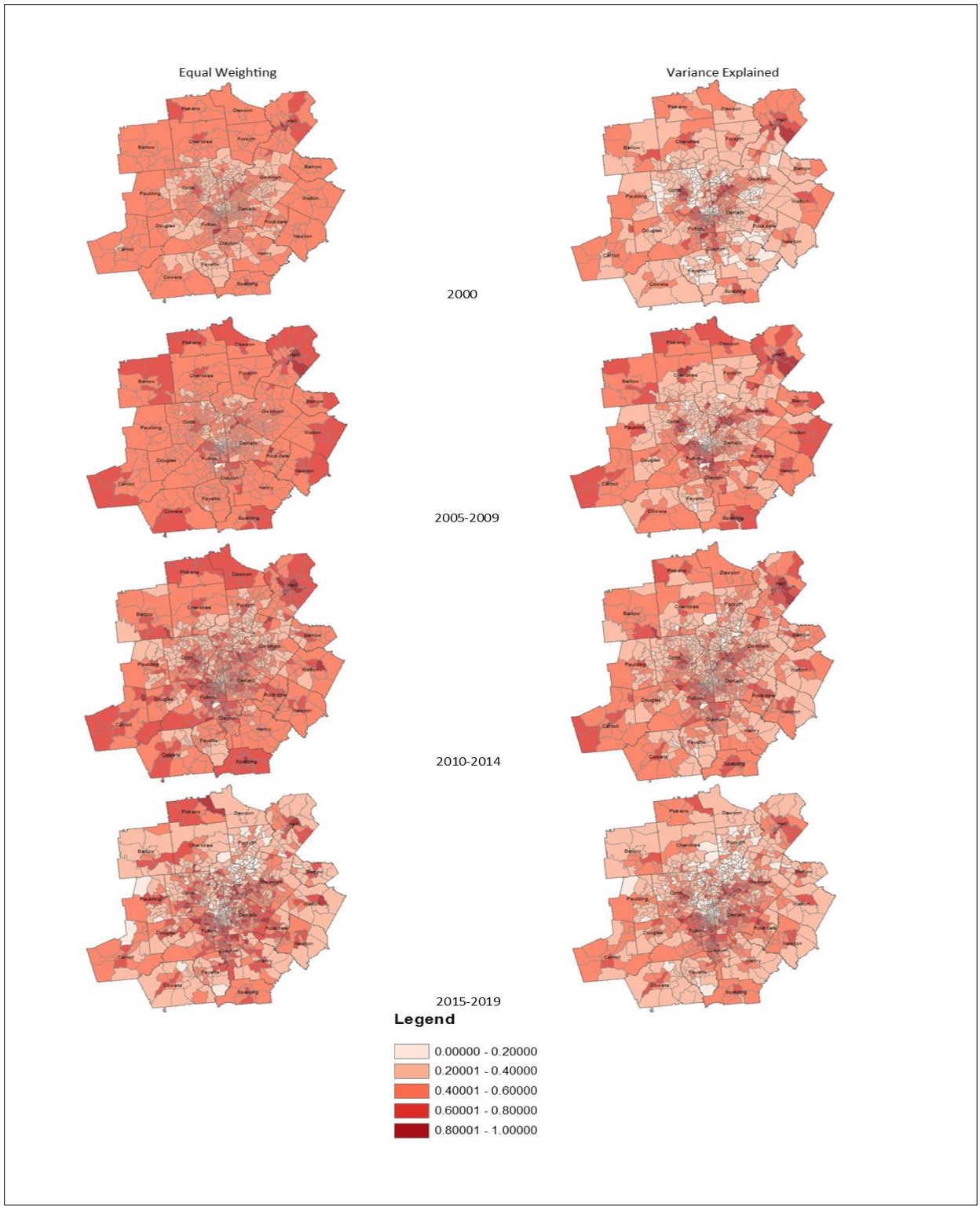


Figure 3-2. Weighting based on variance explained had more tracts in the high and very high classes (0.6 to1.0) compared to equal weighting. Counties in downtown areas were disproportionately susceptible for both weighting mechanics, corroborating the output of Anselin's Moran's analysis.

### *3.3.4 Raster Model*

The raster model had fewer proportions of census tracts in the high and very high classes than the vector model for equal weighting and variance-based weighting. The tracts in the very low class also decreased in the raster model. The vector model consistently had higher proportions of tracts in the low category than the moderate, while for the raster model, the moderately vulnerable class was higher for 2000 and 2005-2009 (table 3-5). The distribution of tracts for eigenvalue weighting was dense in the low category compared to the vector model. Both the raster and vector models established a reduced number of tracts in the high and very high classes throughout the study. The raster and vector models had different spatial distributions of tracts across the classes, although the patterns of increase or decrease in vulnerability were approximately identical. Although both models indicated a reduction in tracts in the high and very high classes, downtown areas have had denser concentrations of vulnerable tracts over time (figure 3-3). The pattern observed in the vector model where low clusters succeeded high clustering, and then moderate vulnerability clusters on the periphery seem to have been diminished in the variance-based weighting for the raster model. The choice of the spatial model of representation has a bearing on the accuracy of the developed SoVI.

Table 3-5. Results of the raster model for equal weighting and eigenvalue weighting.

| Period | Equal weighting | | | | | Variance-based weighting | | | | |
|---|---|---|---|---|---|---|---|---|---|---|
| | Very low | Low | Moderate | high | Very high | Very low | Low | Moderate | High | Very high |
| 2000 | 0.03 | 46.25 | 53.44 | 0.28 | 0.00 | 0.03 | 81.44 | 18.21 | 0.24 | 0.08 |
| 2005-2009 | 0.20 | 34.25 | 65.24 | 0.31 | 0.00 | 0.18 | 67.76 | 31.75 | 0.31 | 0.00 |
| 2010-2014 | 0.13 | 53.83 | 45.94 | 0.10 | 0.00 | 0.13 | 68.02 | 31.62 | 0.23 | 0.00 |
| 2015-2019 | 0.05 | 64.38 | 35.47 | 0.07 | 0.03 | 0.03 | 77.04 | 22.84 | 0.06 | 0.03 |

As a synthesis of the models and weighting mechanics, weighting guided by the variance explained and equal weighting impact on the spatial distribution and magnitude of the SoVI. The data transformations adopted also influence the nature of the derived SoVI evinced by the variations of the local and global Moran's I indices against the vector model. The global and local Moran's I outputs inherently anchored on the vector model returned different results from our vector model. Notably, the data transformation choices differentiate our vector model from the global and local Moran's vector-based model, signifying the alterations attributable to disparate data transformation techniques. Given that testing for validity of the metrics is beyond the scope of this study, the contrasting results should be interpreted as complementary and meant to enrich multiple facets of decision-making, as argued by Holand et al. (2011). Data transformation is inevitable and could be masking perspectives of vulnerability as much as it reveals. For instance, our vector model normalized the factors across time, ensuring uniformity, while the global and local Moran's may not be consistent for longitudinal studies. The SoVI is also a relative measure that is not hazard-specific, complicating its validation (Cutter et al., 2003; Karanja and Kiage, 2021). The multiple outputs generated should yield a broader spectrum of rational decision-making, strengthening the utility of the SoVI. The inadequacies of the models should not limit applications of the SoVI. The raster and vector models in a broader sense had similar visualization patterns but significantly differed at a closer look at the distribution in the classes. Future studies must explore smaller spatial scales to detect the evolving patterns for a specific locality. Our models are population-based, and subsequent studies should attempt area-based models. Testing the efficacy of the SoVI pre-and post-disaster should be evaluated across multiple disasters to enrich conceptualizations of the SoVI.

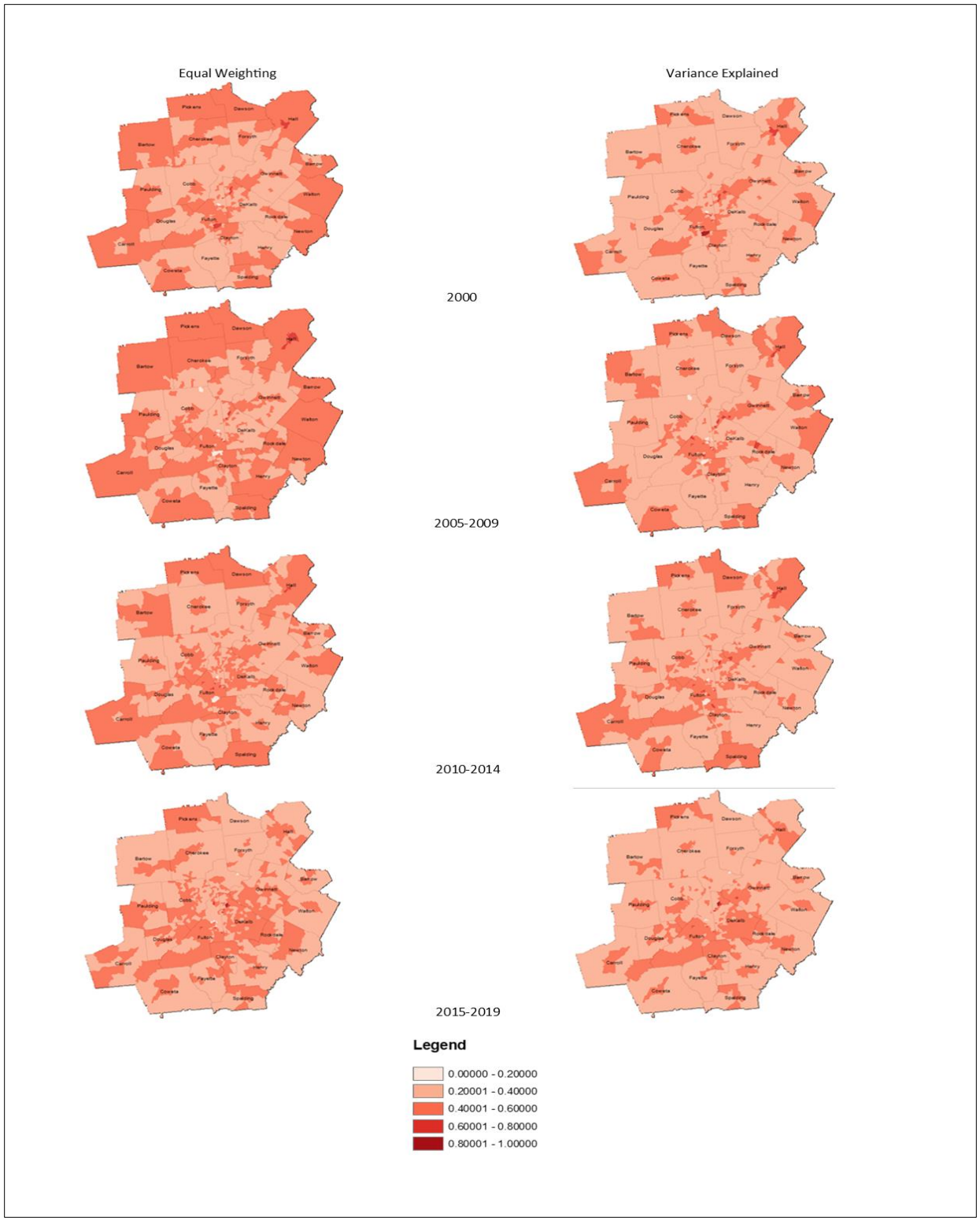


Figure 3-3. The raster model consistently indicated denser clusters of vulnerable tracts in downtown areas similar to the vector model. Equal weighting and variance-based weighting produced varied distributions of vulnerability.

## 3.4 Conclusion

Vulnerability comprises the biophysical and socioeconomic patterns. The difference between a hazard and a disaster could be attributed to socioeconomic and demographic characteristics. Given the geographical and spatial inequalities in coping, responding, and recovering from disasters, it is compelling to understand how the SoVI varies spatially and across time for targeted mitigation and adaptation measures. The biophysical dimension can hardly be prevented, but planning strategies modulate the SoVI. Understanding the dynamics of the SoVI and its evolution and key drivers is a salient undertaking. The SoVI is not hazard-specific, limiting tests of validity predicated on a specific hazard. The viable pathway is to explore the multi-dimensionality of the SoVI using multiple models and weighting mechanics to offer a broader spectrum for rational decision making. The inconsistencies in the models should be interpreted as complementarities meant to strengthen the utility of the metric rather than stifling its applicability. Our study applied equal weighting and weighting guided by variance explained using both and raster and vector models. Failure to capture the multiple facets of the SoVI could be the actual vulnerability (Cardona, 2003).

We chose PCA as the data reduction technique, and all the variables were subjected to the KMO and Bartlett's test of sphericity to check suitability for the PCA. The scree plot and Kaiser criterion extracted five components for 2000, 2005-2009, 2010-2014, but retained six for 2015-2019. The key drivers of vulnerability across time in Atlanta were: Hispanics where the English language was not spoken at home, Black/African Americans below poverty, recipients of social security income for populations above 65 years, individuals below 18 years, living alone, female gender, and those employed in primary productivity. Weighing based on variance explained had more clustering, and higher magnitude of the SoVI than equal weighting for both local and global

Moran's I indices. No correlation was detected between the total variance explained and the spatial autocorrelation analysis. Similarly, a high global Moran's index did not always translate to more tracts in the High-High clustering. The patterns of increases or reduction in vulnerability over time were similar for both weighting mechanics for the global and local Moran's analysis. High-high clustering was dense in the core metro counties, succeeded by Low-Low clusters in the suburban, whereas the peripheral counties had no significant clusters.

Both the raster and vector models had patterns of a reduced proportion of tracts in the high and very high classes, which differed from the local Moran's I index's output. Our vector model and the Local Moran's index established that downtown Atlanta was disproportionately vulnerable. Weighting based on the variance explained had a higher percentage of tracts in the high and very high classes than equal weighting for the vector model. The raster model had fewer tracts in the high and very high classes than the vector model. The raster and vector models had different spatial distributions of tracts across the classes, although the patterns of increases and decreases were identical. Therefore, varying spatial models, data transformation techniques, and weighting mechanics have a bearing on the magnitude and intensity of the SoVI. Contrasting outputs are essential in highlighting the multi-dimensionality of the SoVI, enriching planning strategies.

## 3.5 Statement of Authorship

The student, Joseph Karanja, is the lead author under the guidance of Dr. Lawrence Kiage.

**References:**

Abdi, H., & Williams, L. J. (2010). Principal Component Analysis. *Wiley Interdisciplinary Reviews: Computational Statistics, 2*. doi:https://doi.org/10.1002/wics.101

Alonso, L., & Renard, F. (2020, February 5). A comparative study of the physiological and socio-economic vulnerabilities to heat waves of the population of the metropolis of Lyon (France) in a climate change context. *International Journal of Environmental Research and public health, 17*(1004). doi:doi:10.3390/ijerph17031004

Atyia, M. S. (2015). A Framework to Understand the Relationship between Social Factors that Reduce Resilience in Cities: Application to the City of Boston. *International Journal of Disaster Risk Reduction, 12*, 53-80. doi:10.1016/j.ijdrr.2014.12.001

Aubrecht, C., & Ozceylan, D. (2013). Identification of heat risk patterns in the U.S. national capital region by integrating heat stress and related vulnerability. *Environment International, 56*, 65-77. doi:http://dx.doi.org/10.1016/j.envint.2013.03.005

Binita, KC., Shepherd, J. M., & Gaither, C. J. (2015). Climate change vulnerability assessment in Georgia. *Applied Geography, 62*, 62-74. doi:http://dx.doi.org/10.1016/j.apgeog.2015.04.007

Borden, A. K., Schmidtlein, C. M., Emrich, T. C., Piergosch, W. W., & Cutter, L. S. (2007). Vulnerability of US cities to environmental hazards. *Journal of homeland security and emergency management, 4*(2). doi:https://doi.org/10.2202/1547-7355.1279

Cardona, O. D. (2003). The need for rethinking the concepts of vulnerability and risk from a holistic perspective: A necessary review and criticism for effective risk management. In G. Bankoff, G. Frerks, & D. Hilhorst (Eds.), *Mapping vulnerability: Disasters, development*

*and people*. London: Earthscan Publishers. Retrieved from https://www.researchgate.net/publication/254267457

Carr, L. D., Pricope, G. N., Aukema, E. J., Jankowska, M. M., Funk, C., Husak, G., & Michaelsen, J. (2014, March 6th). A spatial analysis of population dynamics and climate change in Africa: potential vulnerability hotspots emerge where precipitation declines and demographic pressures coincide. *Population and Environment, 35*, 323-339. doi:https://doi.org/10.1007/s11111-014-0209-0

Caruana, J. E., Marius, R., Sanchez, H. J., & Solli, P. (2015, October 9th). Longitudinal studies. *Thoracic Disease, 7*(11), 537-545. doi:https://doi.org/10.3978/j.issn.2072-1439.2015.10.63

Chen, W., Cutter, S. L., Emrich, C. T., & Shi, P. (2013). Measuring social vulnerability to natural hazards in the Yangtze river delta region, China. *International journal of disaster risk science, 4*(4), 169-181. doi:10.1007/s13753-013-0018-6

Conlon, K. C., Mallen, E., Gronlund, C. J., Berrocal, V. J., Larsen, L., & O'Neill, M. S. (2020, September). Mapping human vulnerability to extreme heat: A critical assessment of heat vulnerability indices created using Principal Component Analysis. *Environmental health perspectives, 128*(9). doi:https://doi.org/10.1289/EHP4030

Connor, M. A. (2015). Metropolitan Secession and the Space Color-Blind Racism in Atlanta. *Journal of Urban Affairs, 37*(4), 436-461. doi:https://doi.org/10.1111/juaf.12101

Cooley, H., Moore, E., Heberger, M., & Allen, L. (2012, July). Social vulnerability to climate change in California. Retrieved from https://pacinst.org/wp-content/uploads/2012/07/social-vulnerability-climate-change-ca.pdf

Cutter, L. S., Boruff, J. B., & Shirley, L. W. (2003, June). Social vulnerability to environmental hazards. *Social Science Quarterly, 84*(2). doi:https://doi.org/10.1111/1540-6237.8402002

Cutter, S. L., Emrich, C. T., Webb, J. J., & Morath, D. (2009). *Social vulnerability to climate variability hazards: A review of the literature.* Final report, Oxfam America, Hazard and Vulnerability Research Institute. Retrieved from https://citeseerx.ist.psu.edu/viewdoc/download?doi=10.1.1.458.7614&rep=rep1&type=pdf

Dintwa, K. F., Letamo, G., & Navaneetham, K. (2019, May 6). Measuring social vulnerability to natural hazards at the district level in Botswana. *Jàmbá: Journal of Disaster Risk Studies, 11*(1). doi:https://doi.org/10.4102/jamba.v11i1.447

Eakin, H., & Luers, A. L. (2006, July 18). *Annual Review of Environment and Resources, 31*, 365-394. doi:10.1146/annurev.energy.30.050504.144352

Eisenman, D. P., Wilhalme, H., Tseng, C.-H., Chester, M., English, P., Pincetl, S., . . . Dhaliwal, S. K. (2016). Heat death associations with the built environment, social vulnerability and their interactions with rising temperature. *Health and Place, 41*, 89-99. doi:http://dx.doi.org/10.1016/j.healthplace.2016.08.007

Evans, J. M., Hardy, D., & Hauer, M. (2014). *Social vulnerability and local hazard mitigation planning: Application and evaluation of a "SoVI-Lite" approach for Glynn County, Georgia.* Carl Vinson Institute of Government, University of Georgia, Athens. doi:10.13140/2.1.2017.0566

Flanagan, B. E., Gregory, E. W., Hallisey, E., Heitgerd, J. L., & Lewis, B. (2011). A social vulnerability index for disaster management. *Journal of Homeland Security and Emergency Management, 8*(1). doi:https://doi.org/10.2202/1547-7355.1792

Flanagan, B. E., Hallisey, E. J., Adams, E., & Lavery, A. (2018). Measuring community vulnerability to natural and anthropogenic hazards: The Centers for Disease Control and Prevention's social vulnerability index. *80*(10), 34-36. Retrieved from https://svi.cdc.gov/Documents/Publications/CDC_ATSDR_SVI_Materials/JEH2018.pdf

Fothergill, A., & Peek, L. A. (2004). Poverty and disasters in the United States: A review of recent sociological findings. *Natural Hazards, 32*, 89-110. doi:https://doi.org/10.1023/B%3ANHAZ.0000026792.76181.D9

Goodling, E., Jamaal, G., & McClintock, N. (2015). Uneven development of the sustainable city: shifting capital in Portland, Oregon. *Urban Geography, 36*(4), 504-527. doi:http://dx.doi.org/10.1080/02723638.2015.1010791

Hansen, A., Bi, L., Saniotis, A., & Nitschke, M. (2013, July 29). Vulnerability to extreme heat and climate change: is ethnicity a factor? *Global Health Action, 6*(1). doi:https://doi.org/10.3402/gha.v6i0.21364

Harlan, S. L., Declet-Barreto, J. H., Stefanov, W. L., & Petitti, D. B. (2013, February). Neighborhood effects on heat deaths: Social and environmental predictors of vulnerability in Maricopa County, Arizona. *Environmental Health Perspectives, 121*(2), 197-204. doi:http://dx.doi.org/10.1289/ehp.1104625

Hayden, M. H., Brenkert-Smith, H., & Wilhelmi, O. (2011). Differential adaptive capacity to extreme heat: A Phoenix, Arizona, case study. *American Meteorological Society, 3*, 269-280. doi:10.1175/WCAS-D-11-00010.1

Ho, H. C., Knudby, A., & Huang, W. (2015, December 18). A Spatial Framework to Map Heat Health Risks at Multiple Scales. *International Journal of Environmental Research and Public Health, 12*, 16110-16123. doi:10.3390/ijerph121215046

Ho, H. C., Knudby, A., Chi, G., Aminipouri, M., & Lai, D. Y.-F. (2018). Spatial-Temporal Analysis of Regional Socio-Economic Vulnerability Change Associated with Heat Risks in Canada. *Applied Geography, 95*, 61-70. doi:https://doi.org/10.1016/j.apgeog.2018.04.015

Holand, I. S., Lujala, P., & Rød, J. K. (2011). Social vulnerability assessment for Norway: A quantitative approach. *Norwegian Journal of Geography, 65*, 1-17. doi:10.1080/00291951.2010.550167

Hondula, D. M., Davis, R. E., Leisten, M. J., Saha, M. V., Veazey, L. M., & Wegner, C. R. (2012). Fine-scale spatial variability of heat-related mortality in Philadelphia County, USA, from 1983-2008: a case series analysis. *Environmental Health, 11*(16). doi:http://www.ehjournal.net/content/11/1/16

Juntunen, L. (2006). Addressing social vulnerability to hazards. *TsuInfo Alert, 8*(2). Retrieved from https://file.dnr.wa.gov/publications/ger_tsuinfo_2006_v8_no2.pdf

Karanja, J., & Kiage, L. (2021). Perspectives on spatial representation of urban heat vulnerability. *Science of the Total Environment, 774*. doi:https://doi.org/10.1016/j.scitotenv.2021.145634

Kashem, B. S., Wilson, B., & Zandt, V. S. (2016, January). Planning for climate adaptation: evaluating the changing patterns of social vulnerability and adaptation challenges in three coastal cities. *Journal of Planning Education and Research, 36*(3), 304-318. doi:https://doi.org/10.1177/0739456X16645167

Kim, D. W., Deo, R. C., Lee, J. S., & Yeom, J. M. (2017, June 5th). Mapping Heat Vulnerability in Korea. *Natural Hazards, 89*, 35-55. doi:10.1007/s11069-017-2951-y

Kruse, K. M. (2005, July). The politics of race and public space: Desegregation, privatization and the tax revolt in Atlanta. *Journal of Urban History, 31*(5), 610-633. doi:https://doi.org/10.1177%2F0096144205275732

Lee, Y. J. (2014). Social Vulnerability Indicators as a Sustainable Planning Tool. *Environmental Impact Assessment Review, 44*, 31-42. doi:http://dx.doi.org/10.1016/j.eiar.2013.08.002

Lo, C. P., & Quattrochi, A. (2003, September). Land Use and Land Cover Change, Urban Heat Island Phenomenon, and Health Implications: A Remote Sensing Approach. *Photogrammetric Engineering and Remote Sensing, 69*(9), 1053-1063. doi:https://doi.org/10.14358/PERS.69.9.1053

Macnee, G. R., & Tokai, A. (2016, August). Heatwave vulnerability and exposure mapping for Osaka Japan. *Journal on Environmental systems and decisions, 36*, 368-376. doi:https://doi.org/10.1007/s10669-016-9607-4

Maier, G., Grundstein, A., Jang, W., Li, C., Naeher, L. P., & Shepherd, M. (2014, April). Assessing the Performance of a Vulnerability Index During Oppressive Heat Across Georgia, United States. *6*, 253-263. doi:10.1175/WCAS-D-13-00037.1

Markley, S. N., Hafley, T. J., Allums, C. A., Holloway, S. R., & Chung, H. C. (2020). The limits of homeownership: Racial capitalism, Black wealth, and the appreciation gap in Atlanta. *International Journal of Urban and Regional Research*. doi:https://doi.org/10.1111/1468-2427.12873

Mendes, J. d. (2009, January). Social vulnerability indexes as planning tools: beyond the preparedness paradigm. *Journal of Risk Research, 12*(1), 43-58. doi:https://doi.org/10.1080/13669870802447962

Mitchell, B. C., & Chakraborty, J. (2014, October). Urban Heat and Climate Justice: A Landscape of Termal Inequity in Pinellas County, Florida. *Geographical Review, 104*, 459-480. doi:https://doi.org/10.1111/j.1931-0846.2014.12039.x

Nayak, S. G., Shrestha, S., Kinney, P. L., Ross, Z., Sheridan, S. C., Pantea, C. I., . . . Hwang, S. A. (2018). Development of a Heat Vulnerability Index for Newyork State. *Public Health, 161*, 127-137. doi:https//:doi.org/10.1016/j.puhe.2017.09.006

Ployhart, E. R., & Vandenberg, J. R. (2010, January). Longitudinal research: the theory, design, and analysis of change. *Journal of Management, 36*(1), 94-120. doi:https://doi.org/10.1177/0149206309352110

Reid, C. E., Gronlund, C. J., O'Neill, M., Brines, S. J., Brown, D. G., Diez-Roux, A. V., & Shwartz, J. (2009, November). Mapping Community Determinants of Heat Vulnerability. *Environmental Health Perspectives, 117*(11), 1730-1735. doi:https://doi.org/10.1289/ehp.0900683

Shelton, T. (2018). Rethinking the RECAP: mapping the relational geographies of concentrated poverty and affluence in Lexington, Kentucky. *Urban Geography, 39*(7), 1070-1091. doi:https://doi.org/10.1080/02723638.2018.1433927

US Government. (2011). *The financial crisis inquiry report.* Official Government edition, Financial crisis inquiry commission. Retrieved from https://www.govinfo.gov/content/pkg/GPO-FCIC/pdf/GPO-FCIC.pdf

Wilson, B., & Chakraborty, A. (2019). Mapping Vulnerability to Extreme Heat Events: Lessons from Metropolitan Chicago. *Journal of Environmental Planning and Management, 62*(6), 1065-1088. doi:https://doi.org/10.1080/09640568.2018.1462475

Yong, A. G., & Pearce, S. (2013). A beginner's guide to factor analysis: Focusing on exploratory factor analysis. *Tutorials in quantitative methods for psychology, 9*(2), 79-94. doi:10.20982/tqmp.09.2.p079

Zhang, W., Zhao, Q., & Pei, M. (2021). How much uncertainty does the choice of data transforming methods brings to heat risk mapping? Evidence from China. *Natural Hazards, 106*, 349-373. doi:https://doi.org/10.1007/s11069-020-04466-y

Zhou, Y., Li, N., Wu, W., Wu, J., & Shi, P. (2014). Local Spatial and Temporal Factors Influencing Population and Societal Vulnerability to Natural Disasters. *Risk Analysis, 34*(4), 614-639. doi:10.1111/risa.12193

**Data Reference:**

Manson, S., Schroeder, J., Riper, D. V., Kugler, T., & Ruggles, S. (2020). IPUMS National Historical Geographic Information System: Version 15.0 [datasets]. Retrieved from http://doi.org/10.18128/D050.V15.0

# CHAPTER 4

## Comparing Integrated Metrics of Heat Vulnerability using Multiple Weighting Mechanics

### 4.0 Synopsis

Extreme heat events are among the climate change-related hazards that affect urbanized environments in many parts of the world. Heat hazards are likely to increase in frequency and magnitude, augmenting heat-related population morbidity and mortality depending on exposure and adaptive capacities. Heat metrics, constructed from socioeconomic indicators, biophysical variables, and composites, seek to mainstream heat susceptibility to policymaking. However, there is no scientific consensus about the accuracy and precision of these metrics. Data transformation techniques, especially weighting mechanics, influence the intensity and spatial distribution of hotspots. In this study, we used composite images to determine the extent to which the weighting mechanics moderate composite heat metrics in Atlanta, Southeastern North America. Land Surface Temperature-Based (LST)-based composites indicated increased spatial vulnerability in Atlanta concentrated in urban core counties and encroaching to the suburbs. Our findings show that the integrated spectral indices through a PCA approach do not combine additively and return different results from LST composites. The magnitude of vulnerability change was higher for the LST biophysical metric than its composites, attributed to the moderating effects of the SoVI. All the composites comprising the spectral indices and the SoVI reduced vulnerability. All the metrics, biophysical or composites visualized core metro areas with disproportionately concentrated hotspots. Although the spectral indices are correlated to the LST, their weighting should receive scrutiny despite the absence of systematic conceptual frameworks, given the disparate results established in this study.

INDEX WORDS: Biophysical heat metrics, spectral indices, weighting mechanics, integrated indices, Moran's index, Land Surface Temperature (LST).

**Highlights:**

- Weighting mechanics moderate the intensity and spatial distribution of composite heat metrics.
- Integrated spectral indices do not combine additively, thus not an ideal proxy for LST
- The core metro counties in Atlanta are increasingly susceptible, portraying high sensitivity and exposure to heat.
- Weighting mechanics at the SoVI level, and the biophysical-SoVI integration level, impact the spatial distribution of exposure and sensitivity

## 4.1 Introduction

Extreme heat events have been shown to increase mortality in the United States by 3.7%, especially in urban areas, where more than 80% of the population resides (Atyia, 2015; Bera, 2019). Urban areas are 6°C to 8°C warmer than surrounding rural locations (Weber et .2015), a hallmark of the Urban Heat Island (UHI) phenomena (Adeyeye et al., 2019: Berko et al.,2014; EPA, 2006; Wang et al., 2019). The average global temperature in 2019 was close to 1°C greater than pre-industrial times, and the cascading ramifications will be profound if continued warming remains unmitigated (Habeeb et al., 2015). Extreme heat events are projected to increase in intensity, frequency, duration, and magnitude, creating pockets of thermal inequality (Berko et al., 2014; Habeeb et al., 2015; Harlan et al., 2013). The combined effects of local warming resulting from the built environment and increasing global temperatures resulting from greenhouse gas emissions raise concerns for heat-related morbidity and mortality across urban areas. Heat hazard is arguably the deadliest weather-related hazard (Johnson et al., 2012; Maier et al., 2014; Shepherd

and Zhou, 2009; Sheridan and Dolney, 2004). Environmental health studies have consistently shown a strong relationship between temperature-related metrics and a wide range of health outcomes (c.f., Chuang and Gober, 2015; Harlan et al., 2013; Hondula et al., 2015; Maier et al., 2014). However, scientific consensus about the metrics' accurate and precise characterization remains inconclusive (Chuang and Gober., 2015; Eakin and Luers, 2006: Tate 2013). Varied use of surface metrics, near-surface metrics, original variables versus principal components, and/or various metrics combinations has accelerated the urgency for novel, comprehensive and comparative approaches geared toward mainstreaming heat vulnerability in policymaking (Wolf et al., 2015). Variable weighting problems have marred attempts to visualize combined heat vulnerability indices and scale incompatibility between demographic datasets and satellite datasets that compound the modifiable areal unit problem (MAUP) (Ho et al., 2015). Data transformation techniques have been found to deplete the authenticity of individual suites of variables (Kashem et al., 2016). The evaluation of disparate weighting schemes has received little attention yet could influence the intensity and accuracy of derived metrics, limiting the applicability of outputs from heat vulnerability studies (Brenkert and Malone, 2005; Turner II et al., 2003). Our research explores how the social vulnerability weighting mechanics impact the nature of composite indices when coupled with the biophysical metric. We seek to answer how the spectral indices combine to characterize heat. Apart from this, we explore how the composite heat metrics have evolved spatially and temporally in Atlanta. We determine how the SoVI combines with spectral indices, and we compare LST-based metrics with spectral indices-based metrics.

Several studies have used various spectral indices, including the Normalized Difference Vegetation Index (NDVI), Normalized Difference Bareness Index (NDBaI), Normalized Difference Water Index (NDWI), and Normalized Difference Built-up Index (NDBI) (Harlan et

al., 2013; Jonsonn and Lundgren, 2015; Mushore et al., 2018) to characterize heat. These indices have been used as proxies for the LST or independently to denote heat, yet little is known whether they integrate additively. Composite metrics have been developed to remedy the shortcomings associated with either the SoVI or the exposure metrics. To date, the relative importance of weighting either index remains unknown (Tate, 2013), yet they are integral for policy prioritization (Harlan et al., 2013: Wolf et al., 2015). These studies use single scene imagery, which could be unrepresentative. However, Pelta and Chudnvosky (2017) concluded that a single satellite overpass provides a good relative metric of the actual day's temperature conditions. Despite this assertion, a single snapshot may not capture episodic heat events and general patterns of exposure. Although the surface temperature was found helpful in determining the most exposed (Harlan et al., 2013), incorporating social-economic dimensions provides an additional analytical perspective (Karanja and Kiage, 2021). The expanded portfolio for vulnerability representation that we adopt in this study is a salient approach that narrows the gap between geographical visualization and policy development (Hondula et al., 2015: Wolf et al., 2015). Current literature overly focuses on vulnerability identification and not its evolution temporally (Carr et al., 2014); hence our study analyzes between 2000 and 2019 to understand vulnerability dynamics that are manifestly longitudinal (Caruana et al., 2015).

## 4.2 Methodology

### *4.2.1 Area of Study*

The study was conducted in Atlanta, covering 22 counties in the urban core, suburban, and periphery regions (figure 4-1). Understanding intra-urban variations and focusing on the major cities is critical, given massive populations reside (Berko et al., 2014: Wolf et al., 2015). Furthermore, Atlanta is likely to experience an accelerated heatwave magnitude of between 4°C

and 5°C from simulations (Broadbent et al., 2020). Urban heat episodes vary in space and time, and city expansion in isolation could account for augmented temperature conditions between 1°C and 2°C (Georgescu et al., 2014). Besides, Habeeb et al. (2015) established that Atlanta would experience more frequent heat events that would last longer. The core counties of Fulton, DeKalb, and Cobb were found to experience a higher heat vulnerability index (Maier et al., 2014). The US Department of Housing (2018) indicated a growing population in Atlanta attributed to emerging job prospects. This city is bound to grow in size, complexity, and population, which potentially indicates accelerated vulnerability to disasters (Borden et al., 2007). Historical weather analysis by Shepherd and Zhou (2009) verified that Atlanta is susceptible to extreme heat with a mean UHI of $1.31^{0}$C between 1984-2007. Heat susceptibility was highly clustered in metro Atlanta (Sunhui, 2017). Given the city status as a premium commercial, transportation hub and industrial capital of the South (Lo and Quattrochi, 2003), it is justifiable to understand how vulnerability manifests, how the changes and their consequences are amplified and attenuated, and how the biophysical and socioeconomic interact to create pockets of thermal inequality.

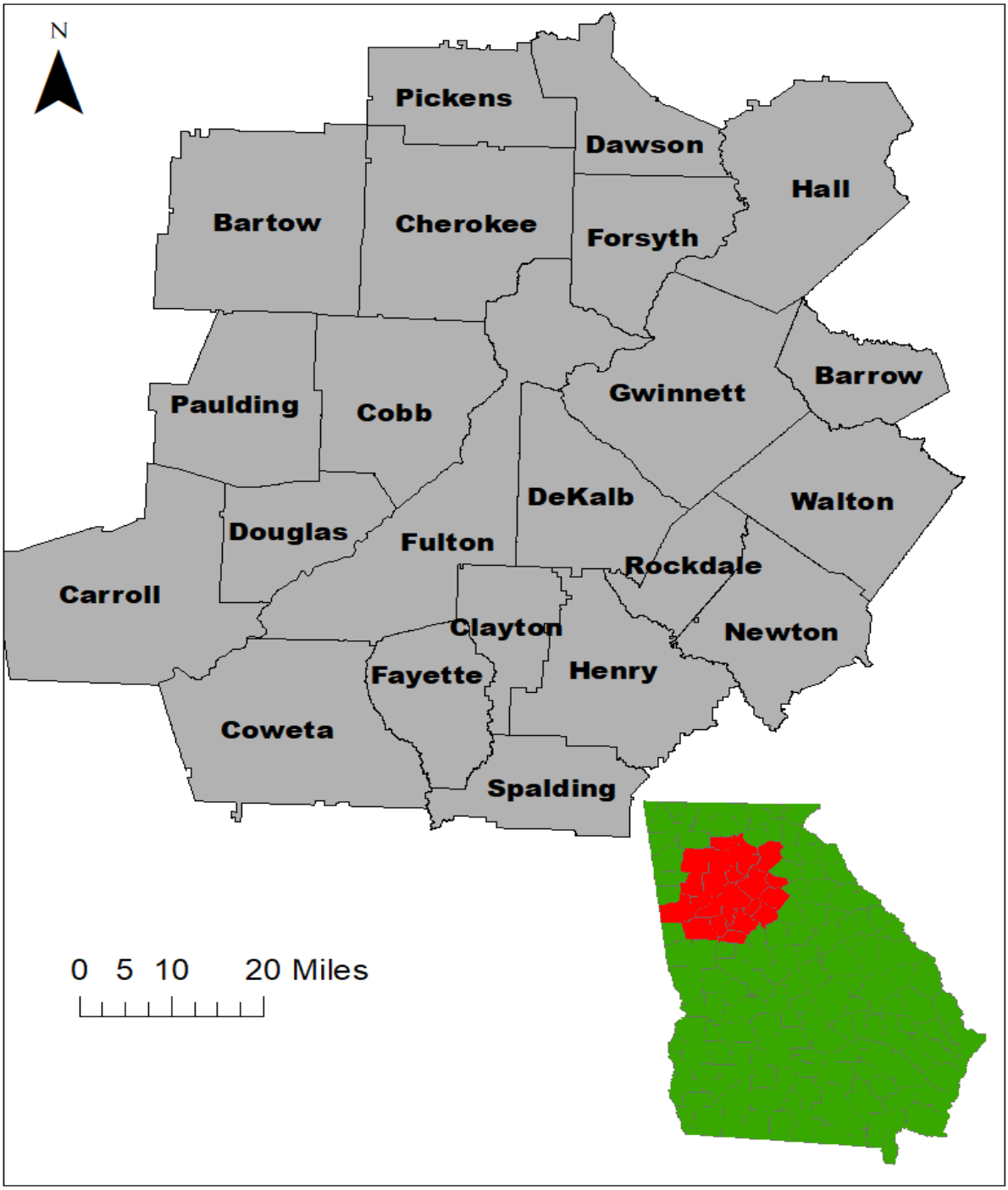


Figure 4-1. Area of study covering 17,686 km$^2$ for 22 metro Atlanta Counties allows for comparative analysis of heat evolution for Atlanta city core, suburban locations, and the city periphery.

### *4.2.2 Data Acquisition and Analysis*

Image data were acquired from the Google Earth Engine (GEE) (Gorelick et al., 2017) by modifying the LST computation code for the Landsat series (e.g., Ermida et al., 2020) to include the computation of the four indices of the NDVI, NDBI, NDWI, and NDBaI using band combination formulae (Bramhe et al., 2018; Mushore et al., 2018; Tran et al., 2018). The images covered the warmest periods of the year, between 20$^{th}$ May to 10$^{th}$ September for each period, capturing early summer to late summer. The study deviates from previous computations (e.g., Harlan et al., 2013; Ho et al., 2015; Mushore et al., 2018) that predominantly use a single sensor scene by aggregating all available images for a determined date range, resulting in a composite image. The composite images were generated, translating to minimal missing data points and leveraging on mean conditions across time. Extraction based on the average value ensured the inclusion of outliers, potentially capturing the extreme heat events. The data were masked for clouds, water, and other atmospheric substances (Ermida et al., 2020). The periods for biophysical analysis were informed by time-series data for generation of Social Vulnerability Index (SoVI) from the American Community Survey (ACS) five-year estimates (2000, 2005-2009, 2010-2014, and 2015-2019). We picked the years 2000, 2007, 2011, and 2019 for the biophysical analysis. 2007 was selected as it was the first mid-point year for the first ACS 5-year estimate. 2019 was preferred over 2017 and 2018 because it had more data points and was proximal to the most recent year of the ACS series selected. There were no satellite datasets for 2012 while 2013 images had numerous cloudy pixels; thus, the 2011 dataset was preferred. The specific codes for the acquisition and computation of the LST and the spectral indices are shown below.

2000: https://code.earthengine.google.com/446612503c34984b43e84f76da6ab74e

2007: https://code.earthengine.google.com/73f56852c117e65b5f7716ddd01cf2fa

2011: https://code.earthengine.google.com/5a5919389f695993f9c31f8f0ece08ed?hl=it

2019: https://code.earthengine.google.com/769632b37df75c05672abd34d83eb6dc?hl=it

Landsat 5 Thematic Mapper was used for 2000, 2007, and 2011 while Landsat 8 Thermal Infrared Sensors (TIRS) was used for 2019. The following band combinations were used to generate the indices: NDVI (Near Infrared and Red), NDBI (Shortwave Infrared and Near Infrared), NDWI (Near Infrared and Shortwave Infrared), NDBaI (Shortwave Infrared and Thermal Infrared) using the formulae shown below:

NDVI = (NIR – Red) / (NIR + Red)

NDBI = (SWIR – NIR) / (SWIR + NIR)

NDWI = (NIR – SWIR) / (NIR + SWIR)

NDBaI= (SWIR – TIR) / (SWIR + TIR)

All the rasters were clipped through extraction by mask using a feature class layer covering the 22 counties that constitute the urban, suburban, and periphery of Atlanta, including: Pickens, Dawson, Cherokee, Bartow, Cobb, Paulding, Douglas, Carroll, Coweta, Fayette, Fulton, Clayton, Spalding, Henry, Rochdale, Newton, DeKalb, Gwinnett, Walton, Barrow, Hall, and Forsyth, allowing for spatial comparison with distance from the urban core. Two metrics were derived to characterize the biophysical vulnerability, based on LST (Ho et al., 2015) and the other based on spectral indices (Mushore et al., 2018). To visualize LST, we rescaled the rasters to range between 0 and 1, using maximum-minimum normalization for consistent comparison of changes over time using the formula ((raster-minimum) / (maximum-minimum)) (e.g., Dintwa et al., 2019). The normalized LST rasters were reclassified into five classes with a uniform class interval of 0.2. The missing data values were assigned the value 99, while the other classes were assigned values between 1 and 5, representing very low vulnerability and very high vulnerability, respectively. The

reclassification process outputs were then extracted by mask to eliminate the background pixels and the processing extent specified using the study location's polygon's layer area. The proportions of pixels in each class were then computed to establish the changes between 2000 to 2019. The missing data points were symbolized using a dark shade. The second biophysical metric entailed conducting a PCA on the indices and determining whether they work additively and whether they could result in an integrated biophysical metric, a robust proxy for the LST representing multiple land cover characteristics. Each retained component was multiplied by the equivalent eigenvector and summed up to derive the integrated spectral index.

We generated four composites using disparate weighting mechanics. The first composite integrated LST with SoVI derived using a raster model for equal weighting (Ho et al., 2015; Ho et al., 2018). The second composite consisted of LST and raster-based SoVI through variance explained. The goal was to determine how SoVI weighting mechanics impact heat metrics for integrative models. The LST and the SoVIs were assigned an equal weighting of 50% each, using a weighted sum tool, which supports floating rasters. The LST-based composites were reclassified into five equal interval classes, masked for background pixels, and the percentage of pixels in each category was computed. Zonal statistics were computed using the mean value, and both the local and global Moran's I tracked over time to visualize hotspots (Kashem et al., 2016; Zhou et al., 2014). The third composite metric was generated by combining the spectral indices and the SoVI and subjected to the weighted sum tool (Mushore et al., 2018). In the weighted sum analysis, each spectral index and the SoVI were apportioned each 20% weighting. The indices were first rescaled between 0 and 1 using the maximum-minimum normalization to guarantee internal data consistency before summing them up. The NDVI and NDWI were inverted to ensure high values translated to high vulnerability since they are negatively correlated to the LST (Mushore et al.,

2018: Sunhui, 2017). The rasters were inverted using the formula shown below from **https://support.esri.com/en/technical-article/000006694,** (("Rasterlayer" - Maximum_value) * -1) + Mininimum_value. The proportion of pixels in the various classes was computed and compared across time. Zonal statistics to extract the mean value were conducted, and then the global and local Moran's I indices were computed to establish the hotspots and their changes over time. The fourth composite was PCA-based, where the spectral indices and the SoVI were all subjected to data reduction. The goal was to determine how PCA-based weighting differs from the other weighting mechanics and the relationships among the biophysical and socioeconomic indices.

## 4.3 Results

### *4.3.1 Land Surface Temperature*

The LST trends indicated a progressive increase in heat vulnerability, with many areas shifting from low to moderate exposure using equal interval classification. The percentage of pixels in the low category reduced from 57% in 2000 to 29% in 2019 (table 4-1). Simultaneously, the percentage of pixels in the moderate class increased from 42% to 70%. 2019 did not record pixels in the very low category. The high class generally had an increasing pattern with a marginal dip between 2011 and 2019. No significant changes were observed in the high and very high classes. The mean of the LST surfaces increased across time, with 2000 having the lowest average temperatures in Kelvin while 2019 had the highest. The minimum and maximum temperature values also increased, signifying higher intensity. High-High clusters were concentrated in core metro counties whose spatial distribution increased over the period of study. There was consistency in the patterns of the Global Moran's I and the mean value of the LST surfaces. The percentage of census tracts in the High-High clustering increased over the period but did not fit the trends of the Global Moran's I. Low-Low clustering trend also increased across time. Low-High clustering and High-Low clustering hardly accounted for 15% of the census tracts. Locations of non-significant clusters reduced, mostly transitioning to Low-Low clusters, followed by High-High clusters. The spatial distribution of the hotspots varied over time. For 2000, the hotspots were further South of Atlanta, predominantly in Spalding, Henry, and Clayton. The core metro counties of DeKalb and Fulton had a blend of High-High clustering and Low-High clusterings. Gwinnett, Rockdale, and central Cobb also had pockets of High-High clustering. For 2007, vast sections of Spalding and Clayton transitioned to areas of no significant clustering and cold spots. The Hotspots emerged in Fulton, DeKalb, Gwinnett, and parts of Forsyth. The exposure increased in Rockdale,

Bartow, and Forsyth, while it shrunk in Cobb. In 2011, the hotspots for 2007 expanded further southwards to Clayton and Henry and advanced further North to Cobb. A similar pattern was observed in 2019, only that High-High clusters reduced towards the South but advanced towards the North Eastern section of the map encompassing Gwinnett and Forsyth (figure 4-2).

Table 4-1. Analysis of the LST using equal interval classification, local and global Moran's I

| | 2000 | 2007 | 2011 | 2019 |
|---|---|---|---|---|
| **Equal Interval Classification** | | | | |
| Very low | 0.003 | 0.002 | 0.001 | 0.000 |
| Low | 57.055 | 47.432 | 40.638 | 29.255 |
| Moderate | 42.409 | 52.286 | 58.458 | 70.093 |
| High | 0.441 | 0.229 | 0.847 | 0.606 |
| Very high | 0.002 | 0.000 | 0.004 | 0.002 |
| Missing pixels | 0.090 | 0.051 | 0.052 | 0.043 |
| Mean (Kelvins) | 303.53 | 304.27 | 305.13 | 305.70 |
| **Local and Global Moran's I** | | | | |
| Global Moran's | 0.334 | 0.480 | 0.576 | 0.619 |
| % High-High clustering | 32.46 | 28.80 | 32.71 | 36.89 |
| % High-Low clustering | 2.49 | 1.32 | 2.19 | 1.67 |
| % Low-High clustering | 12.43 | 11.11 | 11.60 | 10.03 |
| % Low-Low clustering | 16.52 | 13.89 | 21.53 | 23.51 |
| % No significant clusters | 36.10 | 44.88 | 31.97 | 27.90 |

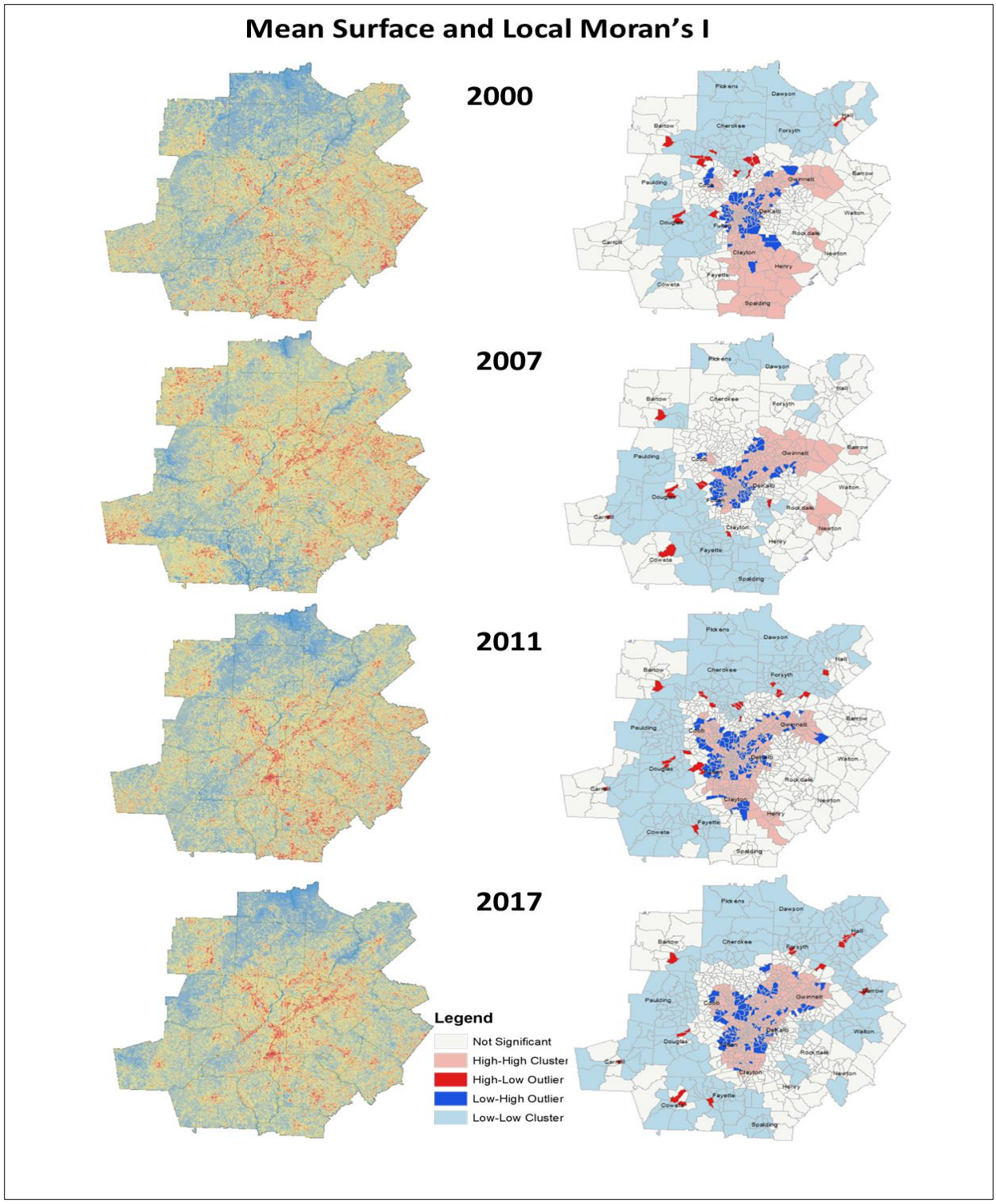


Figure 4-2. Core metro counties are consistently disproportionately exposed where most of the hotspots are located. The Southern county of Spalding progressively transitioned to a coldspot. The Hotspots expanded towards the North Eastern section while the coldspots emerged towards the periphery. The suburbs progressively shifted to areas of no significant clusters.

### *4.3.2 Integrated Spectral Index*

The integrated spectral index constituting the NDVI, NDBI, NDBaI, and NDWI, PCA analysis resulted in the retention of 2 components across the analysis periods, which accounted for approximately 98% of the cumulative percentage variance. Component 1 accounted for about 80.6%, while component 2 explained nearly 18% for 2000, 2007, and 2011. Slight variation occurred in 2019, with component 1 explaining 73%, whereas component 2 accounted for 24.7%. For the entire period, the NDBaI essentially explained component 1, followed by the NDBI and NDWI that had equivalent loadings but with inverse direction of influence (table 4-2). The NDBI and NDWI dominantly explained component 2 with equal loadings, yet opposite in influence. The NDBaI and NDVI also had high loadings for component 2, with the former consistently having a higher load than the latter, although influencing inversely. Equal interval classification demonstrated reduced vulnerability for the integrated spectral metric with 73.48% of the census tracts in the very low class in 2019. The mean value of the raster surfaces also decreased across the period (table 4-3). There was no discernible trend for spatial autocorrelation. The local Moran's I indicated significant clustering in the High-High, and Low-Low, although areas of no significant clustering accounted for nearly 50% of the census tracts across the period.

Table 4-2. Loadings of Spectral Indices on the components

| Period | 2000 | | | | 2007 | | | | 2011 | | | | 2019 | | | |
|---|---|---|---|---|---|---|---|---|---|---|---|---|---|---|---|---|
| CPNTs | 1 | 2 | 3 | 4 | 1 | 2 | 3 | 4 | 1 | 2 | 3 | 4 | 1 | 2 | 3 | 4 |
| NDBaI | 1.00 | 0.83 | -0.33 | -0.83 | 1.00 | 0.85 | -0.36 | -0.85 | 1.00 | 0.85 | -0.35 | -0.85 | 1.00 | 0.67 | -0.23 | -0.67 |
| NDBI | 0.83 | 1.00 | -0.72 | -1.00 | 0.85 | 1.00 | -0.73 | -1.00 | 0.85 | 1.00 | -0.73 | -1.00 | 0.67 | 1.00 | -0.79 | -1.00 |
| NDVI | -0.33 | -0.72 | 1.00 | 0.72 | -0.36 | -0.73 | 1.00 | 0.73 | -0.35 | -0.73 | 1.00 | 0.73 | -0.23 | -0.79 | 1.00 | 0.79 |
| NDWI | -0.83 | -1.00 | 0.72 | 1.00 | -0.85 | -1.00 | 0.73 | 1.00 | -0.85 | -1.00 | 0.73 | 1.00 | -0.67 | -1.00 | 0.79 | 1.00 |

Key: CPNTs = Components

Table 4-3. Breakdown of equal interval classification, local and global Moran′s I for integrated spectral index

| | 2000 | 2007 | 2011 | 2019 |
|---|---|---|---|---|
| Global and Local Moran's I | | | | |
| Spatial Autocorrelation | 0.60 | 0.65 | 0.48 | 0.59 |
| Z-score | 75.02 | 80.90 | 73.91 | 90.79 |
| Mean | 0.44 | 0.43 | 0.35 | 0.16 |
| High-High clustering | 23.68 | 20.32 | 20.48 | 25.18 |
| High-Low clustering | 1.90 | 2.63 | 2.51 | 2.09 |
| Low-High clustering | 9.94 | 8.92 | 9.20 | 11.18 |
| Low-Low clustering | 14.62 | 18.13 | 9.19 | 19.85 |
| No significant clustering | 49.85 | 50.00 | 49.63 | 41.69 |
| Equal Interval Classification | | | | |
| Very low | 0.000 | 0.000 | 0.002 | 73.480 |
| Low | 45.833 | 47.534 | 72.505 | 26.197 |
| Moderate | 46.517 | 51.166 | 27.354 | 0.305 |
| High | 7.492 | 1.268 | 0.108 | 0.000 |
| Very high | 0.039 | 0.003 | 0.003 | 0.000 |
| Missing pixels | 0.069 | 0.028 | 0.028 | 0.018 |

### *4.3.3 LST-Based Composites*

The composite index constituting LST with two different raster-based SoVIs returned different spatial distributions across classes but demonstrated a consistent increasing heat vulnerability trend. The Eigen-based SoVI consistently showed a reduction of the low category from 70.7% in 2000 to 54.7% in 2019 (table 4-4). The equally weighted SoVI saw a marginal decrease from 53.4% to 45.1% in the same period, albeit with lower proportions in 2007 and 2011. The moderate class proportion increased consistently for Eigen weighted SoVI from 28.9% to 45.1%, while equal weighting was from 46.2% to 54.7%. The variance-based SoVI had lower proportions consistently for the moderate class and consistently higher proportions in the low class than equal-weighted SoVI. The magnitude of change was lower for both LST-based integrated metrics compared to the LST biophysical metric. The Anselin's local Moran's I generally indicated an increased number of tracts in the High-High clustering with the variance-based SoVI

occasionally having higher proportions. Trends of increases and decreases of spatial autocorrelation were similar to that of Local Moran's I. However, a heightened global Moran's I did not invariably translate to more clustering for High-High class for equally weighted SoVI, unlike the Variance-based SoVI.

Table 4-4. Results of the LST-based composites using different SoVIs

| | Eigen weighted SoVI + LST | | | | Equally weighted SoVI + LST | | | |
|---|---|---|---|---|---|---|---|---|
| | 2000 | 2007 | 2011 | 2019 | 2000 | 2007 | 2011 | 2019 |
| Very Low | 0.000 | 0.000 | 0.000 | 0.000 | 0.000 | 0.000 | 0.000 | 0.000 |
| Low | 70.753 | 59.325 | 55.049 | 54.769 | 53.451 | 36.399 | 42.706 | 45.127 |
| Moderate | 28.929 | 40.459 | 44.806 | 45.108 | 46.251 | 63.448 | 57.179 | 54.740 |
| High | 0.139 | 0.077 | 0.067 | 0.043 | 0.119 | 0.015 | 0.027 | 0.053 |
| Very High | 0.000 | 0.000 | 0.000 | 0.000 | 0.000 | 0.000 | 0.000 | 0.002 |
| Missing pixels | 0.179 | 0.139 | 0.078 | 0.079 | 0.179 | 0.139 | 0.088 | 0.079 |

Global and Local Moran's I

| | H-H | H-L | L-H | L-L | NS | SA |
|---|---|---|---|---|---|---|
| 2000 EW | 22.51 | 1.46 | 8.19 | 20.03 | 47.81 | 0.30 |
| 2000 VE | 28.07 | 1.75 | 10.67 | 19.59 | 39.91 | 0.34 |
| 2007 EW | 20.61 | 3.80 | 3.80 | 24.27 | 46.64 | 0.24 |
| 2007 VE | 20.61 | 1.61 | 6.87 | 16.67 | 54.24 | 0.28 |
| 2011 EW | 29.78 | 3.87 | 10.03 | 22.88 | 33.33 | 0.36 |
| 2011 VE | 29.89 | 4.39 | 15.20 | 30.70 | 47.81 | 0.35 |
| 2019 EW | 31.35 | 2.93 | 8.78 | 18.27 | 38.67 | 0.27 |
| 2019 VE | 31.35 | 3.13 | 8.36 | 23.51 | 33.65 | 0.39 |

Key: EW (Equal Weighting), VE (Variance Explained) H-H (High-High), L-H (Low-High), L-L (Low-Low), NS (No Significant), SA (Spatial Autocorrelation)

### *4.3.4 PCA-Based Composites*

PCA-Based Composite (Spectral Indices and SoVI) retained 3 components across the entire period accounting for approximately 98% of the total variance. Component 1 ranged between 71.5% and 73.3% for 2000 and 2011 (table 4-5). A significant drop was established in 2019, where the variance explained reduced to 66.72%. Component 2 explained approximately 16% for the first three periods but increased for 2019 to 22.6%. Component 2 was explained by the NDBaI, NDBI, and NDWI. Component 3 was favorably explained by all the spectral indices accounting for 8.74%, 11.29%, 10.26%, and 8.68%, respectively, for the specific periods in chronological order. The SoVI exclusively explained the first component for the entire period. The mean value of the rasters decreased over time, translating to reduced vulnerability. By 2019, 75% of the census tracts were in the very low class and nearly 25% in the low class, and no tracts in the high and very high classes (table 4-6). Values in the moderate class also significantly reduced across time, and by 2019 there were negligible tracts for this class. Patterns of spatial autocorrelation were dissimilar to the mean value, corresponding to the integrated spectral index. Similarly, spatial autocorrelation did not dictate the clustering of hotspots for the local Moran's I. Hotspots and coldspots were evident from Moran's analysis even with reduced vulnerability. The hotspots were clustered in the core metro counties and diminished with distance from downtown areas, succeeded by suburbs with no significant clustering and the periphery that constituted coldspots.

Table 4-5. Loadings of the SoVI and the spectral indices from the PCA analysis

| | 2000 | | | | | 2007 | | | | |
|---|---|---|---|---|---|---|---|---|---|---|
| | 1 | 2 | 3 | 4 | 5 | 1 | 2 | 3 | 4 | 5 |
| SoVI | 1.00 | 0.03 | 0.02 | -0.06 | -0.02 | 1.00 | 0.05 | 0.02 | 0.00 | -0.02 |
| NDBaI | 0.03 | 1.00 | 0.83 | -0.33 | -0.84 | 0.05 | 1.00 | 0.85 | -0.36 | -0.85 |
| NDBI | 0.02 | 0.83 | 1.00 | -0.72 | -1.00 | 0.02 | 0.85 | 1.00 | -0.73 | -1.00 |
| NDVI | -0.06 | -0.33 | -0.72 | 1.00 | 0.72 | 0.00 | -0.36 | -0.73 | 1.00 | 0.73 |
| NDWI | -0.02 | -0.84 | -1.00 | 0.72 | 1.00 | -0.02 | -0.85 | -1.00 | 0.73 | 1.00 |
| Variance | 73.37 | 16.35 | 8.74 | 1.55 | 0.00 | 71.55 | 15.81 | 11.29 | 1.35 | 0.00 |
| | 2011 | | | | | 2019 | | | | |
| SoVI | 1.00 | 0.03 | 0.01 | -0.03 | -0.01 | 1.00 | 0.04 | 0.05 | -0.07 | -0.05 |
| NDBaI | 0.03 | 1.00 | 0.85 | -0.35 | -0.85 | 0.04 | 1.00 | 0.68 | -0.23 | -0.68 |
| NDBI | 0.01 | 0.85 | 1.00 | -0.73 | -1.00 | 0.05 | 0.68 | 1.00 | -0.79 | -1.00 |
| NDVI | -0.03 | -0.35 | -0.73 | 1.00 | 0.73 | -0.07 | -0.23 | -0.79 | 1.00 | 0.79 |
| NDWI | -0.01 | -0.85 | -1.00 | 0.73 | 1.00 | -0.05 | -0.68 | -1.00 | 0.79 | 1.00 |
| Variance | 72.68 | 15.71 | 10.26 | 1.35 | 0.00 | 66.72 | 22.57 | 8.68 | 2.03 | 0.00 |

Table 4-6. Results for the equal interval analysis, local and global Moran's analysis

| Equal Interval Analysis | | | | | Global and Local Moran's I | | | | |
|---|---|---|---|---|---|---|---|---|---|
| | 2000 | 2007 | 2011 | 2019 | | 2000 | 2007 | 2011 | 2019 |
| Mean | 0.428 | 0.450 | 0.384 | 0.152 | SA | 0.579 | 0.606 | 0.452 | 0.600 |
| Very Low | 0.000 | 0.000 | 0.000 | 75.110 | H-H | 22.515 | 18.421 | 19.854 | 23.720 |
| Low | 50.509 | 35.189 | 62.911 | 24.544 | H-L | 2.485 | 3.216 | 2.717 | 2.403 |
| Moderate | 42.992 | 61.432 | 36.446 | 0.302 | L-H | 11.404 | 11.111 | 9.718 | 11.703 |
| High | 6.310 | 3.261 | 0.581 | 0.000 | L-L | 14.766 | 16.667 | 17.555 | 19.436 |
| Very High | 0.039 | 0.009 | 0.000 | 0.000 | NS | 48.830 | 50.585 | 50.157 | 42.738 |
| Missing pixels | 0.150 | 0.107 | 0.054 | 0.044 | Z-Score | 72.525 | 75.983 | 69.632 | 91.776 |

### *4.3.5 Spectral Indices and SoVI Equally Weighted Composite*

This composite portrayed reduced vulnerability over time by clustering more tracts in the low category consistent with the PCA-based composite but differed with the LST-based composites. No significant changes were established for the high and very high classes (table 4-

7). The mean value showed a decreasing trend except for 2007, where there was a slight increase and had no relationship with the High-High clustering. The High-High and Low-Low clusters increased over time, showing coldspots and hotspots, reducing the number of areas of no significance similar to the trends established in the LST-based composites. There was no established relationship between spatial autocorrelation and High-High clustering, nor between the global Moran's I and the mean.

Table 4-*7.* Analysis of the spectral indices and the SoVI, equally weighted

| | 2000 | 2007 | 2011 | 2019 |
|---|---|---|---|---|
| Global and Local Moran's I | | | | |
| Spatial Autocorrelation | 0.54 | 0.51 | 0.43 | 0.47 |
| Z-score | 67.41 | 63.88 | 67.03 | 73.16 |
| Mean | 0.41 | 0.43 | 0.41 | 0.32 |
| High-High clustering | 23.20 | 20.91 | 23.82 | 26.75 |
| High-Low clustering | 1.75 | 3.22 | 3.66 | 2.30 |
| Low-High clustering | 10.23 | 6.58 | 8.78 | 11.18 |
| Low-Low clustering | 17.98 | 21.64 | 22.05 | 22.26 |
| No significant clustering | 46.93 | 47.66 | 41.69 | 37.51 |
| Equal Interval Classification | | | | |
| Very low | 0.000 | 0.000 | 0.000 | 0.000 |
| Low | 55.538 | 44.184 | 53.447 | 88.460 |
| Moderate | 44.065 | 55.491 | 46.349 | 11.483 |
| High | 0.239 | 0.208 | 0.140 | 0.001 |
| Very high | 0.000 | 0.000 | 0.000 | 0.000 |
| Missing pixels | 0.158 | 0.116 | 0.064 | 0.055 |

## 4.4 Discussion

### *4.4.1 Land Surface Temperature (LST)*

Metro Atlanta is experiencing elevated exposure to heat vulnerability, findings corroborating Habeeb et al. (2015), who identified heat events accelerating in frequency and intensity in Atlanta. Equal interval classification, global and local Moran's I, and the mean of the LST raster surfaces indicated a progressive increase in exposure to temperature conditions. The modes of analysis differed on either the intensity or spatial distribution of vulnerable locations. We extracted the raster surfaces using the mean value to capture extreme events. Still, the desired effect seemed to have been depleted by the maximum-minimum rescaling that clusters values towards the middle (Tate,2013). The diminished impact of extreme values could also be attributed to the generation of composite images, including data outside of the consummate summer months, instead of relying on a single snapshot. We also speculate that since temperature changes vary marginally, and the changes occur over large temporal scales, the short period of analysis may not depict the outliers, and the equal interval visualization may not disclose significant changes. For instance, the mean value increased from 303.53 Kelvins to 305.70 Kelvins; although it is a substantive increase, data transformations and visualization options may mask the nuances. Locations of no significance decreased over time, which largely transitioned to coldspots.

The hotspots were predominantly concentrated in the core metro counties of Fulton, Cobb, Gwinnett, Clayton, and DeKalb. Similar findings were observed by Maier et al. (2014). In contrast, the suburbs formed a ring of no significant clusters, while the peripheral counties were coldspots. The projected acceleration of intensity, magnitude, and frequency of heatwaves (Alexander 2020) means a substantial proportion of Atlanta could flip to high and very high classes unless mitigation and adaptation measures are overwhelmingly embraced. The spatial distribution highlights the

disproportionate exposure to heat hazards defined by location where core counties that are most populous characterized by people of color and high poverty rates are potentially at higher risk. The affluent suburbs were primarily coldspots or areas of no significant clusters yet constituted of low population density with wealthy households that could modify heat exposure. The peripheral counties were dominantly coldspots, possibly driven by higher elevations. The minimum and maximum values were also increasing, meaning even the cooler areas were getting warmer while warmer areas were getting hotter. The Low-Low clusters increased over time, but the affected counties were outside of the core metro area. Our study established that for the LST, trends of spatial autocorrelation were not similar to Anselin's local Moran's I. On the other hand, a higher mean did not translate to higher spatial autocorrelation, and neither did it guarantee more of the High-High clustering. We established that the mean value was the best predictor of vulnerability trends for equal interval classification.

### *4.4.2 Integrated Spectral Indices*

The integrated spectral indices metric returned inconsistent results from the LST, meaning the indices do not combine additively in Atlanta. LST was used as the standard metric. Previous studies have concluded that it is a great measure of actual temperature conditions (c.f., Frigerio and Amicis 2016; Ho et al., 2018; Mushore et al., 2018; Weber et al., 2015). The findings differ with Mushore et al. (2018), who established that the spectral indices combined additively in Zimbabwe. Equal interval classification had more clustering in the low and very low classes. The clustering of tracts in the low vulnerable classes is attributed to the significantly decreasing mean across the periods. Despite the low vulnerability, downtown Atlanta had significant clustering of hotspots (figure 4-3). Areas of no significant clustering accounted for nearly 50% of the census tracts across time, unlike the LST, where this class had a reduced proportion across the periods.

Similar to LST, there was no relationship between the mean value and spatial autocorrelation. Furthermore, a high spatial autocorrelation did not translate to a higher percentage of tracts in the High-High clustering. All the spectral indices favorably loaded on either component 1 or 2, signifying their relative importance on the final derived metric. Expectedly, the NDBaI and NDBI had positive loadings, thus increased vulnerability. Contrary, the NDWI, and NDVI loaded negatively. The strength of the NDBI and NDWI was equal across the spectrum but inverse in the direction of influence. Reduction of the cumulative variance for component 1 in 2019 correlated with loadings reduction for the NDBI and NDWI, with a slight increase for the NDVI.

Future studies must explore why the indices do not combine additively by analyzing other biophysical parameters such as topography. Despite the reduced vulnerability trend, core downtown areas had disproportionately more High-High clusters, with sections of Northern Fulton dotted with Low-High clusters. These were cooler areas surrounded by high clusters attributable to affluence where landscaping activities and denser trees could have lessened the increased exposure. Other than the core Counties, Gwinnett and sections of Northwest Bartow had higher exposure. Like the LST, the suburbs were essentially areas of no significant clustering, while peripheral counties were extensively coldspots. There is consistency in the distribution of hotspots between the LST and the integrated spectral index, albeit differing on vulnerability trends over time. In terms of visualization, differences were apparent in the maps for the hotspots maps. In 2000, the integrated spectral index only visualized hotspots around the metro area. The LST showed the existence of hotspots further South, including Spalding county. In 2007, the LST metric indicated hotspots in Rockdale and Newton county sections that were absent for the integrated spectral index. For 2011, the LST visualized hotspots in Cobb and had continuous series of hotspots from core metro counties to Gwinnett. Such a trend was not replicated for the integrated

spectral indices metric. The spatial distribution for 2017 was approximately the same for both biophysical metrics. We concluded that the integrated spectral index metric is not a good proxy for LST in Atlanta, although they had nearly similar hotspots and coldspots identification patterns.

Although correlated to the LST individually, the spectral indices do not combine additively to generate a robust integrated biophysical metric. Following these findings, we recommend further studies to establish spectral indicators' suitability in spatial modeling of heat. Most studies have used the indices individually or in limited combination, ascribing disparate weights for lack of a theoretical underpinning regarding the variables' weighting. Tate (2013) explained that data aggregation might result in compensability; Low values in one variable could mask higher values in another and observed that data-driven frameworks could generate loadings non-conformal to conceptual associations. The spectral indices' PCA analysis established that areas with high NDVI and NDWI had very low NDVI and NDBaI, potentially intensifying compensability. Karanja and Kiage (2021) proposed harmonizing theoretical constructs and statistical relationships when deriving the metrics. There is a need to re-examine the subjective choices made in heat representation as adaptation and mitigation measures can only be as good as the derived metrics. Tate (2013) acknowledged the subjectivity in the construction of vulnerability metrics but emphasized the need to evaluate the decisions even in the absence of systematic conceptual frameworks. Despite the disparity in the outputs, Hondula et al. (2015) suggested they are unlikely to constrain their functionality in response efforts, but reliability tests should be upheld. We chose multiple spectral indices to capture diverse urban characteristics (Broadbent et al., 2020), assuming that each index provides a separate independent feature of the urban establishment (Mushore et al., 2018). For instance, tree extent and built-up density accounted for 68% of the LST variation (Alexander, 2020). The author recommended enhanced use of spectral indices utilizing the infrared

window as they have better spatial resolution than thermal bands. However, our study establishes that this approach is only possible if they result in a robust proxy. Furthermore, Bramhe et al. (2018) advocated for including the bareness index alongside the built-up index to guarantee the characterization of built-up areas and bare spaces. Weng et al. (2004) argued that NDVI and LST relationship needs enhanced scrutiny, and the former metric may fail to show areal estimates of vegetational abundance. Several studies (e.g., Harlan et al., 2013; Johnson et al., 2012) only utilized the NDVI. Mushore et al. (2018) applied multiple spectral indices since the NDVI saturates at a high vegetational fraction. Land cover characteristics modulate heat vulnerability (Aubrecht and Ozceylan, 2013), and attempting to incorporate multiple indices is imperative, yet the value of most spectral indices remains unexplored (Mushore et al., 2018).

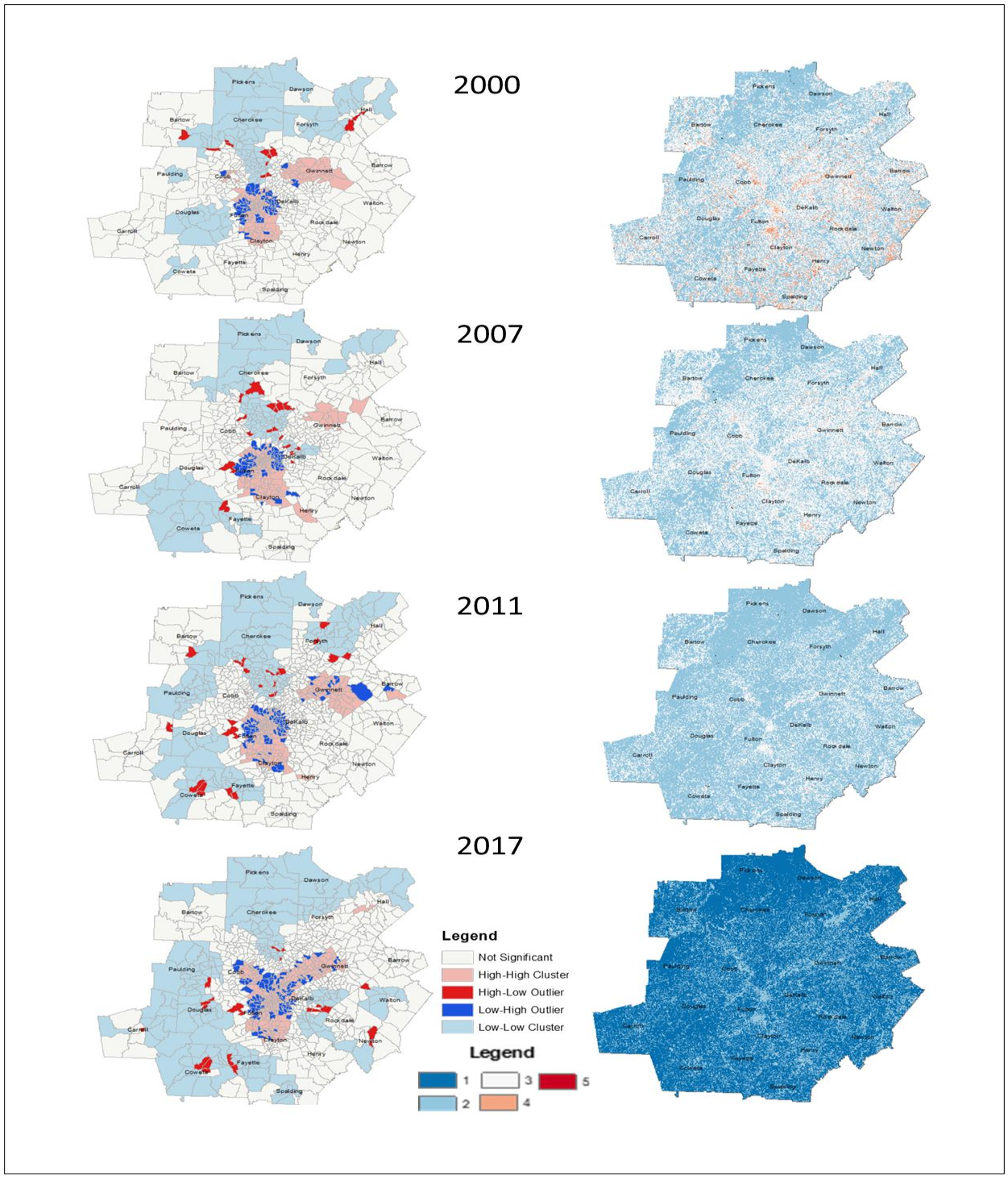


Figure 4-3. Equal interval classification (images on the right) indicated reduced vulnerability. The spatial distribution of the hotspots was similar to the LST using Local Moran's I, with downtown areas experiencing augmented temperature conditions (images to the left). Trends of the mean value were a good predictor of the trends of the equal interval classification.

### *4.4.3 LST-Based Composites*

LST-based composites had no significant variations in the high and very high classes for equal interval classification similar to the LST, attributable to minimum-maximum rescaling and initial extraction of composite images periods beyond the consummate summer months. Additionally, Small temperature increases coupled with data transformation procedures could mask the progressive temperature escalations that take decades to ubiquitously manifest. Future studies could compare the outputs of disparate normalization methods and the associated consequences on spatial visualization. The very low vulnerability class did not have any values for both LST-based composites, interpreted to mean minimum daily temperatures could be rising, corroborating the LST analysis. The magnitude of heat intensity of the LST-based composites was lower compared to the LST-only biophysical metric. We believe the difference in the intensity could be attributed to the moderating effect of the SoVI as vulnerability constitutes hazard exposure and sensitivity (Bera, 2019; Borden et al., 2007; Frigerio and Amicis, 2016; Turner et al., 2003). For instance, Hall county was consistently a coldspot for the LST metric but is visualized as a hotspot by the LST-based composites, driven by a higher percentage of the Hispanic community. Similarly, parts of Northern Fulton visualized as hotspots by the LST metric have transitioned to cold spots or areas of no significant clustering in the LST-based composite. The variance-based SoVI had lower proportions consistently for the moderate class and consistently higher proportions in the low class than equal-weighted SoVI, reflecting variances in the magnitude introduced by choice of the spatial model. It is crucial to model the SoVI alongside the biophysical metrics to determine how modeling decisions influence results (Chuang and Gober, 2015: Tate, 2013). The results emphasize the urgent need to institute policy changes to alleviate the biophysical hazard's harmful effects. Furthermore, the models for the construction of the SoVI

should be enhanced since weighting mechanics and data transformation techniques impact the magnitude and distribution of composite biophysical and socioeconomic indices. The derivation of the SoVI could be impaired by the absence of guidelines on selecting, weighting, interpretation, and data reduction techniques (Johnsonn and Lundgren, 2015: Karanja and Kiage, 2021).

A significant percentage of the tracts in the High-high category are clustered in the urban core counties, specifically Southeast Cobb, Southern Fulton, DeKalb, North Clayton, Southwest Gwinnett, and Northwest Rockdale (figure 4-4). This spatial distribution is repeated across the years, although more concentration of the clusters encroaches on Cobb, Gwinnett, and Clayton with time. Low-high clusters started to appear in the initially low vulnerable areas such as North Fulton, Fayette, Cherokee, Forsyth, Bartow, Paulding, Watson, Rockdale, and Barrow. The core urban counties host a massive population for Atlanta, and the increasing heat in these areas should concern policymakers. According to the US Department of Housing and Urban Development, Fulton and DeKalb counties account for 30% of the population in Atlanta, which have experienced a net annual population growth rate of 1.5% propelled by job availability. The counties also host the majority of the low-income people, indicating excessive exposure and sensitivity. These locations have high exposure yet lack the means to safeguard themselves. Going by Atlanta's simulated temperatures (Broadbent et al., 2019), a public health crisis of heat-related mortality and morbidity is a likely scenario in the future unless mitigation and adaptation are commensurate to the increasing magnitude and intensity of heat and its spatial spread (Alexander, 2020). Berko et al. (2014) established that weather-related deaths were 2 to 7 times more in poor localities than in affluent neighborhoods; hence the statistics portend exacerbated sensitivity and exposure for the urban poor. The integrated metrics illustrate that even the affluent suburbs are experiencing warming and that wealth, if not invested in mitigation, then the consequences would be

undiscriminating. The critical finding from both metrics' spatial distribution is that heat vulnerability is increasing in Atlanta, particularly in the urban core, which over time is encroaching to formerly cooler suburban areas. The low-income areas are disproportionately susceptible, yet they are highly exposed to heat vulnerability.

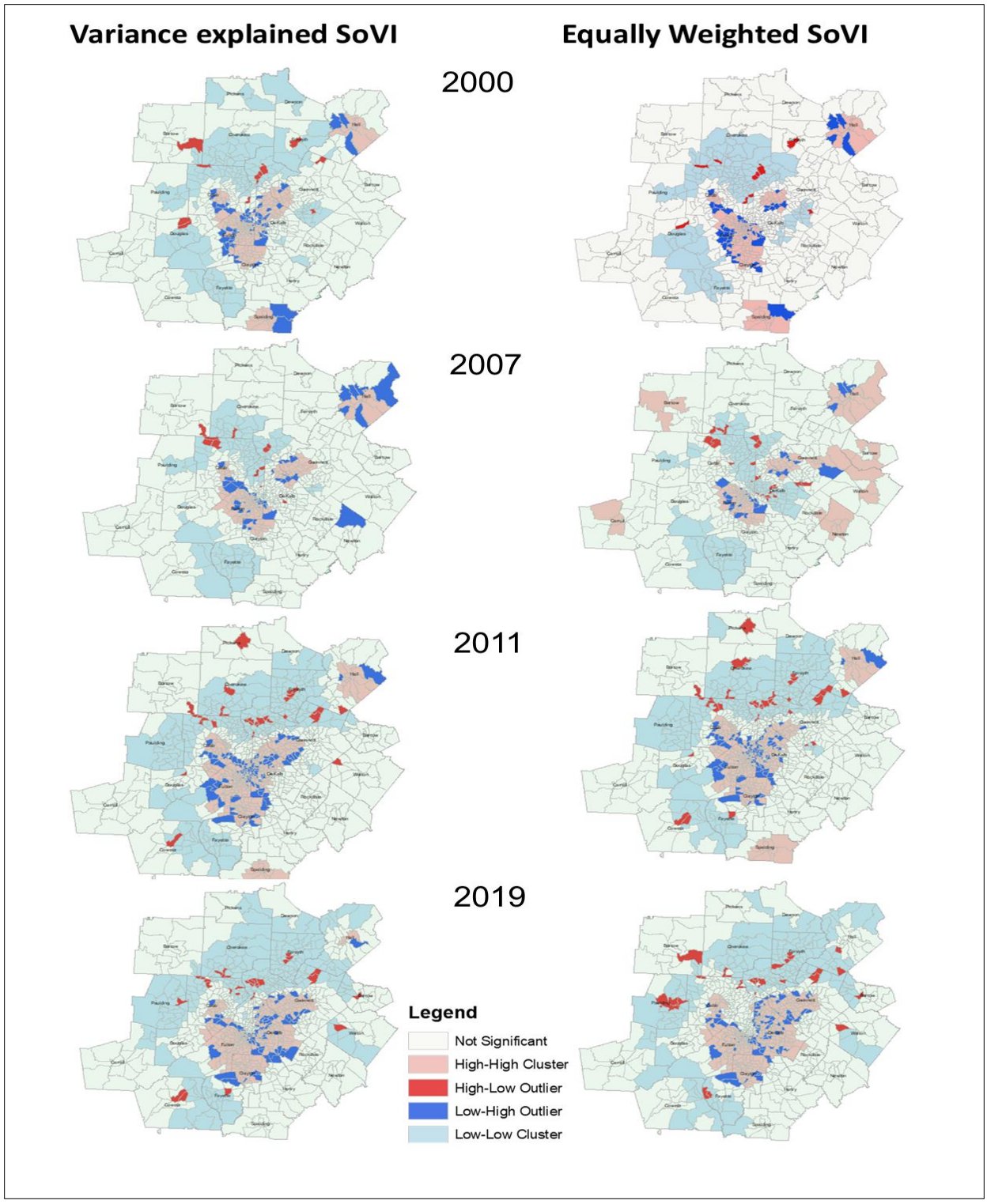


Figure 4-4. Heat vulnerability is disproportionately concentrated in the core metro counties, with increasing spatial spread over time to the suburbs. The urban core counties host massive populations meaning more people at risk of heat-related morbidity and mortality going by the climate simulations. The low-income areas are increasingly sensitive yet highly exposed.

### *4.4.4 PCA-Based Composite*

The PCA-based composite index showed decreased vulnerability over time, consistent with the spectral indices-based metrics, but differed with the LST-based metrics. Any composite metric generated from the combined spectral metrics was found not to correlate with the LST and may not reflect vulnerability. The spectral metrics do not combine additively, and their application to heat vulnerability studies should be carefully determined and evaluated before incorporating them into the spatial models. Despite the applicability of PCA, it could result in variables interactions that fail to reflect the intricacy of interactions (Nayak et al., 2018). Across all the composite metrics, the trends of the mean raster surface determined the trends of vulnerability for equal interval classification. The SoVI exclusively explained component 1 and had no consistent direct association with any of the spectral indices. The NDBaI was more prominent for component 2 and the NDBI and NDWI, which had equal loadings but with different directions, corroborating the results from the integrated spectral index. The global and local Moran's I indicated the core metro counties of Fulton, DeKalb, and Clayton to be disproportionally exposed alongside Gwinnett for the entire period. Northern Fulton had patches of Low-High, which could be attributed to moderating effects of the SoVI, driven by the affluence of the residents in these locations. Compared to the LST-based composite derived from Eigen weighting, the PCA-based metric revealed differences in the spatial distribution of coldspots and hotspots. For instance, in 2000, LST-based composite visualized Spalding county as a hotspot and Fayette as a coldspot, which appeared as areas of no significant clusters for PCA-based composite. In 2011, Hall and Spalding counties were visualized as hotspots by LST-based composite, while they are represented as coldspots and area of no significant clustering by PCA-based. In 2019, the PCA-based showed more Low-High clusters in Northern Fulton, a pattern that is diminished in the LST-based

composite (figure 4-5). It is prudent to consider the spatial model of representation as it impacts the spatial distribution of vulnerability. Following these findings, there is a need to compare metrics based on images extracted using the median and the mean. Future studies should also attempt data fusion techniques (c.f., Pelta and Chudnovsky, 2017; Zhang, 2010) to enhance sensor-based metrics' accuracy for enhanced multi-temporal and spatial resolution. Another opportunity lies in comparing near-surface and surface temperature metrics.

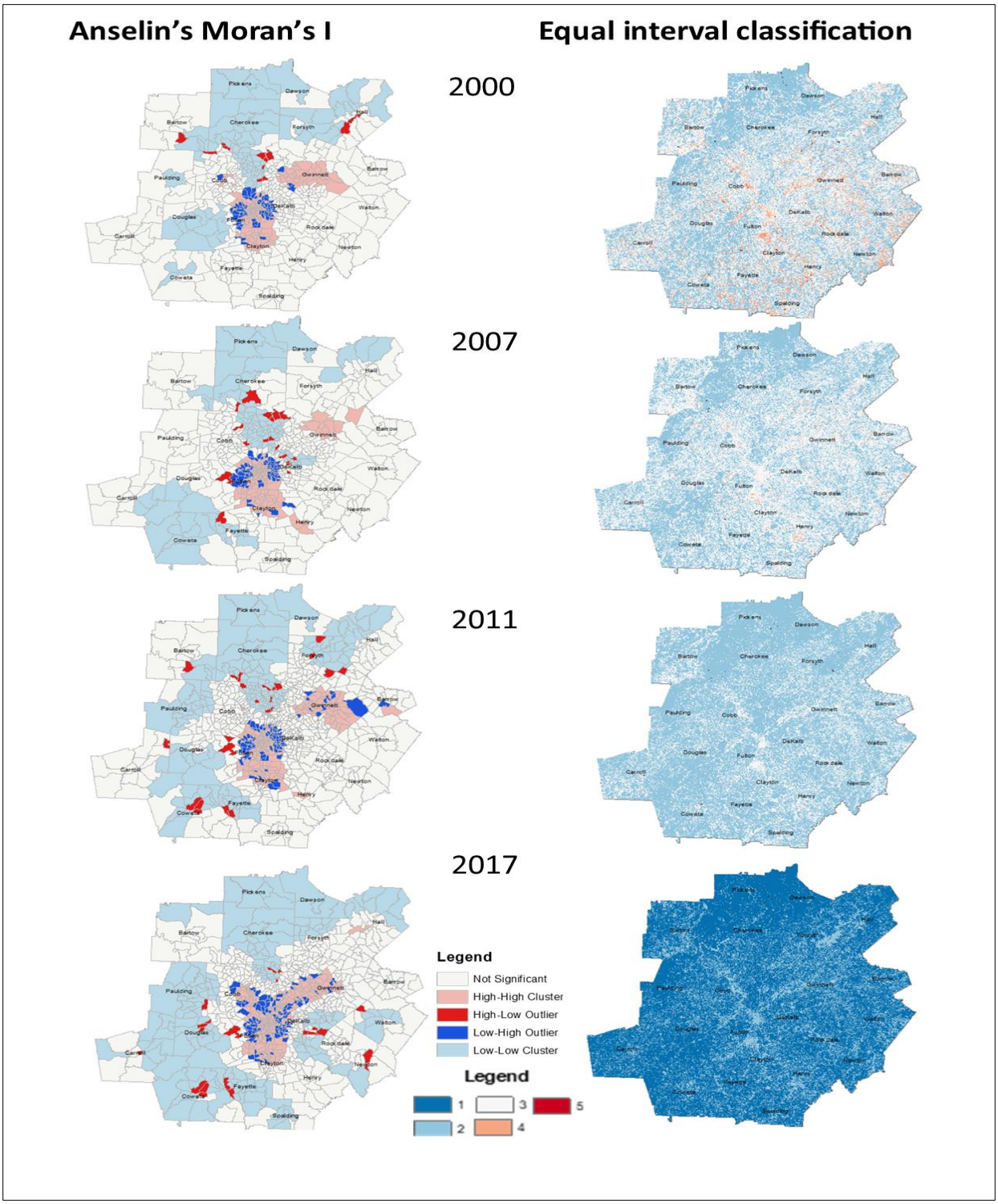


Figure 4-5. Equal interval classification showed a trend of reduced vulnerability, whereas Anselin's Moran's I indicated hotspots in the core metro counties. The hotspots diminish with distance from downtown areas. The mean value is a good predictor of the trends of vulnerability for equal interval classification.

### *4.4.5 Spectral Index and SoVI Equally Weighted*

The equally weighted spectral indices and SoVI composite showed consistent results with the PCA-based composite. A reduced vulnerability was established over time, although they differed on the magnitude of the metric. The mean value seems to be a better predictor of exposure trends consistent with earlier analysis for the other metrics, especially for the equal interval classification adopted. This composite had consistently lower values for spatial autocorrelation than the PCA-based metric. The rate of mean change was lower while the values in the High-High clustering were greater than the PCA-based composite. Similarly, the composite had more Low-Low clusters but less value for areas of no significant clusters. The most profound difference is that the PCA-based metric clustered more tracts in the very low class for 2019, unlike the equally weighted composite, which huddled more in the low class. The local Moran's I and the equal interval classification results indicate that this composite shows greater vulnerability than the PCA-based composite. The results corroborate the findings for the LST-based composite where the Eigen weighted SoVI had less vulnerability than equal weighting. We conclude that composites computed using equal weighting have a higher magnitude of vulnerability than Eigen weighting. The trends of increase and decrease were the same for the moderate class, High-High clustering, and Low-Low clustering. However, the metrics differed on trends of spatial autocorrelation. The differences illustrate how the choice of the spatial model influences the determination of vulnerability and the need for studies to harmonize the weighting mechanics for more precise representations and visualizations. The equally weighted composite best-visualized areas with high SoVI, including Hall County, which had not been a hotspot for any biophysical metric. Like the other composites, hotspots were established in core metro counties, with the periphery consisting of coldspots (figure 4-6).

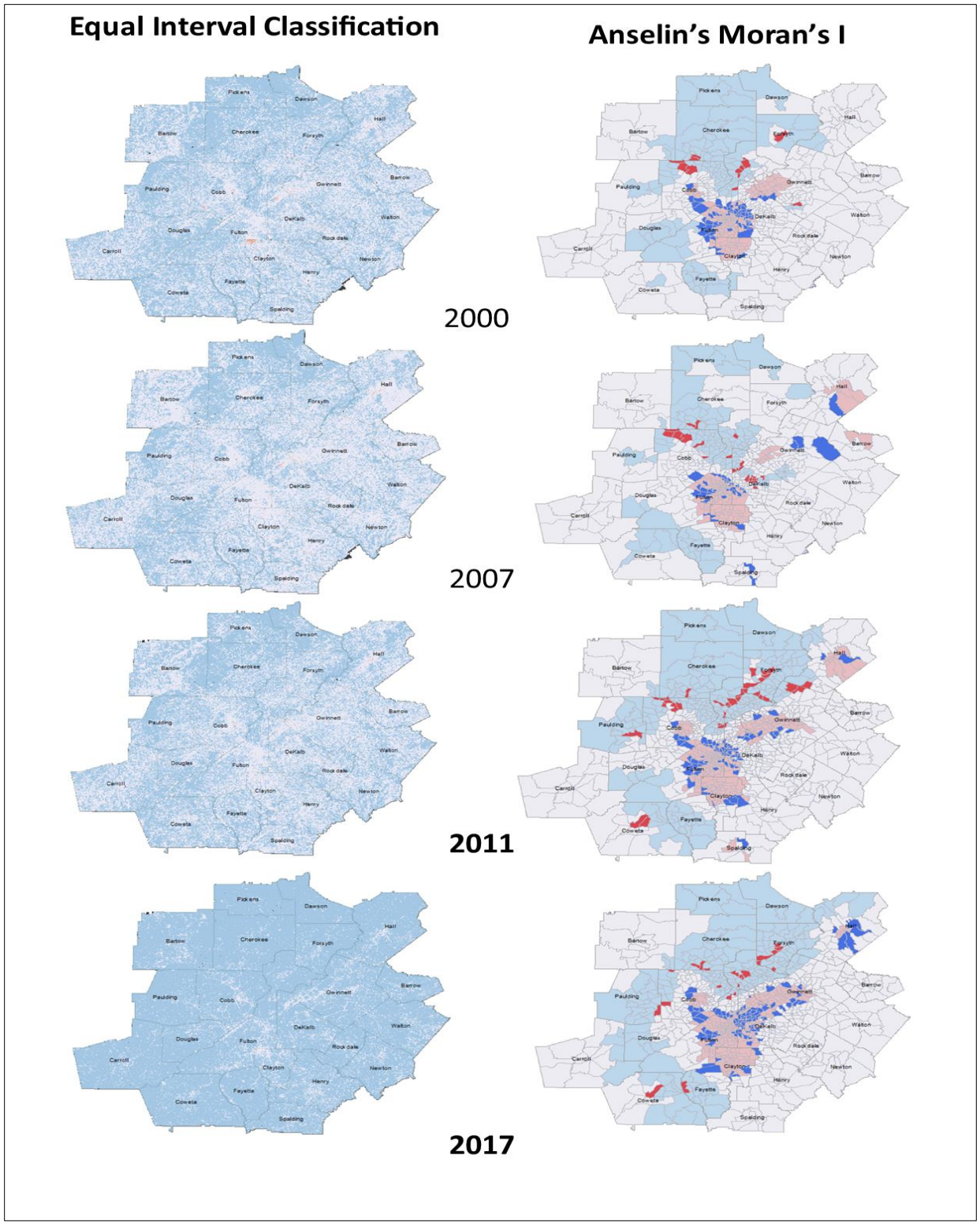


Figure 4-6. The equally weighted composite showed the prevalence of hotspots in downtown areas. The composite had a higher magnitude of vulnerability than the PCA-based composite, corroborating the findings of the LST-based composites.

## 4.5 Conclusion

Heat hazard would increase in intensity, duration, frequency, and magnitude to the future going by the simulations. Policymaking requires novel characterization of the heat metrics, especially composite indices that capture socioeconomic and biophysical variables. The lack of a systematic framework to guide heat metrics conceptualization has marred the construction of the metrics. It is crucial to understand how LST-based metrics differ from those generated from its proxies (e.g., NDVI, NDBI, NDWI, and NDBaI). It is also imperative to probe the variable weighting decisions, data transformation techniques, and the spatial models applied and compare them through longitudinal studies to narrow the gap in the existing methodologies. Our approach compared several composites and their effect on the spatial distribution of vulnerability, the intensity, and the magnitude of the metric. It is crucial to provide a multi-dimensional analysis of risk to enrich broad spectrum decision making as ideal modeling of the real world is nearly impossible. Given the existing fuzzy conceptualizations of heat vulnerability, understanding how the biophysical and socioeconomic metrics interact is a profound undertaking. Establishing the evolution of the metrics and the intricacies involving data transformations, spatial modeling choices, and weighting mechanics could be a pathway towards harmonizing disparate conceptualizations. Exploring the drivers of vulnerability and different visualization paradigms could unlock fundamental systemic dynamics undergirding heat vulnerability.

The first composite was LST-based combined by SoVI generated through equal weighting. The second was LST-based integrated with SoVI generated through Eigen weighting. The objective was to establish how constructs of the SoVI may influence the nature of the eventual integrated metrics. The third SoVI comprised spectral indices, and the SoVI each assigned equal weighting to determine how spectral indices-based metric differed from LST-based. The fourth

composite was PCA-based, including the spectral indices and the SoVI. The goal was to establish how weighting mechanics and the choice of spatial model impact vulnerability representation. LST-based composites had similar trends, although they differed on the spatial distribution in the various classes. The magnitude of vulnerability was lower compared to the LST biophysical metric. LST-based composites established an increased susceptibility, with downtown areas experiencing augmented sensitivity and exposure. The LST composite derived using Eigen weighted SoVI had a lesser magnitude of vulnerability than equally weighted SoVI. The composite from the spectral indices returned different results from LST-based metrics indicating reduced susceptibility. Further analysis established that the flipped outcome could be attributed to the spectral indices. We combined them alone to generate a biophysical metric that reduced exposure over time, thus not a suitable proxy for LST. We concluded that the spectral indices do not combine additively, and their weighting mechanics should be thoroughly evaluated, despite the absence of a substantive theoretical framework. The spectral-based composites using equal weighting and PCA-based established hotspots in core metro counties, which reduced with distance from downtown areas. Our study determined that the SoVI had no association or correlation with any of the spectral metrics. We determined that the mean value trends are the best predictor of patterns of vulnerability for equal interval classification. Generally, composites derived from equal weighting showed higher vulnerability than Eigen-based composites for both the LST and spectral indices metrics. We concluded that variable weighting techniques, data transformation choices, the choice of the spatial model have implications on the magnitude and spatial distribution and identification of hotspots and coldspots.

## 4.6 Statement of Authorship

The student, Joseph Karanja, is the lead author under the guidance of Dr. Lawrence Kiage.

**References:**

Adeyeye, T. E., Insaf, T. Z., Al-Hamdan, M. Z., Nayak, S. G., Stuart, N., DiRienzo, S., & Crosson, W. L. (2019). Estimating Policy-Relevant Health Effects of Ambient Heat Exposures Using Spatially Contiguous Reanalysis Data. *Environmental Health, 18*(35). Retrieved from https://doi.org/10.1186/s12940-019-0467-5

Alexander, C. (2020, April). Normalized difference spectral indices and urban land cover as indicators of land surface temperature (LST). *International journal of applied earth observation and geoinformation, 86*. doi:https://doi.org/10.1016/j.jag.2019.102013

Atyia, M. S. (2015). A Framework to Understand the Relationship between Social Factors that Reduce Resilience in Cities: Application to the City of Boston. *International Journal of Disaster Risk Reduction, 12*, 53-80. doi:10.1016/j.ijdrr.2014.12.001

Aubrecht, C., & Ozceylan, D. (2013). Identification of heat risk patterns in the U.S. national capital region by integrating heat stress and related vulnerability. *Environment International, 56*, 65-77. doi:http://dx.doi.org/10.1016/j.envint.2013.03.005

Bera, K. K. (2019, July). Vulnerability of Rural Areas to Climate Change- Analysis of Similar Units in Terms of Spatial Conditions for Warminsko-Mazurmskie Voivodeship. *Journal of Ecological Engineering*, 20(6), 198-206. https://doi.org/10.12911/22998993/109454

Berko, J., Ingram, D. D., Saha, S., & Parker, J. D. (2014, July). *Deaths Attributed to Heat, Cold, and Other Weather Events in the United States, 2006-2010.* National Center for Health Statistics Report. Hyattsville: National Center for Health Statistics. (76): 1-15. PMID:25073563. Retrieved from https://pubmed.ncbi.nlm.nih.gov/25073563/

Bramhe, V. S., Ghosh, S. K., & Garg, P. K. (2018, November). Extraction of built-up area by combining textural features and spectral indices from Landsat-8 multispectral image. *The international archives of the photogrammetry, remote sensing and spatial information sciences, XLII*(5). doi:https://doi.org/10.5194/isprs-archives-XLII-5-727-2018

Borden, A. K., Schmidtlein, C. M., Emrich, T. C., Piergosch, W. W., & Cutter, L. S. (2007). Vulnerability of US cities to environmental hazards. *Journal of homeland security and emergency management, 4*(2). doi:https://doi.org/10.2202/1547-7355.1279

Brenkert, A. L., & Malone, E. L. (2005). Modeling Vulnerability and Resilience to Climate Change: A Case Study of India and Indian States. *Climatic Change*, 72, 57-102. doi:10.1007/s10584-005-5930-3

Broadbent, A. M., Krayenhoff, E. S., & Georgescu, M. (2020). Efficacy of Cool Roofs at Reducing Pedestrian-Level Air Temperature during Projected 21st Century Heatwaves in Atlanta, Detroit, and Phoenix (USA). *Environmental Research Letters, 15*. Retrieved from https://doi.org/10.1088/1748-9326/ab6a23

Carr, L. D., Pricope, G. N., Aukema, E. J., Jankowska, M. M., Funk, C., Husak, G., & Michaelsen, J. (2014, March 6th). A spatial analysis of population dynamics and climate change in Africa: potential vulnerability hotspots emerge where precipitation declines and demographic pressures coincide. *Population and Environment, 35*, 323-339. doi:https://doi.org/10.1007/s11111-014-0209-0

Caruana, J. E., Marius, R., Sanchez, H. J., & Solli, P. (2015, October 9th). Longitudinal studies. *Thoracic Disease, 7*(11), 537-545. doi:https://doi.org/10.3978/j.issn.2072-1439.2015.10.63

Chuang, W.-C., & Gober, P. (2015). Predicting Hospitalization for Heat-Related Illness at the Census-Tract Level: Accuracy of a Generic Heat Vulnerability Index in Phoenix, Arizona (USA). *Environmental Health Perspective, 123*, 606-612. Retrieved from http://dx.doi.org/10.1289/ehp.1307868

Dintwa, K. F., Letamo, G., & Navaneetham, K. (2019, May 6). Measuring social vulnerability to natural hazards at the district level in Botswana. *Jàmbá: Journal of Disaster Risk Studies, 11*(1). doi:https://doi.org/10.4102/jamba.v11i1.447

Eakin, H., & Luers, A. L. (2006, 18th July). *Annual Review of Environment and Resources, 31*, 365-394. doi:10.1146/annurev.energy.30.050504.144352

EPA (Environmental Protection Agency). (2006). *Excessive Heat Events Guidebook.* Washington, D.C., Pennsylvania Avenue NW: United States Environmental Protection Agency.

Ermida, S. L., Soares , P., Mantas, V., Göttsche, F. M., & Trigo, I. F. (2020, May 6). Google Earth Engine open source code for Land Surface Temperature Estimation from the Landsat series. *Remote Sensing, 12*(9). doi:https://doi.org/10.3390/rs12091471

Frigerio, I., & Amicis, M. D. (2016, June 14). Mapping Social Vulnerability to Natural Hazards in Italy: A Suitable Tool for Risk Mitigation Strategies. *Environmental Science and Policy*, 63, 187-196. Retrieved from http://dx.doi.org/10.1016/j.envsci.2016.06.001

Georgescu, M., Morefield, P. E., Bierwagen, B. G., & Weaver, C. P. (2014, February 25). Urban adaptation can roll back warming of emerging megapolitan regions. (S. Hanson, Ed.) *Proceedings of the National Academy of Sciences of the United States of America, 111*(8), 2909-2914. doi:https://doi.org/10.1073/pnas.1322280111

Gorelick, N., Hancher, M., Dixon, M., IIyushchenko, S., Thau, D., & Moore, R. (2017). Google Earth Engine: planetary-scale Geospatial Analysis for Everyone. *Remote Sensing of Environment, 202*, 18-27. Retrieved from http://dx.doi.org/10.1016/j.rse.2017.06.031

Habeeb, D., Vargo, J., & Stone, J. B. (2015, 1st January). Rising Heatwave Trends in Large US Cities. . *Natural Hazards, 76*, 1651-1665. doi:10.1007/s11069-014-1563-z

Harlan, S. L., Declet-Barreto, J. H., Stefanov, W. L., & Petitti, D. B. (2013, February). Neighborhood Effects on Heat Deaths: Social and Environmental Predictors of Vulnerability in Maricopa County, Arizona. *Environmental Health Perspectives*, *121*(2), 197-204. doi:http://dx.doi.org/10.1289/ehp.1104625

Ho, C. H., Knudby, A., & Huang, W. (2015, Decemeber 18). A Spatial Framework to Map Heat Health Risks at Multiple Scales. *International Journal of Environmental Research and Public Health, 12*, 16110-16123. doi:10.3390/ijerph121215046

Ho, H. C., Knudby, A., Chi, G., Aminipouri, M., & Lai, D. Y.-F. (2018). Spatial-Temporal Analysis of Regional Socio-Economic Vulnerability Change Associated with Heat Risks in Canada. *Applied Geography*, *95*, 61-70. doi:https://doi.org/10.1016/j.apgeog.2018.04.015

Hondula, D. M., Davis, R. E., Saha, M. V., Wegner, C. R., & Veazey, L. M. (2015, March 17). Geographic Dimensions of Heat-Related Mortality in Seven U.S. Cities. *Environmental Research, 138*, 439-452. Retrieved from http://dx.doi.org/10.1016/j.envres.2015.02.033

Johnson, P. D., Stanforth, A., Lulla, V., & Luber, G. (2012). Developing an Applied Extreme Heat Vulnerability Index Utilizing Socio-Economic and Environmental Data. *Applied Geography*, 35, 23-31. doi:10.1016/j.apgeog.2012.04.006

Jonsonn, A. C., & Lundgren, L. (2015). Vulnerability and Adaptation to Heat in Cities: Perspectives and Perceptions of Local Adaptation Decision Makers in Sweden. *Local Environment*, 20(4), 442-458. http://dx.doi.org/10.1080/13549839.2014.896326

Karanja, J., & Kiage, L. (2021, February 13). Perspectives on spatial representation of urban heat vulnerability. *Science of the Total Environment, 774*. doi:https://doi.org/10.1016/j.scitotenv.2021.145634

Kashem, B. S., Wilson, B., & Zandt, V. S. (2016, January). Planning for Climate Adaptation: Evaluating the Changing Patterns of Social Vulnerability and Adaptation Challenges in Three Coastal Cities. . *Planning Education and Research, 36*(3), 304-318. doi:10.1177/0739456X16645167

Lo, C. P., & Quattrochi, A. (2003, September). Land Use and Land Cover Change, Urban Heat Island Phenomenon, and Health Implications: A Remote Sensing Approach. *Photogrammetric Engineering and Remote Sensing, 69*(9), 1053-1063. doi:https://doi.org/10.14358/PERS.69.9.1053

Maier, G., Grundstein, A., Jang, W., Li, C., Naeher, L. P., & Shepherd, M. (2014, April). Assessing the Performance of a Vulnerability Index During Oppressive Heat Across Georgia, United States. *6*, 253-263. doi:10.1175/WCAS-D-13-00037.1

Mushore, D. T., Mutanga, O., Odindi, J., & Dube, T. (2018). Determining Extreme Heat Vulnerability of Harare Metropolitan City using Multi-Spectral Remote Sensing and Socio-economic Data. *Spatial Science, 63*(1), 173-191. Retrieved from https://doi.org/10.1080/14498596.2017.1290558

Nayak, S. G., Shrestha, S., Kinney, P. L., Ross, Z., Sheridan, S. C., Pantea, C. I., . . . Hwang, S. A. (2018). Development of a Heat Vulnerability Index for Newyork State. *Public Health, 161*, 127-137. doi:https//:doi.org/10.1016/j.puhe.2017.09.006

Pelta, R., & Chudnvosky, A. (2017). Spatiotemporal Estimation of Air Temperature Patterns at the Street Level using High Resolution Satellite Imagery. *Science of the Total Environment, 579*, 675-684. doi:http://dx.doi.org/10.1016/j.scitotenv.2016.11.042

Shepherd, M., & Zhou, Y. (2009, May 27). Atlanta's urban heat island under extreme heat conditions and potential mitigation strategies. *Nat Hazards* 52, 639–668. https://doi.org/10.1007/s11069-009-9406-z

Sheridan, S. C., & Dolney, T. J. (2004, September 19). Heat, Mortality, and Level of Urbanization: Measuring Vulnerability Across Ohio, USA. *Climate Research*, 24, 255-265. doi:10.3354/cr024255

Sunhui, S. (2017, October 4). Social Vulnerability to Heat in Greater Atlanta, USA: Spatial Pattern of Heat, NDVI, Socioeconomics and Household Composition. *Remote Sensing Technologies and Applications in Urban Environments II*, 1043105. Warsaw, Poland. doi:10.1117/12.2278678

Tate, E. (2013, 20th August). Uncertainty Analysis for a Social Vulnerability Index. *Annals of the Association of American Geographers, 103*(3), 526-543. doi:10.1080/00045608.2012.700616

Tran, B. N., Tanase, M. A., Bennett, L. T., & Aponte, C. (2018, 24th October). Evaluation of spectral indices for assessing fire severity in Australian temperate forests. *Remote sensing, 10*(1680). doi:doi:10.3390/rs10111680

Turner II, L. B., Kasperson, E. R., Matson, A. P., McCarthy, J. J., Corell, W. R., Christensen, L., & Schiller, A. (2003). A Framework for Vulnerability Analysis in Sustainability Science. *Proceedings of the National Academy of Science of the United States of America (PNAS), 100*(4), 8074-8079.

US Deparment of Housing and Urban Development. (2018). *Atlanta Metropolitan Areas Series focus on: Fulton and DeKalb Counties, Georgia.* Office of Policy Development and Research. Retrieved from https://www.huduser.gov/portal/publications/pdf/Fulton-DeKalb-GA-CHMA.pdf

Wang, W., Liu, K., Tang, R., & Wang, S. (2019, January 3). Remote Sensing Image Based Analysis of the Urban Heat Island Effect in Shenzhen, China. *Physics and Chemistry of the Earth*, 110, 168-175. https://doi.org/10.1016/j.pce.2019.01.002

Weber, S., Sadoff, N., Zell, E., & Sherbinin, A. d. (2015, July 17). Policy Relevant Indicators for Mapping the Vulnerability of Urban Populations to Extreme Heat Events: A Case Study of Philadelphia. *Applied Geography*, 63, 231-243. http://dx.doi.org/10.1016/j.apgeog.2015.07.006

Weng, Q., Lu, D., & Schubring, J. (2004). Estimation of land surface temperature-vegetation abundance relationship for urban heat island studies. *Remote sensing of the environment, 89*, 467-483. doi:doi:10.1016/j.rse.2003.11.005

Wolf, T., Chuang, W.-C., & McGregor, G. (2015, 23rd October). On the Science-Policy Bridge: Do Spatial Heat Vulnerability Assessment Studies Influence Policy ? (J. C. Semenza, Ed.) *International Journal of Environmental Research and Public Health, 12*, 13321-13349. doi:10.3390/ijerph121013321

Zhang, J. (2010, February 17). Multi-source remote sensing data fusion: status and trends. *International journal of image and data fusion, 1*(1), 5-24. doi:https://doi.org/10.1080/19479830903561035

Zhou, Y., Li, N., Wu, W., Wu, J., & Shi, P. (2014). Local Spatial and Temporal Factors Influencing Population and Societal Vulnerability to Natural Disasters. *Risk Analysis, 34*(4), 614-639. doi:10.1111/risa.12193

# CHAPTER 5: SUMMARY AND CONCLUSION

## 5.1 Conclusion

Urban heat stress will increase in magnitude, frequency, intensity, and duration hence the need to accurately and precisely visualize the most susceptible for a targeted policy response. We have provided an iterative holistic conceptual framework that integrates quantitative and qualitative approaches. The UHI phenomenon being multi-dimensional should not be a deterrent to effective spatial representation. Our inclusive framework acknowledges that the interactions between the biophysical, geodemographics and socioeconomic dimensions generate stochastic ecological perturbations, residual risks, and hazard co-productions, often not accounted for in the existing frameworks. These interactions are iterative and need a longitudinal approach that recognizes that scientific theories are explicitly and implicitly longitudinal.

Targeted policy responses are enhanced when specific, accurate, and precise spatial representations are availed. The imperfections observed in the available frameworks are multiple. There is a need to harmonize the different approaches, scale choices, weighting mechanics, and manipulation of variables through longitudinal methods that acknowledge spatiotemporal reference. Alternatives pursued by scientists must meet certain thresholds and be subjected to replication and validation while incorporating the qualitative dimension. Our review has provided a starting point for scientific discourse towards a consistent iterative spatial representation framework. The theoretical and statistical relationships are enhanced, and the definition of vulnerability is made hazard-specific. We have provided flexible decision criteria that transition from simple data aggregation to understanding processes that shape vulnerability. The model allows for pre and post hazard variables determination and avails rational content-driven reasoning in developing the composite HVI.

Our analysis of the SoVI established that weighting guided by the variance explained and equal weighting impact on the spatial distribuion and magnitude of the SoVI. Data transformations and model adopted have a bearing on the developed metrics. The contrasting results highlight the need to enhance the available methodological framework, especially since there is no systematic method for validation of the metric. Although data transformation is inevitable, comparing several metrics offers a broader spectrum for practical evaluation of alternatives, which may provide hints on the most representative methodology, when validated by a number of health outcomes. Analysis of the biophysicals and composite indices established that combining the NDVI, NDWI, NDBaI and NDBI do not interact in an additive manner; hence do not return equivalent results to the LST and whenever the spectral indices are used a thorough evaluation of the weighting mechanics should be done. Combination of the LST and multiple SoVIs determined that weighting decisions at the SoVI construction level results in variations in outputs for the combined metrics. Our research identified the common spatial modeling pathways and adopted some in a case study of Atlanta. All the metrics derived from the spectral indices indicated reduced vulnerability, albeit had consistency in the identification of hospots compared to the LST. The fundamental finding is that the disprate weighting mechanics, data transformation choices, and spatial models adopted have a bearing on the magnitude and spatial distribution of hotspots and coldspots. It is imperative for scientists to start questioning the decision criteria despite the absence of a consistent and systematic framework. Our inclusive framework provides a starting point for convesations on heat vulnerability and visualization. Our composites inform the potential differences arising from data manipulation and the spatial modeling decision criteria, crucial for broad spectrum disaster response strategies and enhancing vulnerability conceptualization.

## 5.2 Directions for Future Research

Our analysis focused on population parameters and eventually transitioning into area-based statistics with the integration of the biophysical parameters. Future studies should compare the outputs of the two methods and determine whether significant variations persist. Scientists interested in social metrics could test their SoVIs pre- and post-disaster efficacy to understand the dynamics and enrich the theoretical and statistical associations of variables. Given that GIScience challenges such as the Modifiable Areal Unit Problem (MAUP) and mixed pixel are likely to constrain spatial representations, it is critical for future studies to explore these two spatial representation challenges. Varying distance lags when using the Local Moran's I may provide insights on geographical variability. Data fusion techniques for satellite sensors could be pursued as an alternative to enhance the temporal, spatial, and spectral resolutions of satellite imagery.